Check for updates

Recent progress in synthesis and applications of monolithic metal–organic frameworks

Donald Muringaniza, Laurencia Zulu, Linia Gedi Marazani, [ID] Piwai Tshuma and Gift Mehlana [ID] *

Monolithic MOFs have so far exhibited significant advantages in various industrial applications such as catalysis, sensing, separation, and gas storage. Compared to their powder counterparts, they have been exceptional in terms of mechanical strength, stability, and improved handling. This addresses the critical challenges with powder MOFs in real-world industrial applications. Despite the notable developments in the synthesis of monolith MOFs, challenges related to their functional optimization and large-scale production are still being encountered. This review presents the synthetic methodologies that have been used to prepare monolithic MOFs. Characterisation techniques are also presented with the hardness test being used to distinguish between a monolith and a powdered MOF. Owing to their tunable structures, flexibility, and unique physicochemical properties, monolithic MOFs are increasingly being adopted in diverse industrial sectors, including catalysis, environmental remediation, energy storage, and sensing. Their ongoing development is poised to play a pivotal role in advancing sustainable and high-performance technologies.

Introduction

The field of metal organic frameworks (MOFs) is a rapidly evolving area of materials science, distinguished by ongoing breakthroughs and broadening research horizons. These crystalline structures, comprised of metal ions or clusters coupled by organic ligands, have received significant scientific attention due to their outstanding architectural diversity and exceptional functional qualities.[1,2] MOFs possess several remarkable characteristics: precisely engineerable porous networks, high catalytic activity, and remarkable structural stability. The porous networks can be tailored at the molecular level, enabling control over material properties, while the catalytic activity and stability make them promising for applications under challenging conditions.[3–6] MOFs have emerged as attractive candidates for advanced technologies such as targeted drug delivery systems, gas storage, sensing and selective molecular separation because of their modular nature which facilitates systematic design and modification.[7–13] The potential of MOFs to address diverse scientific and industrial challenges becomes inherently important as analytical and synthetic technologies continue to advance, thereby placing MOFs at the forefront of contemporary material research and technological innovation.[14,15]

However, the physical and chemical characteristics of MOF powders pose significant practical challenges, with the main

Department of Chemical Sciences, Faculty of Science and Technology, Midlands State University, P Bag 9055 Senga Road, Gweru, Zimbabwe. E-mail: mehlanag@staff.msu.ac.zw

issue being pronounced handling difficulties.[16] Applications like catalysis, gas separation, and energy storage require materials that possess controllable mechanical strength, uniform particle size, consistent geometry, and predictable microscopic morphology. MOF powders often lack these fundamental properties, thereby restricting their industrial applications.[17,18] Additionally, MOF powders are prone to aggregation, fragile, and present challenges in accurate dosing and maintaining consistency during operations.[19]

These multifaceted limitations necessitate pre-processing techniques, such as pelletization, immobilization on support matrices, or advanced morphological engineering, to transform these promising materials from laboratory curiosities into viable technological solutions capable of meeting stringent industrial performance criteria.[20] It is within this context that the development of monolithic MOF materials has emerged as a powerful solution to address the challenges inherent to their powdered counterparts.[21,22]

Monolithic MOFs are defined as macroscopically continuous, self-supporting solid materials composed of a MOF or its composite, which possess structural integrity and can be handled without the need for an additional binder or support matrix. They are hierarchically structured materials that integrate a continuous porous network across multiple length scales, from micro- (<2 nm) and meso- (2–50 nm) to macropores (>50 nm).[23] This nature gives them rigidity, stability, and a high density, and their porosity can be engineered for a wide range of applications.[24]

The transition from loose powders to monolithic architectures resolves several critical limitations: their cohesive, solid

form makes them easy to manipulate and integrate into devices, and they can be readily recovered for reuse.[25–27] A key advantage is their engineered hierarchical pore system,[24] which preserves the essential microporosity of the parent MOF (ensuring high surface area and selectivity) while incorporating meso- and macropores that drastically enhance mass transfer,[28] leading to excellent permeability and powerful separation capabilities suitable for applications like chromatographic columns.[29] Furthermore, monoliths exhibit significantly superior mechanical properties (*e.g.*, enhanced hardness and Young's modulus), providing critical resistance to attrition.[30] Finally, by eliminating interparticle voids, monolithic MOFs achieve a much higher bulk density, which often translates to superior volumetric performance (*e.g.*, gas storage per volume),[31–33] a key metric for practical applications where space is a constraint.

The rapid evolution of monolithic MOFs is marked by key developments in synthetic strategies and conceptual advances. Fig. 1 outlines this progress timeline, highlighting pioneering works that have demonstrated the potential of monolithic MOFs in creating hierarchically porous, mechanically robust, and application-ready structures. The field has progressed from early shaping methods to advanced manufacturing techniques like 3D printing and sophisticated templating approaches, leading to increasingly complex and high-performance monolithic structures for multifunctional applications.

This review focuses on these advancements in monolithic MOFs, highlighting their importance due to enhanced structural stability and handling compared to powdered MOFs. Key synthetic methods, particularly sol–gel processes and 3D printing, are discussed for their ability to create materials with customized geometries and functionalities. We further examine the characterisation techniques and industrial applications of monolithic MOFs in gas storage, catalytic processes, water treatment, sensing, and drug delivery. Moving beyond pure monolithic MOF systems, the review also explores the design and utility of multifunctional composites. Finally, the review presents current trends, ongoing challenges, and future directions in the field, with a specific emphasis on emerging applications and their potential to meet complex technological needs across various sectors.

Monolithic MOF synthesis methods

Sol–gel synthesis

Sol–gel synthesis is a versatile and widely used method for creating monolithic materials with defined shapes and porous, continuous structures. The process involves the transition from a liquid colloidal suspension (sol) into a solid, interconnected network (gel). This is typically initiated by distributing MOF precursors in a solvent to form a stable sol system.[34,35] A key indicator of the gelation process is a sharp increase in the solution's viscosity.

The formation of the monolith is governed by several critical stages: supersaturation, nucleation, growth, and Ostwald ripening. These stages collectively determine the final material's size, morphology, and properties. Supersaturation often occurs as precursors undergo hydrolysis and condensation reactions, forming small clusters. These clusters then develop into stable nuclei through homogeneous (throughout the solution) or heterogeneous (on surfaces) nucleation. Subsequent growth occurs as more material deposits onto these nuclei. Finally, during Ostwald ripening, larger, more stable particles grow at the expense of smaller ones, further densifying the structure.[30,36,37] As shown in Fig. 2, the high concentration reaction (HCR) method utilizes a base, triethylamine (NEt_3), to deprotonate the organic linker. This accelerates the formation of metal–organic clusters, creating a high density of nucleation sites. The resulting nanoparticles are sufficiently small to form a gel. Upon drying at room temperature, this gel network solidifies into a monolithic structure.[38]

This is also demonstrated in the work of Tian *et al.*,[30] who synthesized monolithic HKUST-1 ($_{mono}$HKUST-1) *via* a sol–gel process. Their work exemplifies how precise control over nucleation and growth conditions yields a densely packed, robust monolith. The synthesis began with the formation of approximately 51 nm primary nanoparticles. A subsequent mild drying process at room temperature promoted epitaxial growth at the particle interfaces, effectively using the MOF itself as a binder to create a continuous monolith without external additives or high-pressure compaction. In contrast, rapid drying at elevated temperatures resulted in a powdered material with interparticle voids and lower density.
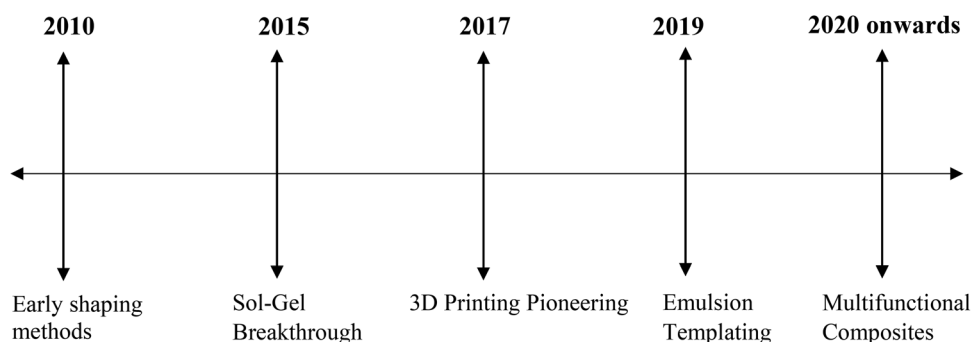

Fig. 1 Timeline of key developments in the synthesis and application of monolithic MOFs.
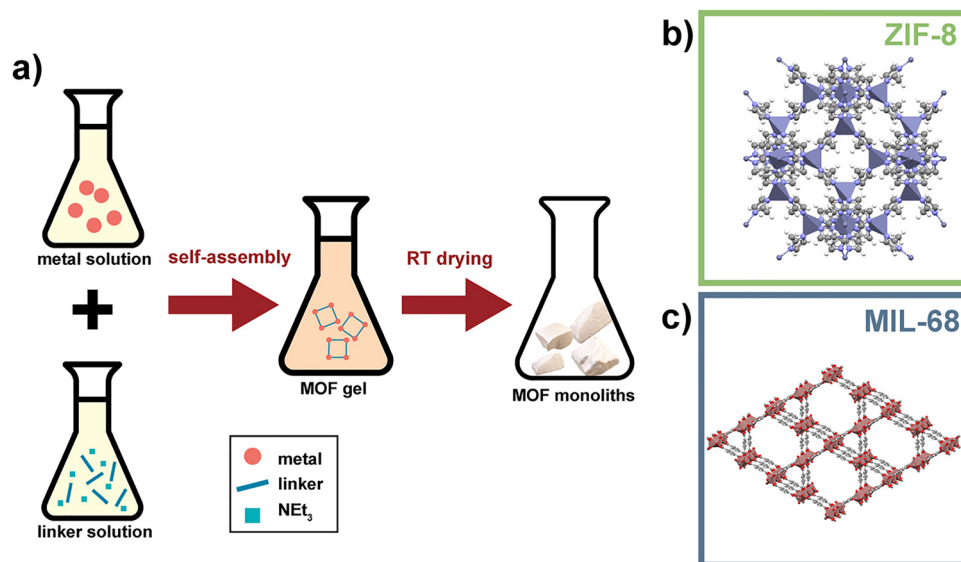
| 2010 | 2015 | 2017 | 2019 | 2020 onwards |
| Early shaping methods | Sol-Gel Breakthrough | 3D Printing Pioneering | Emulsion Templating | Multifunctional Composites |

Fig. 2 (a) An illustration of the sol–gel synthesis of monolith MOFs, (b) and (c) shows two monolith MOFs prepared using this method.[38] Note that in some instances after self-assembly centrifugation is applied prior to drying. Reproduced from ref. 38, with permission from the Royal Society of Chemistry.

The advantages of this approach are multifaceted. For instance, the achieved bulk density of $_{mono}$HKUST-1 (1.06 g cm^{-3}) significantly exceeded that of hand-packed powder and even the theoretical crystal density. This high density directly contributed to superior mechanical properties, with a hardness of 460 MPa and a Young's modulus of 9.3 GPa. Concurrently, the material exhibited a exceptional volumetric methane storage capacity of 259 cm^3 (STP) cm^{-3} at 65 bar and 298 K, nearly meeting the U.S. DOE target, without sacrificing adsorption kinetics.

He *et al.*[39] developed a sophisticated synthesis route to create monolithic MOF-801, this represented a significant advancement of the sol–gel method that combined sol–gel phase separation with a subsequent acid-heat treatment as illustrated in Fig. 3.

The process began by dissolving zirconyl chloride and fumaric acid in DMF before adding poly(propylene glycol) (PPG) as a phase separation inducer. This mixture was stirred at 60 °C to form a homogeneous emulsion, which was then transferred to a mold and heated at 80 °C for gelation and aging. During this step, phase separation occurred, where the DMF phase formed continuous MOF skeletons and the PPG phase created continuous macroporous channels, which were later washed away. A critical acid-heat post-treatment using formic acid was then employed to enhance the crystallinity and micropore volume. This innovative method yielded a robust, centimetre-scale monolith with a hierarchically porous structure, exhibiting a high porosity of 59.7%, a superior specific surface area of 977.8 m^2 g^{-1}, and a micropore volume of 0.234 cm^3 g^{-1}. Crucially, the monolith also possessed excellent mechanical strength, with a compressive Young's modulus of up to 61.3 MPa, enabling its practical use in scaled-up applications.

Beyond this example, the sol–gel process offers remarkable simplicity and cost-effectiveness while delivering products of high purity and versatility.[40,41] It allows for the creation of various product forms, including fibres and aerogels, and is particularly suited for producing materials with enhanced physical properties. The solution-phase nature of the process provides detailed control over the material's structure through adjustable variables during the early stages of its formation and network development.[42] However, challenges remain, including scalability, the risk of cracking during drying if not properly handled, and potential diffusion limitations due to the dense monolithic structure. Table 1 provides a summary of selected monolithic MOFs monoliths prepared *via* sol–gel synthesis, their applications, advantages, and disadvantages are also presented.

3D Printing

3D printing enables control over structure, geometry, and porosity, making it a valuable technique for creating tailored MOF materials.[47] The process allows for the fabrication of complex structures without expensive retooling and with less waste than traditional methods.[48] 3D-printed monoliths are usually created by synthesizing MOF particles or utilizing commercial MOF powders, which are then mixed into a paste that includes a binder, co-binder, solvents, and plasticizer. A general schematic of the 3D printing technique for deriving carboxylate MOFs is shown in Fig. 4, which outlines the key steps from ink formulation and printing to the necessary post-processing treatments required to achieve a functional monolith.

The following sections will explore the primary strategies employed in 3D printing MOF monoliths, including direct ink writing (DIW), seed-assisted *in situ* growth, matrix incorporation, selective laser sintering (SLS), digital light processing (DLP), and template-assisted methods.

Direct ink writing

Direct ink writing (DIW), a form of 3D printing, is a technique that offers high precision and versatility. It is a simple, flexible
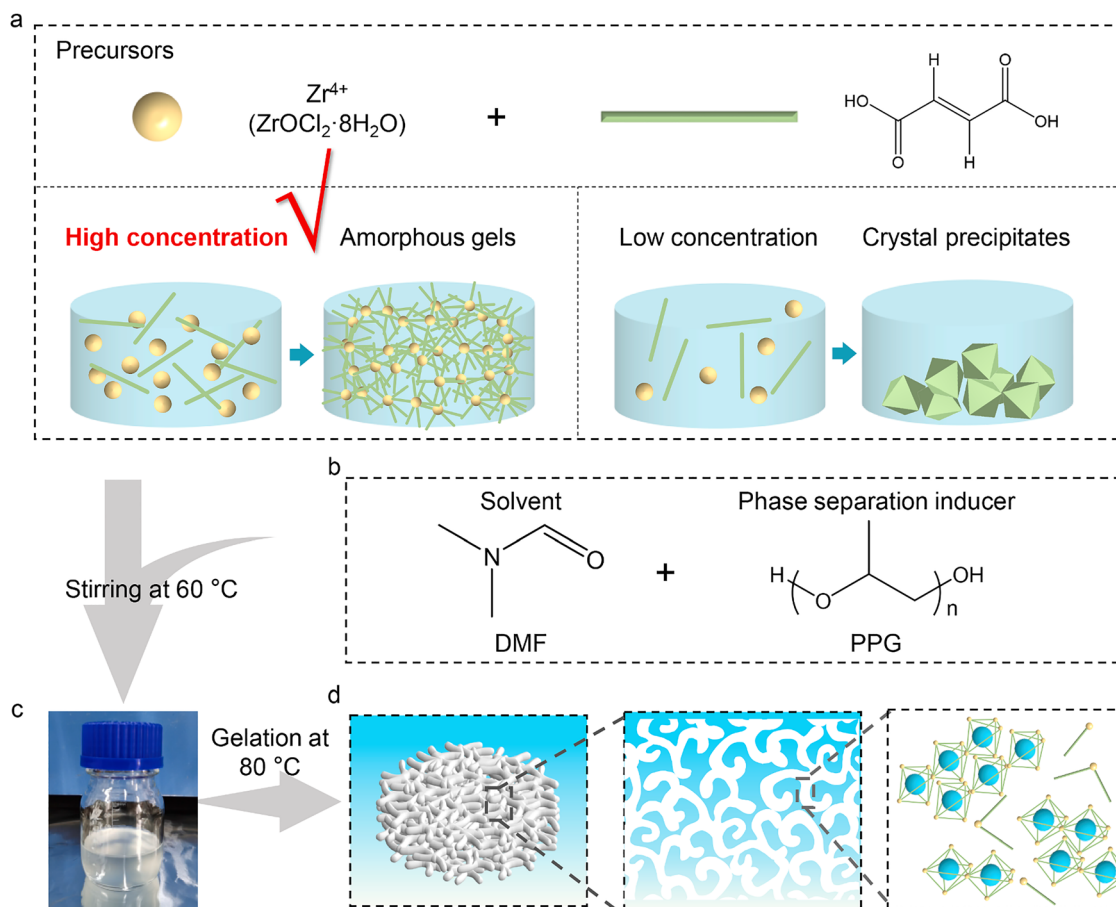
Fig. 3 Schematic of the synthesis of the macroporous MOGs. (a) ZrOCl$_2$·8H$_2$O and fumaric acid precursors in DMF; (b) introduction of PPG as a phase separation inducer; (c) formation of a homogeneous emulsion after stirring at 60 °C; (d) formation of macroporous MOGs after gelation at 80 °C accompanied by phase separation.[39] Reproduced from ref. 39. Copyright (2023) Elsevier B. V.

and cheap technique whereby a paste or ink is ejected layer-by-layer through a fine nozzle.[50] A critical requirement of the process in that the active material must be made into an ink with ideal viscosity and must also be able to flow through a nozzle continuously and then solidify quickly to preserve its shape.[48] Once formulated, the prepared ink is typically rolled at room temperature for 1 to 2 days during the binding process to ensure proper interaction between the various components and achieve the desired results. During the densification step, the prepared ink is slowly heated to a temperature range of 40–60 °C for several hours to ensure that all the solvent is evaporated, resulting in a paste with the desired rheological properties for printing.[51,52]

The feasibility of fabricating ZIF-8 monoliths *via* DIW was demonstrated by Verougstraete *et al.*[53] providing a clear example of the 3D printing fibre deposition method, as shown in Fig. 5. ZIF-8 powder (66.7 wt%), bentonite (16.7 wt%) and methylcellulose (16.7 wt%) were mixed with water to form a printable paste. This was followed by activation under Argon at 450 °C, to remove the methylcellulose binder, yielding a final composition of 80 wt% ZIF-8 and 20 wt% bentonite.

Building upon this foundational work, Claessens *et al.*[54] subsequently employed a similar DIW approach to fabricate

ZIF-8 monoliths for biobutanol recovery. Their study provided a detailed analysis of how printing parameters dictate monolith architecture and, consequently, separation efficiency. Using a paste of ZIF-8, bentonite, and methylcellulose, they produced monoliths with 600 μm and 250 μm nozzles. After thermal treatment, the monoliths exhibited a dark-brown colour due to binder degradation. As shown in Fig. 6, SEM analysis revealed the 600 μm monolith had a fibre thickness of 540 μm and open side channels (260 μm), while the 250 μm monolith had blocked side channels (<60 μm). This structural difference, clearly visible in the figure, caused flow maldistribution in the smaller monolith, leading to broader breakthrough profiles, whereas the larger monolith demonstrated superior performance with high butanol capacity (0.2 g g^{-1}) and selectivity.

Beyond ZIF-8, the DIW technique has been successfully applied to other MOFs. For instance, Lim *et al.*[48] successfully fabricated a self-standing HKUST-1 monolith using the DIW strategy as illustrated in Fig. 7. Their key innovation was formulating a printable colloidal gel from only HKUST-1 nanoparticles and ethanol, entirely omitting the need for a binder, which demonstrated excellent printability and rheological properties. The figure shows photos of the HKUST-1 gel and various 3D-printed structures, SEM images of the filament and

Table 1 Summary of selected monolith MOF prepared using the sol–gel, including their application, advantages and disadvantages

Monolith MOF examples	Application	Advantages	Disadvantages
ZIF-8 and ZIF-67	Toluene vapour adsorption[43]	– Simple, ambient temperature synthesis – High surface area (e.g., 1450–1732 m^2 g^{-1} for ZIF-8) and hierarchical porosity[43–45] – Narrow particle size distribution (e.g., 55 nm).[44] – High vapour capacity[45]	– Can require longer aging time (e.g., 96–120 hours)[44] – Potential pore blockage.
HKUST-1	– Hydrogen storage.[31] Methane uptake[32]	– Enhanced mechanical stability (hardness: of 460 MPa, young modulus: 3 GPa).[32] – High volumetric storage capacities[31,32] (e.g., 259 cm^3 (STP) cm^{-3} for CH$_4$ at 65 bar; 10.1 g L^{-1} for H$_2$ at 100 bar) – Improved handling.	– Scale up challenges. – Susceptible to cracking during drying if not properly handled.
MIL-101	CO$_2$ adsorption, methylene dye removal from water[46]	– Easier handling and integration into systems – High thermal stability (stable up to 300 °C) – Reduces pressure drop in fixed-bed reactors, facilitating scale up.	– Requires multi step solvothermal synthesis with tight control of solvent composition and temperature, icreasing process cost. – Limited adaptability for post-synthetic functionalisation due to rigid chromium terephthalate framework. – Susceptible to cracking during drying or activation because of capillary stress in the dense monolithic matrix. – Dense framework may impede desorption kinetics, making regeneration slower and less energy-efficient after multiple adsorption cycles.
UiO-66[33]	Gas storage[33]	– Cohesive solid form simplifies packaging and reactor loading. – High bulk density with preserved porosity and surface area (BET ~ 1000–1200 m^2 g^{-1})	– Scaling up limited by the need for uniform gelation and solvent exchange, which can cause structural inhomogeneity in larger batches. – Synthesis requires careful control of washing solvents and drying conditions to avoid framework collapse and residual solvent contamination. – Susceptible to cracking during solvent removal due to capillary stress in dense monolithic matrices.
MOF 801	Atmospheric water harvesting.[39]	– Robust hierarchical porosity (BET: 977.8 m^2 g^{-1}, micropore volume: 0.234 cm^3 g^{-1}) – High water uptake from air under low humidity (≥ 0.2 g·g^{-1} at 30% RH) – Fabrication of centimetre scale monolith demonstrated. – High structural stability under cycling – Suitable for passive water harvesting applications.	– Synthesis requires multi-step sol–gel and phase-separation control with post-synthetic acid treatment to enhance crystallinity, increasing process complexity. – Relatively higher material cost due to use of zirconium precursors (e.g., ZrOCl$_2$·8H$_2$0) and formic acid treatment reagents. – Performance consistency depends on optimising solvent ratio, gelation temperature (68–80 °C), and aging time to achieve uniform pore structure.

nanoparticles, and rheological data proving the ink's shear-thinning behaviour and solid-like gel properties. Crucially, the process preserved the MOF's original pore volume, resulting in a monolith with a high specific surface area (1134 m^2 g^{-1}) and significant methane uptake of 64 cm^3 (STP) cm^{-3} at 65 bar.
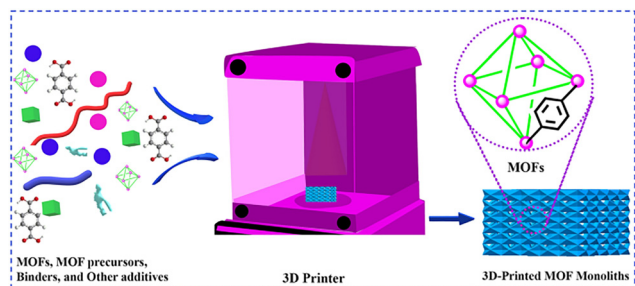
Fig. 4 3D printing pathway of carboxylate derived MOFs.[49] Reproduced from ref. 49, with permission from Springer.

Bouzga et al.[55] developed 3D-printed UTSA-16 monoliths using a non-aqueous ink formulation. The ink, tailored with boehmite and hydroxypropyl cellulose as rheology modifiers, exhibited optimal printability and enhanced the dispersion of UTSA-16 nanoparticles within the monolithic structure. The study demonstrated that the resulting 3D-printed monoliths function as efficient CO$_2$ adsorbents, exhibiting high uptake capacity and notable structural stability under humid conditions. This stability was attributed to the hydrophobic nature of the hydroxypropyl cellulose component, which effectively shields the MOF centres from water molecules.

In a related study, Lawson et al.[56] developed 3D-printed monoliths from amine-functionalized MIL-101 for CO$_2$ capture in enclosed environments. They employed a DIW technique using two strategies: pre-impregnation (where the MIL-101 powder was first impregnated with polyethylenimine (PEI) or polyethylenimine (TEPA) and then printed) and post-impregnation (where the monolith was printed first and then functionalized). The study
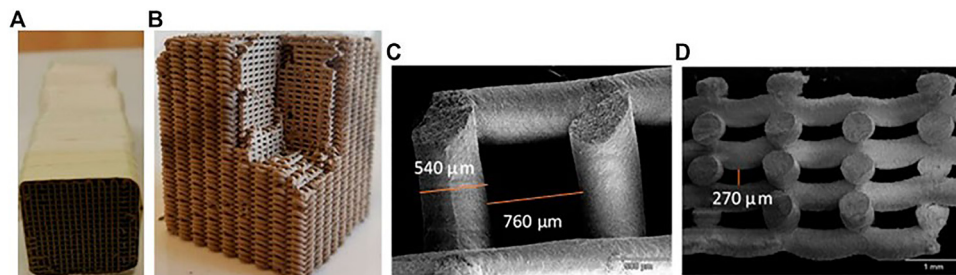
Fig. 5 3D printed ZIF-8 monolith. (A) Monolith used for breakthrough experiments. Several pieces were stacked and held together with Teflon tape. (B) Side view showing the presence of channels in the radial direction. (C) Scanning electron microscopy-picture of the top-view of the monolith. (D) Scanning electron microscopy-picture of side view visualizing the radial gaps present in the structure.[53] Reproduced with permission from ref. 53, under the terms of the Creative Commons Attribution License (CC BY).
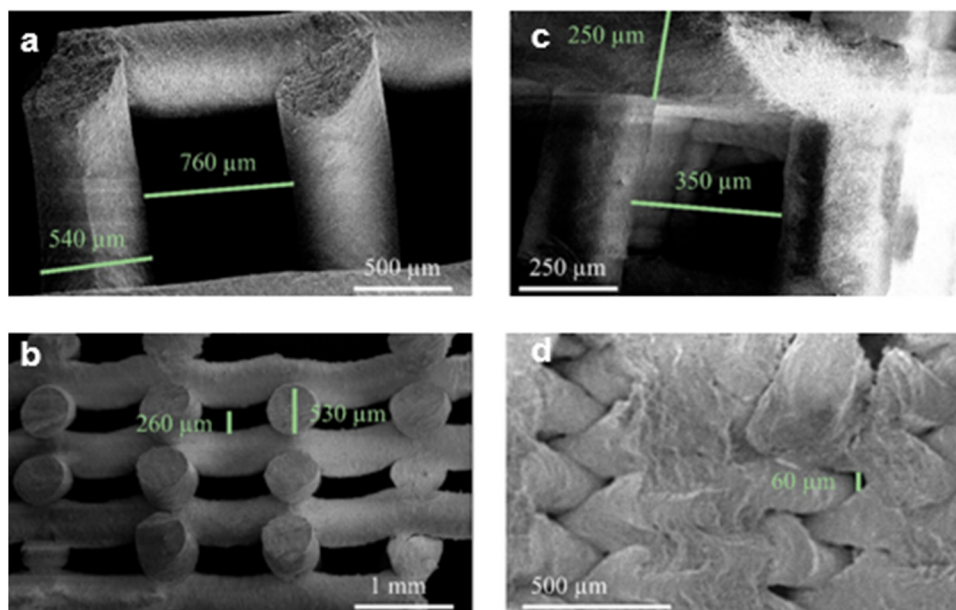

Fig. 6 SEM images of 3D printed 600 μm monolith (a) and (b) and 250 μm monolith (c) and (d)[54] Reprinted with permission from ref. 54. Copyright (2020), American Chemical Society.

concluded that the pre-impregnation approach was superior, yielding higher amine loadings and CO_2 capacities (1.6 mmol g^{-1} for TEPA and 1.4 mmol g^{-1} for PEI at 3000 ppm) due to successful amine grafting within the pores during paste densification. However, despite their high capacity, the adsorption kinetics were slow, leading to the conclusion that future work must focus on tuning the monolith dimensions to optimize CO_2 diffusion.

Monolith MOFs synthesised via 3D technology have the following advantages: (1) interconnected channels are formed which facilitate heat and mass transfer during operation conditions, (2) MOFs can be used in large-scale practical applications, (3) 3D printing enables the incorporation of different materials within a single structure, allowing for multifunctional applications, (4) allows for the creation of complex and customized shapes that meet specific application requirements[49] and finally (5) the creation of complex structural networks while generating minimum waste.[57]

The main challenge with 3D-printed MOF monoliths is that they typically have lower specific surface areas and pore volumes than their powdered equivalents. This problem occurs due to several factors like, the need for high temperatures and pressure during the printing process which makes the MOFs deform, the presence of additives in the paste can result in several issues, including pore blockage, surface coverage, and the build-up of dead mass.[58]

Template-assisted synthesis of monolithic MOFs

The inherent microporosity of MOFs, while ideal for molecularly selective applications, imposes significant mass transfer limitations in processes requiring high flow rates or involving viscous media. To overcome this, template-assisted synthesis has emerged as a powerful strategy to engineer hierarchical pore systems within scalable, monolithic structures.[34] By using dynamic soft templates, this approach creates well-defined
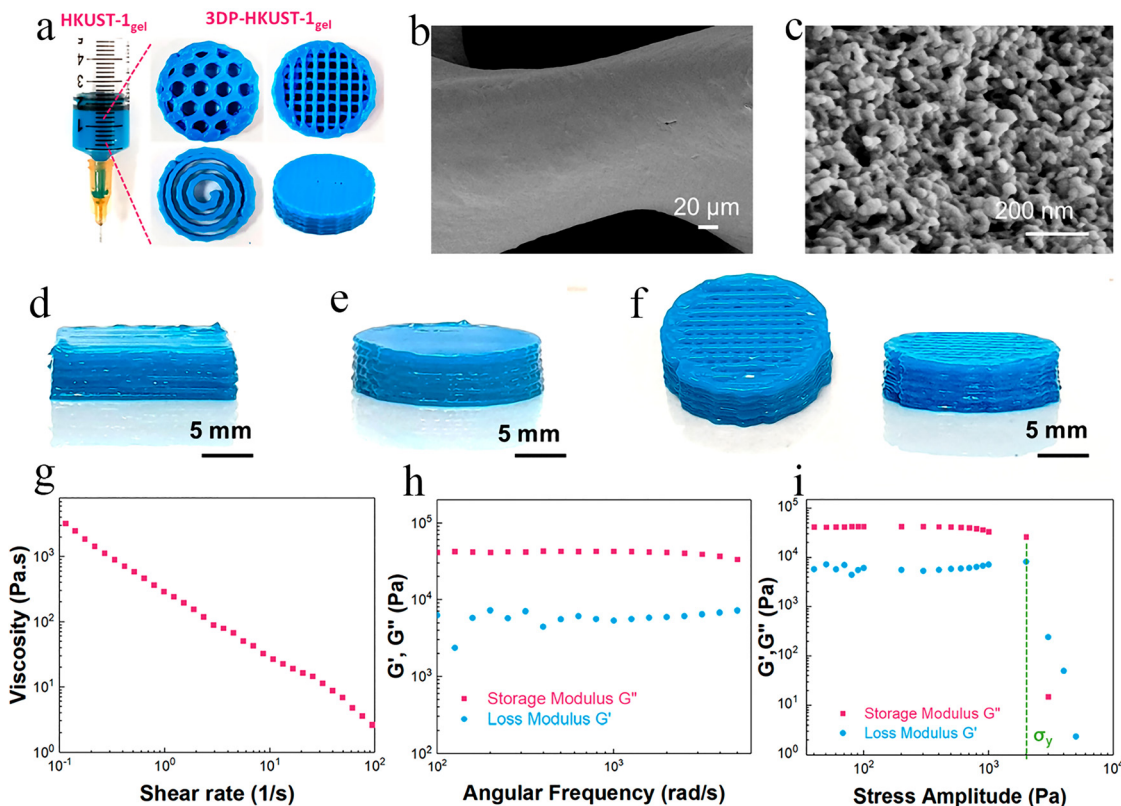
Fig. 7 Characterization of the HKUST-1 gel and 3D-printed monoliths, including (a) photos of the gel and printed structures, (b) and (c) SEM images of a filament and its nanoparticles, (d)–(f) photos of monoliths with different geometries, and (g)–(i) rheological profiles of the ink.[48] Reprinted with permission from ref. 48. Copyright (2020), ResearchGate GmbH.

macropores that facilitate convective flow, which are seamlessly integrated with the intrinsic micro- and mesopores of the MOF to combine efficient mass transport with high surface area and selectivity. This versatile pathway enables the rational design of MOF monoliths with enhanced functionality for demanding applications in catalysis, adsorption, and separation.

A foundational approach to creating hierarchical MOFs is the bottom-up, direct templating of mesoporosity during crystal growth. Do *et al.*[59] pioneered this concept by using amphiphilic block copolymers as structure-directing agents to synthesize mesostructured MIL-53(Al), designated L-MOF. Instead of using a solid scaffold, they employed soft templates in the form of block copolymers (Pluronic P123 and F127). Under solvothermal conditions, these surfactants self-assemble into micelles. The MOF precursors (for MIL-53(Al)) then crystallize around these micellar templates. Subsequent removal of the polymer leaves behind a material whose walls are made of microporous MIL-53(Al) crystals. The successful creation of intrinsic mesoporosity was confirmed by N_2 physisorption (Fig. 8). The Type IV isotherm with distinct hysteresis steps (Fig. 8A) provided definitive evidence of mesopores, while the corresponding pore size distribution (Fig. 8B) revealed a trimodal system comprising the native micropores alongside two mesopore networks: a wormhole-like system ($\sim$4 nm) and larger channels (5.4–7.6 nm) templated by the block copolymers. This exemplifies the direct synthesis of a MOF with hierarchical porosity, ideal for catalysis involving bulky molecules.

While the approach by Do *et al.*[59] exemplifies the templating of internal porosity within a MOF crystal, the challenge of assembling MOFs into macroscopic, handleable objects still remains. To advance the concept of soft templating to a larger scale, Sun *et al.*[20] demonstrated how a dynamic emulsion template could be used not only to structure porosity but to shape an entire monolithic device. Their strategy utilized a Pickering high internal phase emulsion (HIPE), where ZIF-8 nanoparticles acted as the sole stabilizer for oil droplets dispersed in a water phase containing molecular MOF precursors. As illustrated in Scheme 1, the process begins with ZIF-8 nanoparticles stabilizing droplets of cyclohexane (the internal phase) within an aqueous solution containing ZIF-8 precursors. A key innovation was the subsequent *in situ* growth of additional ZIF-8 within the continuous phase, which acts as a natural "cement" to bond the nanoparticle stabilizers together without any foreign polymeric binder.

After synthesis, the emulsion is freeze-dried to remove the liquid oil template, leaving behind a solid, monolithic structure. The resulting morphology, revealed in the SEM images of Fig. 9, shows a highly interconnected macroporous network that is a direct inverse replica of the original emulsion droplets, while the walls consist of microporous ZIF-8. This unique structure endowed the monolith with exceptional performance in dual applications: it served as an extremely efficient flow-through catalyst, achieving complete conversion in a Knoevenagel
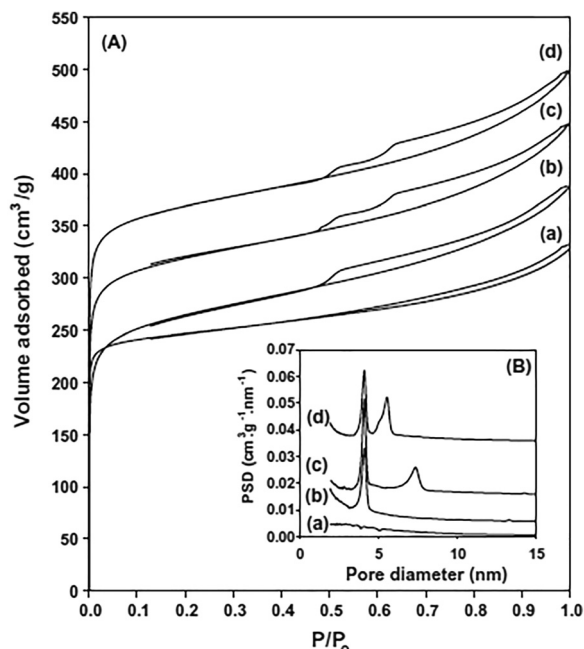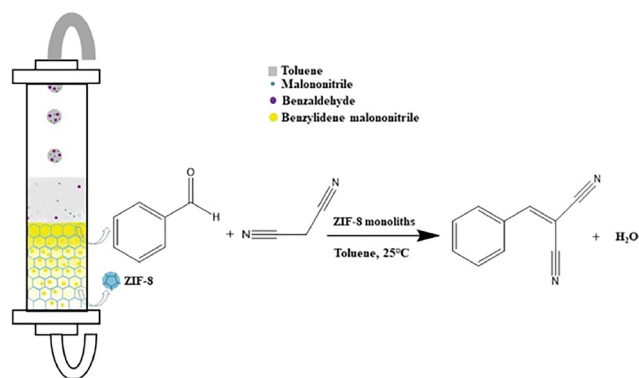
Fig. 8 Pore structure analysis of mesostructured MOFs. Mesopore structures analysis of mesostructured MOFs: (A) N₂ adsorption–desorption isotherms at 77 K for (a) MIL-53(Al), (b) L-MOF(0), (c) L-MOF(1), and (d) L-MOF(2); (B) pore size distribution for (a) MIL-53(Al), (b) L-MOF(0), (c) L-MOF(1), and (d) L-MOF(2).[59]

Scheme 1 Knoevenagel reaction of benzaldehyde with malononitrile in toluene using the 3D ZIF-8 monolith as a flowthrough catalyst.[20] Reprinted with permission from ref. 20 Copyright (2021), American Chemical Society.

reaction within 130 seconds, and as a rapid oil absorbent, reaching absorption equilibrium for hydrocarbons in less than 5 seconds due to its open, permeable architecture.

The synergy between these two approaches illustrates the power and versatility of dynamic soft templating for structuring MOFs across multiple length scales. The work of Do et al.[59] illustrates an intrinsic strategy, templating mesopores within the MOF crystal to enhance molecular diffusion. To complement this work, Sun et al.[20] demonstrate an extrinsic assembly strategy, templating macropores between crystals to create a functional monolith. Both methods effectively decouple molecular selectivity from mass transport, providing valuable blueprints for designing hierarchical MOF architectures tailored to specific applications.

Seed assisted *in situ* growth

The seed-assisted *in situ* growth strategy is analogous to the Direct Ink Writing (DIW) technique in its initial stage, as it also begins with the formulation of a printable ink containing solvents, inert binders, and plasticizers. However, a key distinction is that the structured monoliths produced do not require a large amount of the active MOF material to be functional. Instead, the 3D-printed substrate itself acts as a nucleation site, containing metal oxides or MOF precursors that enable the coordination and growth of an active MOF layer after a primary densifying step.[49]

This strategy has been effectively applied to the interfacial synthesis of MOF-74 onto 3D-printed monoliths, as demonstrated by Lawson et al.[60] The process began by printing MOF-74 nanoparticles into a dope of a Torlon polymer solution. Although the crystalline structure of these initial MOF particles was degraded during the subsequent solvent extraction process, they successfully served as growth seeds. When these monoliths were exposed to MOF precursors in a secondary solvothermal synthesis step, new MOF-74 crystals grew from the seeds, resulting in the fabrication of monoliths with a high MOF loading of 40 wt%.

As illustrated in Fig. 10, this two-step approach, direct printing of seeds followed by secondary growth enables the formation of a dense, continuous MOF film on the polymer scaffold. This approach effectively created chemically active monoliths with significantly enhanced CO_2 adsorption capacity, increasing from 0.5 mmol g^{-1} for the directly printed monolith to 2.5 mmol g^{-1} after secondary growth and improved mass transfer kinetics due to the formation of a thin, continuous MOF film on the surface. However, it was noted to be relatively time-consuming and produced extra waste, making it less suitable for large-scale production.

Matrix incorporation

The matrix incorporation strategy involves dispersing pre-synthesized, chemically active MOF particles as a filler within an inert polymeric stabilizer or binder. This method is primarily used to overcome the rheological limitations of pure MOF inks, enhance the mechanical properties of the final structure, and modulate its hierarchical porosity.

A foundational example of this approach is the work by Kreider et al.[61] They were among the first to employ this strategy to fabricate 3D-printed MOF monoliths by creating composites of acrylonitrile butadiene styrene (ABS) and MOF-5. The process involved the solvent casting of an ABS mixture containing 10 wt% MOF-5 particles to produce a liquid-phase dope with suitable printability. This ink was then used to print structures with various geometries as illustrated in Fig. 11.

However, a significant limitation was identified, the MOF content could not exceed 10 wt% without the ink exhibiting shear-thickening behaviour, rendering it unprintable. Furthermore, the high temperature and pressure involved in the
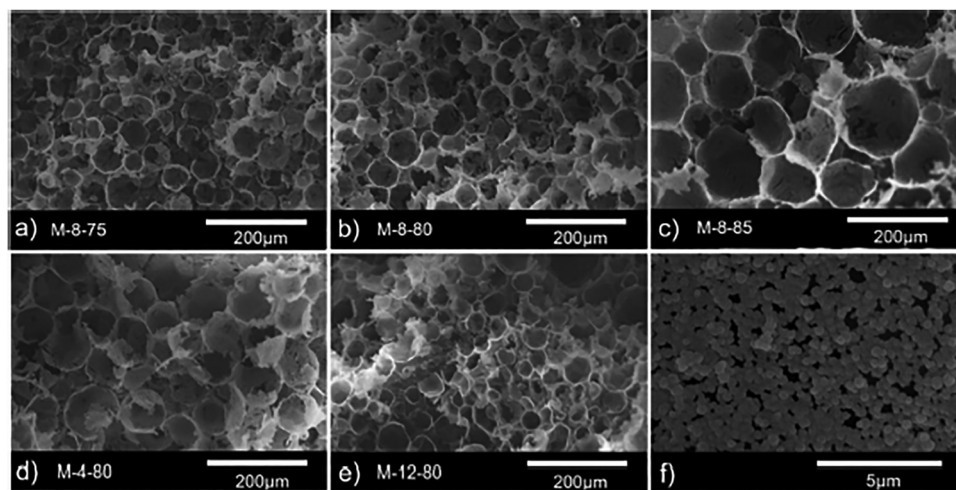
Fig. 9 SEM images of 3D ZIF-8 monoliths: (a) M-8-75, (b) M-8-80, (c) M-8-85, (d) M-4-80, (e) M-12-80, and (f) surface of the void wall of M-8-80.[20] Reprinted with permission from ref. 20 Copyright (2021), American Chemical Society.
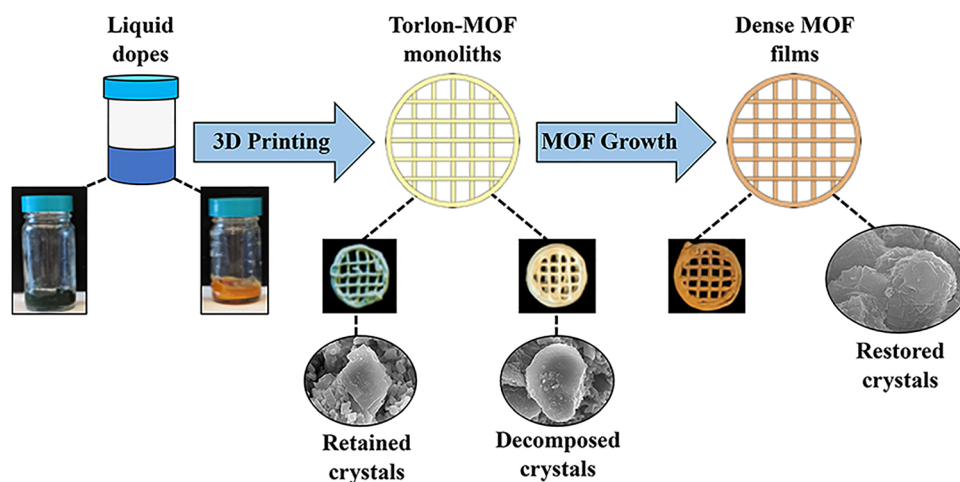

Fig. 10 Schematic representation of the two-step strategy for fabricating polymer–MOF monoliths: (Step 1) direct ink writing of a polymer dope containing MOF particles, which act as seeds, and (Step 2) secondary growth *via* solvothermal synthesis to form a dense, continuous MOF film on the monolithic scaffold.[60] Reprinted with permission from ref. 60 Copyright (2019), American Chemical Society.

thermoplastic processing, combined with the presence of the polymer matrix, typically lead to a reduction in the specific surface area and accessible pore volume compared to the pure MOF powder. Despite this partial degradation, the study confirmed that the MOF-5 particles retained their functionality for applications like hydrogen storage.

Selective laser sintering (SLS)

Selective laser sintering (SLS) strategy involves using a program-controlled laser beam to sinter powdered materials, such as thermoplastic polymers, layer-by-layer into a 3D solid structure.[49] A key advantage of this method is that the operating conditions can be finely tuned to only partially melt the polymer powders, creating a porous, solid monolith with micro-voids between the sintered particles. When MOF nanoparticles are mixed with the polymer powder, these micro-voids form open channels that

improve the exposure of the MOF fillers to the external environment, allowing fluids to pass through the monolith. A series of polymer-based MOF mixed matrix films (MMFs) have been prepared by Li *et al.*[62] utilizing thermoplastic polyamide 12 (PA12) powder as the printable polymer matrix and five kinds of powdered MOFs, MOF-801, ZIF-67, ZIF-8, HKUST-1, and NH_2-MIL-101(Al) as the porous fillers (Fig. 12a). In their study, single-layer MMFs with a lacing structure were printed to evaluate their mechanical properties, BET surface area, and performance. The resulting films were flexible, free-standing, and could be shaped or folded, indicating excellent mechanical stability. The NH_2-MIL-101(Al)-PA12 MMF, with the smallest pore size, was identified as an efficient adsorbent for methylene blue (MB) dye removal, showing high adsorption capacity and kinetics. The reusability was demonstrated through cyclic adsorption/desorption tests, where the adsorbent maintained an 83% removal efficiency after
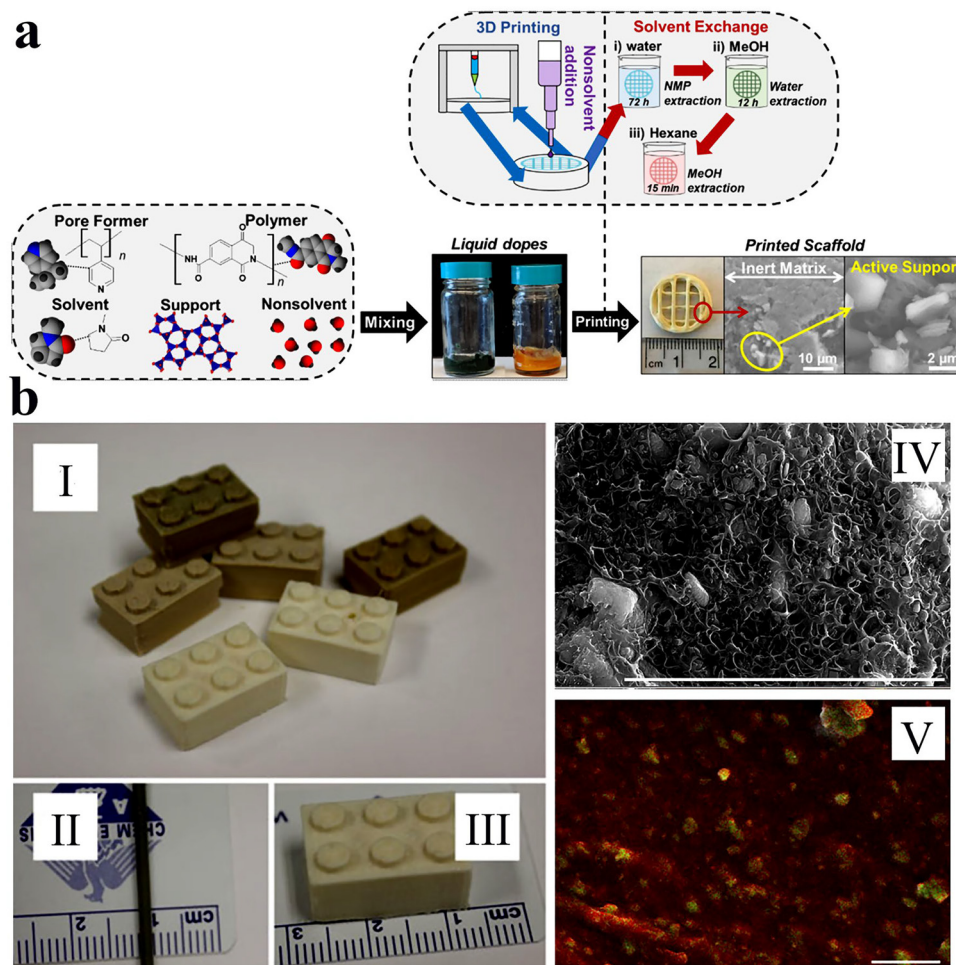
Fig. 11 (a) Schematic representation for the 3D-printed monolith MOF monolith *via* the matrix incorporation strategy. (b) Photoimages of the ABS-MOF-5 filament and the 3D-printed structures: (I) 3D-printed block, (II) filament utilized in the printing process, (III) 3D-printed structure shows scale with corresponding (IV) SEM and (V) zinc maps.[61] Reprinted with permission from ref. 61. Copyright (2021), American Chemical Society.

five consecutive cycles (Fig. 12b), highlighting its durability and potential for practical water treatment applications.

Digital light processing

Digital light processing (DLP) approach generally involves localized photopolymerization of monomers or oligomers with appropriate photoinitiators. This technique uses photoinduced cross-linking to solidify liquid resins on locally illuminated regions, replicating a 3D structure sequentially in a layer-by-layer manner. This enables rapid prototyping and provides precise control over layer thickness and resolution, which is crucial for fabricating functional MOF-based devices.[63]

This method was used by Halevi *et al.*[64] to fabricate flexible and complex 3D monoliths containing HKUST-1 nanoparticles, as shown in Fig. 13. The images demonstrate the printing process, the intricate designs achieved, and the material's flexibility. Crucially, the graph reveals that while the adsorption capacity of the 3D-printed monolith matched that of pure HKUST-1 powder initially, the printed structure proved superior over time by preventing the dye release caused by the hydrolysis and decomposition that degraded the pure powder.

The diverse 3D printing strategies for fabricating MOF monoliths offer distinct advantages and face specific limitations, making them suitable for different applications. Table 2 provides a comparative overview of the primary techniques, summarizing their key benefits, challenges, and typical use cases to guide the selection of an appropriate method.

Characterization of monolith based MOFS

Several techniques have been employed to understand the structural, thermal, and functional properties of monolithic-based MOFs. These include, but are not limited to, powder X-ray diffraction (PXRD) for assessing crystallinity and phase purity, Fourier-transform infrared spectroscopy (FTIR) for analyzing chemical bonding and functional groups, thermogravimetric analysis (TGA) for evaluating thermal stability, scanning electron and Transmission electron microscopy (SEM and TEM) for morphological analyses, and gas sorption measurements for determining porosity and surface area. A good
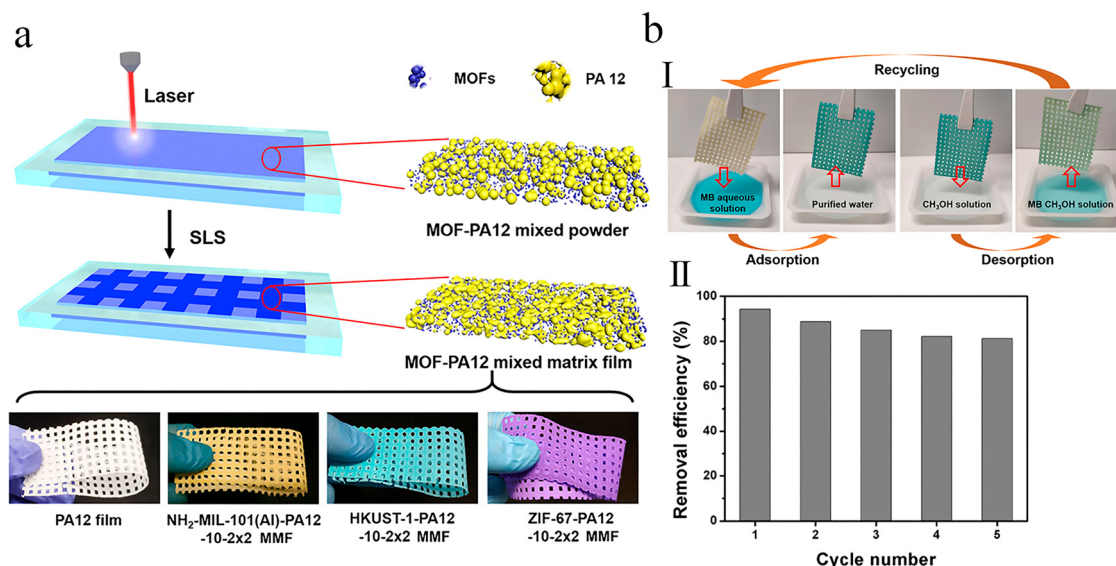
Fig. 12 Fabrication and performance of 3D-printed MOF-PA12 mixed matrix films (MMFs): (a) schematic of the manufacturing process and photographs of PA12 and MOF-PA12 MMFs with various MOF fillers; (b) recyclability assessment of the NH_2-MIL-101(Al)-PA12 MMF, including (I) visual documentation of the adsorption−desorption cycles and (II) quantitative methylene blue (MB) removal efficiency over five consecutive cycles.[62] Reproduced from ref. 62, under the terms of Creative Commons (CC BY) licence Copyright 2019, American Chemical Society.
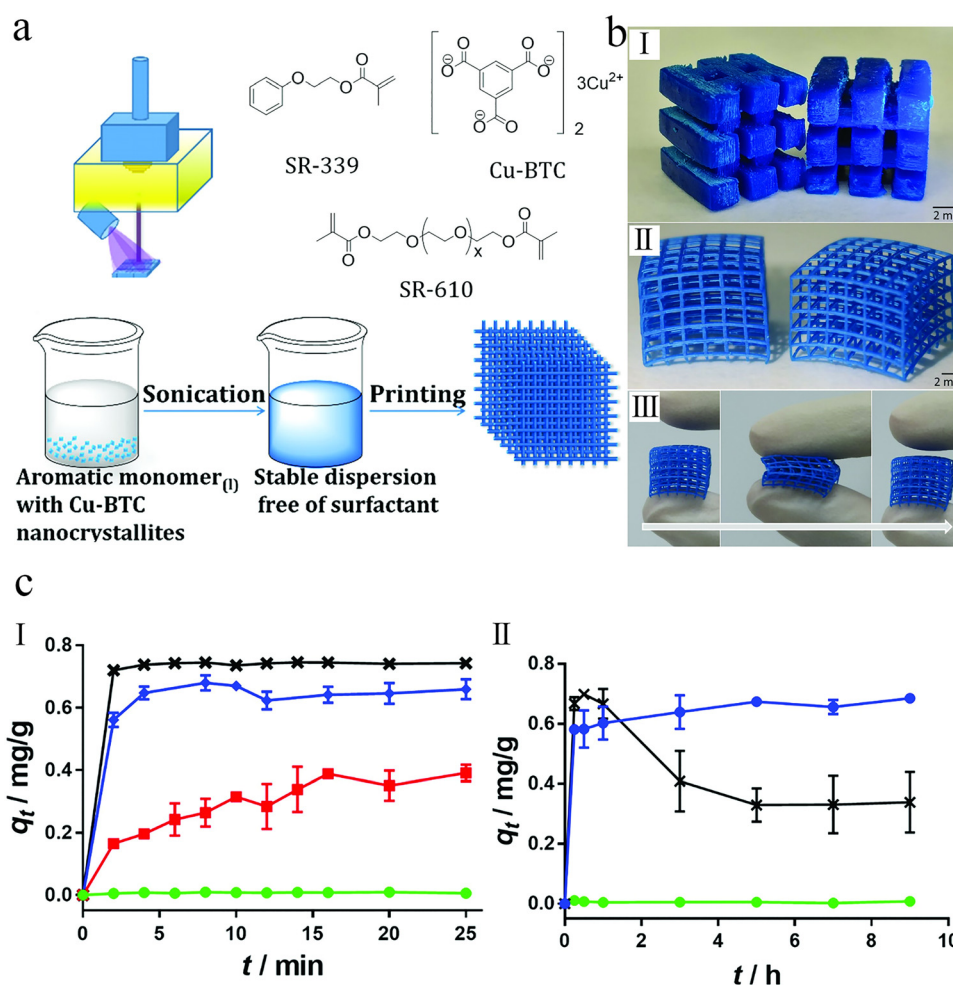

Fig. 13 Digital light processing (DLP) of HKUST-1 composites: (a) schematic of the DLP strategy and material chemistries, (b) photographs of the resulting flexible 3D-printed monoliths, and (c) evaluation of their methylene blue (MB) adsorption performance over time.[64] Reproduced from ref. 64, under the terms of Creative Commons (CC BY) licence.

understanding of monolith MOF properties will allow for their rational design and optimization in specific applications such as catalysis, gas storage, sensing, separation, and drug delivery. This knowledge also provides insights into their structural integrity, chemical resilience, and performance under various operational conditions.

Powder X-ray diffraction (PXRD)

PXRD is a critical tool for identifying the crystallinity and structural integrity of MOFs.[47,69] PXRD gives detail on phase purity of materials, which is necessary to guarantee the mechanical stability and reliable use of monolithic MOFs. The PXRD profiles of monoliths and powders can exhibit distinct variations due to differences in crystal orientation and sample morphology. Powder samples consist of many small crystallites oriented randomly. This ensures that all crystal planes are statistically represented during diffraction, and this usually produces sharp, intense and well-defined peaks. These peaks are also easily compared with simulated or database patterns. In monolithic samples (especially dense, compacted, or shaped samples), however, the crystals may be aligned in specific directions, leading to non-random orientation. This results in intensity variations, some peaks may be enhanced, suppressed, broadened or even missing. This makes it best for checking bulk crystallinity and phase retention after monolith fabrication, but not always quantitative for crystallographic detail.

Furthermore, PXRD analysis is able to unmask a lot about the material for example, the degree of crystallinity within the monolith is indicated by the PXRD pattern's strong, distinct diffraction peaks.[70] The broadening of these peaks in some monoliths, may indicate the existence of an amorphous material, which could affect its mechanical stability and functionality. However, in monolithic UiO-66, significant peak broadening has been identified and this was attributed to the nanocrystallites causing nano-convergence of diffraction peaks.[33,51] Additionally, PXRD is also used to identify any phase transitions or structural alterations[70] that may occur in the monolithic MOF due to external factors, such as mechanical stress, temperature, or exposure to different environments.[72] The preservation of the monolithic MOF's original crystalline structure is essential for its long-term stability and dependable operation, and researchers may verify this by tracking the PXRD patterns over time or under various circumstances.

Over the years there has been a marked advancement in the development of new and more advanced techniques which has made material analysis easy, notable examples include High-resolution PXRD and Synchrotron radiation PXRD.[73,74] These techniques provide detailed information on the crystalline structure, including unit cell parameters, atomic positions, and the presence of minor impurities or defects.[75] By utilizing PXRD as a reliable and comprehensive characterization tool, researchers can confidently validate the crystallinity and structural integrity of monolithic MOFs,[76–79] ensuring that these materials meet the stringent requirements for their intended applications,[76] such as gas storage,[80] catalysis or separation processes.[81] The insights gained from PXRD analysis, coupled

with other characterization methods, play a crucial role in the development and optimization of high-performance monolithic MOF materials.[28,82]

However, it must be noted that while PXRD provides valuable information on the crystallinity and phase purity of MOFs, it does not always distinguish if a MOF is powdered or monolithic. Takahashi et al.[83] used powder X-ray diffraction (XRD) characterisation to verify the crystallinity of HKUST-1 structures. The resulting pattern, presented in Fig. 14, indicated the presence of the target MOF but was dominated by crystalline material of $Cu_2(OH)_3NO_3$ and $Cu(NH_3)_4(NO_3)_4$ phases.

Scanning electron microscopy (SEM) analysis

Scanning electron microscopy is a fundamental tool for comprehensive characterisation of monolithic MOFs, offering unprecedented insights into their structural, morphological, and compositional characteristics.[84,85] The measurements allow for the analysis of both pore structure and overall morphology.[86,87] Due to its high-resolution imaging capabilities, SEM enables researchers to meticulously examine the intricate microstructure of MOFs, revealing critical details about crystal morphology, surface topology, and potential structural defects that might significantly impact material performance.[85,88,89]

The profound impact of synthesis conditions on morphology is eloquently illustrated in the work of Hunter-Sellars et al., as shown in Fig. 15.[41] The well-defined, faceted crystals of conventional ZIF-8 and ZIF-67 powders provide a stark contrast to the structures formed by monolithic synthesis. The transition to a monolithic form via a ligand-assisted sol–gel method using n-butylamine (NB) as a modulator result in a dramatic morphological change. For instance, ZIF-67 (NB) consists of densely packed, much smaller nanoparticles that appear agglomerated with what is assumed to be amorphous material. This evolution is even more pronounced when a mixture of modulators (n-butylamine and 1-methylimidazole, ML) is used. The resulting ZIF-8 (ML) and ZIF-67 (ML) monoliths lack any distinct or well-defined particles altogether, an observation that aligns with PXRD data indicating a severe loss of crystallinity. This suppression of crystal growth is attributed to monodentate linkages formed between metal ions and the modulating ligands, which inhibit the formation of long-range crystalline order.

Beyond revealing this microstructural evolution, SEM, when coupled with energy-dispersive X-ray spectroscopy (EDS), allows for the mapping of elemental composition across the monolith's surface. This is crucial for confirming the homogeneous distribution of metal nodes and organic linkers, ensuring the chemical integrity of the monolith and the absence of phase segregation.

Transmission electron microscopy (TEM)

TEM is a critical characterization tool in the study of MOFs, offering nanoscale insights that complement other techniques such as PXRD, BET surface area analysis, and SEM. In monolithic MOFs, where the morphology, internal nanoparticle arrangement, and nanoparticle interactions are key to performance, TEM allows researchers to directly observe the size,

Table 2 3Dprinting methods for monolithic MOFs including their advantages, disadvantages and applications

3D printing strategies	Advantages	Disadvantages	Application	Examples
Direct ink writing	– Simple and flexible process. – Operating at room temperature.[48]	– Clogging of printing nozzle. – Potential deformation of MOFs due to high pressure during processing.[58]	Methane uptake[48] – CO_2/CH_4, CO_2/N_2 and CO_2/H_2 separation[54,65,66]	HKUST-1[48] UTSA-16(Co)[54,55]
	– Compatible with diverse range of MOFs (e.g., HKUST, ZIF-8, UiO-66, MIL-101)	– Laborious, multi-step ink preparation (e.g., 1 to 2 days of rolling and densification).[51,52]	CO_2, N_2, CH_4 and H_2O uptake[55]	MOF-74(Ni)[65]
	– Moderate to high production rate (faster than seed-assisted, slower than LDP).	– Can be brittle, depending on binder.	– Butanol recovery[54]	ZIF-8[54,66]
		– Particle agglomeration in high MOF loadings.	– CO_2 capture[56]	UiO-66[51]
		– Requires rheological modifiers (e.g. bentonite, cellulose).[50,53] – Low resolution compared to light based techniques. – Require post-processing (e.g. thermal activation).[53]		MIL-101[56]
Seed-assisted in situ growth	– Forms a dense, continuous MOF film on the printed scaffold. – Good interaction between MOFs and matrices. – Uniform distribution of MOFs within the matrices. – Significantly enhances CO_2 capacity (from 0.5 to 2.5 mmol g^{-1}) and improves mass transfer kinetics.	– Not suitable for high MOF loadings (typically $<$50 wt%)[60] – Poor crystallinity of MOF phases – Multi-step process leading to long fabrication times – Generate liquid waste; not ideal for scale-up.	CO_2 adsorption[60]	MOF-74[60]
Matrix incorporation	– Effective dispersion of MOF particles within the polymer matrix.	– Not suitable for high MOF loadings (e.g., limited to $\sim$10 wt% in some cases).[61]	– Hydrogen storage[61]	– MOF-5[61]
	– Ink exhibits suitable viscoelasticity for printing.	– Possibility of partial decomposition of the MOF crystals and pore blockage.	– CO_2 uptake[60]	– MOF-74[60]
	– Relies on inexpensive polymer matrices like acrylonitrile butadiene styrene (ABS). – Fabricating MOF monoliths via a simple solvent-casting process.	– Batch process with limited throughput.		
Selective laser sintering	– High resolution and good control over physical characteristics.	– Limited range of applicable materials.	– Water adsorption, purification[62]	MOF-801, ZIF-67, ZIF-8, HKUST-1,[62] ZIF 8[67]
	– Formation of micropores between MOF and polymer powders, improving exposure.[62]	– Limited by small build chambers, resulting in lower throughput. – High processing temperatures ($>$100 °C) can degrade some MOFs.[62] – Poor interaction between MOF and matrices.	– CO_2 conversion[67]	
Digital light processing	– High resolution and very fast layer-by-leyer curing.	– Limited to photosensitive resin	– Adsorption of methylene blue dye[64]	– HKUST-1[64]
	– Good control over thickness and monolith formation.	– Needing photo initiators	– CO_2/CH_4 separation[63]	– MIL-53(Fe)-NH$_2$[63]
	– Enables rapid fabrication of complex-high resolution 3D monolith.	– Needing a light source. – Can result in reduced mechanical properties for some composites.		
Template-assisted synthesis	– It is a more versatile technique as it offers a chance to achieve more diverse structures (e.g., macroporous networks).	– Limited template availability.	– Oil–water separation and Knoevenagel reaction[20]	– ZIF-8[20]
	– Templating results in control over the chemical reactivity of guests.	– Template removal challenging, often requiring calcination, or solvent extraction.		– MIL-53(Al)[68]

shape, and dispersion of these nanoparticles that aggregate into the final monolithic structure. It has been proven through TEM that monoliths of Al-BDC and UiO-66 are comprised of nanoparticles of sizes that are around 10 nm.[33,90] One of the most important contributions of TEM to monolithic MOF research is its ability to reveal how synthesis parameters such as solvent choice, concentration, or aging time directly influence the nucleation and final morphology of colloidal precursors.

A study by Pathak et al.[44] powerfully illustrates this, using TEM to deconvolute the effects of solvent system and temperature on ZIF-8 monolith MOF formation. Their TEM analysis, summarised in Fig. 16, was pivotal in explaining why certain synthesis yielded powdered (pZIF-8) and other monoliths (mZIF-8-R, mZIF-8-Δ). The images reveal that synthesis in pure water resulted in very large particles which hinder the dense packing required for monolithicity. Conversely, the optimised 15% v/v EtOH–H$_2$O solvent system produced significantly
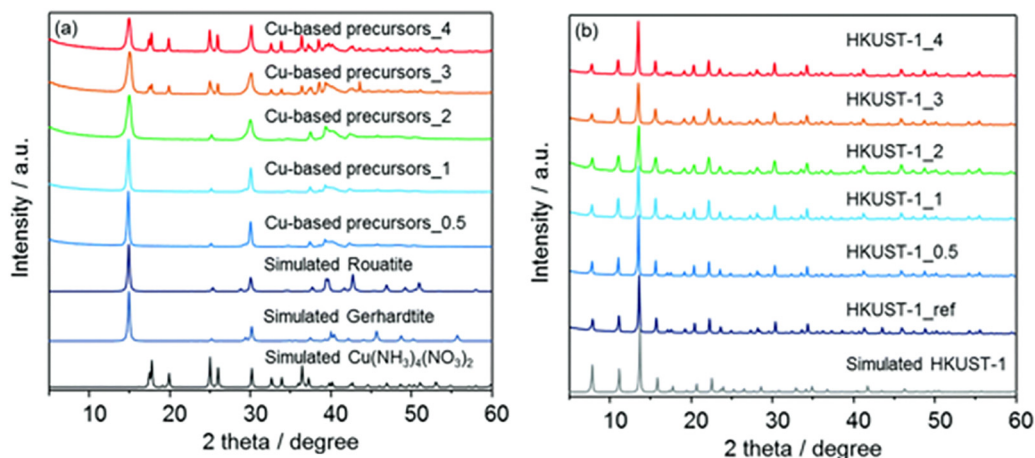
Fig. 14 XRD analysis of copper based monoliths.[83] (a) the solvent insoluble Cu-based precursors (Cu-based precursors X) with simulated patterns for $Cu_2(OH)_3NO_3$ (rouaite and gerhardite) and $Cu(NH_3)_4(NO_3)_2$ and (b) corresponding HKUST-1-X with HKUST-1 reference and simulated pattern for HKUST-1.[83] Reproduced from ref. 83, with permission from the Royal Society of Chemistry.
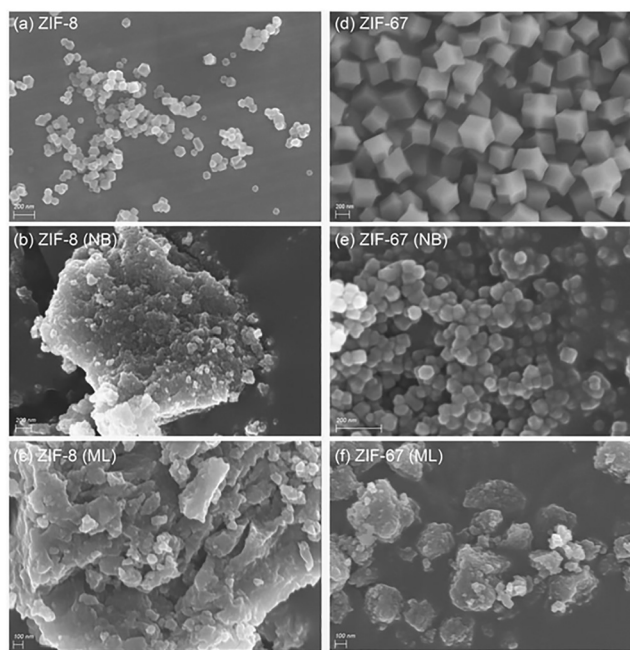

Fig. 15 SEM images of monolithic ZIF-MOF family. (a) ZIF-8, (b) ZIF-8 (NB), (c) ZIF-8 (ML), (d) ZIF-67 (e) ZIF-67 (NB) and (f) ZIF-67 (ML).[41] NB stands for n-butylamine and ML stands for mixed ligands. Reproduced with permission from ref. 41 under the terms of the Creative Commons Attribution License (CC BY).

smaller, uniform primary nanocrystallites, with mean size of 55 ± 10 nm for mZIF-8-Δ. This precise control over particle size was identified as the key factor enabling the particles to agglomerate into coherent, robust monolith rather than a powder.

Furthermore, the study used TEM to track the reaction progress *in situ*. Aliquots taken from the reaction mixture at various times showed that primary particles formed rapidly but required extended periods (96–120 hours) to achieve their final,

well-defined state. This TEM evidence directly supported the conclusion that the solvent mixture's primary effect was to drastically slow down the reaction kinetics and colloidal aggregation. This ability to visually corroborate kinetic data makes TEM an indispensable tool for understanding the complex sol–gel process that underpin monolithic MOF formation.

TEM also enables the detailed examination of structural features that are difficult to detect using other techniques. These include the interfaces between aggregated nanoparticles, mesoporous interparticle spaces, the presence of defects or amorphous regions, and the degree of fusion or continuity within the monolith.[90] Such information is essential for understanding how microstructural features affect macroscopic properties like mechanical strength, gas permeability, or catalytic activity.

In addition, it is particularly useful for characterizing hybrid or composite monoliths, where MOFs are combined with polymers, carbon materials, or other functional components. It can resolve the nanoscale interfaces between phases and provide insights into compatibility, dispersion, and potential phase separation. These factors are critical when designing monoliths for real-world applications such as gas separation membranes, adsorbents, or catalytic reactors.

Porosity and surface area analysis

The applications of MOFs in gas storage, separation and heterogeneous catalysis fundamentally relies on their extraordinary intrinsic porosity and massive surface areas, properties that often surpass those of traditional porous materials like zeolites and activated carbons.[91] This porosity is a direct consequence of their modular, crystalline architecture, where metal nodes are connected by organic linkers to form well-defined cages and channels. Precise characterization of these textural properties is therefore a critical endeavour that links synthetic design and molecular-scale structure directly to application performance.

The most established technique for this purpose is gas physisorption, most commonly using nitrogen (N_2) at 77 K.
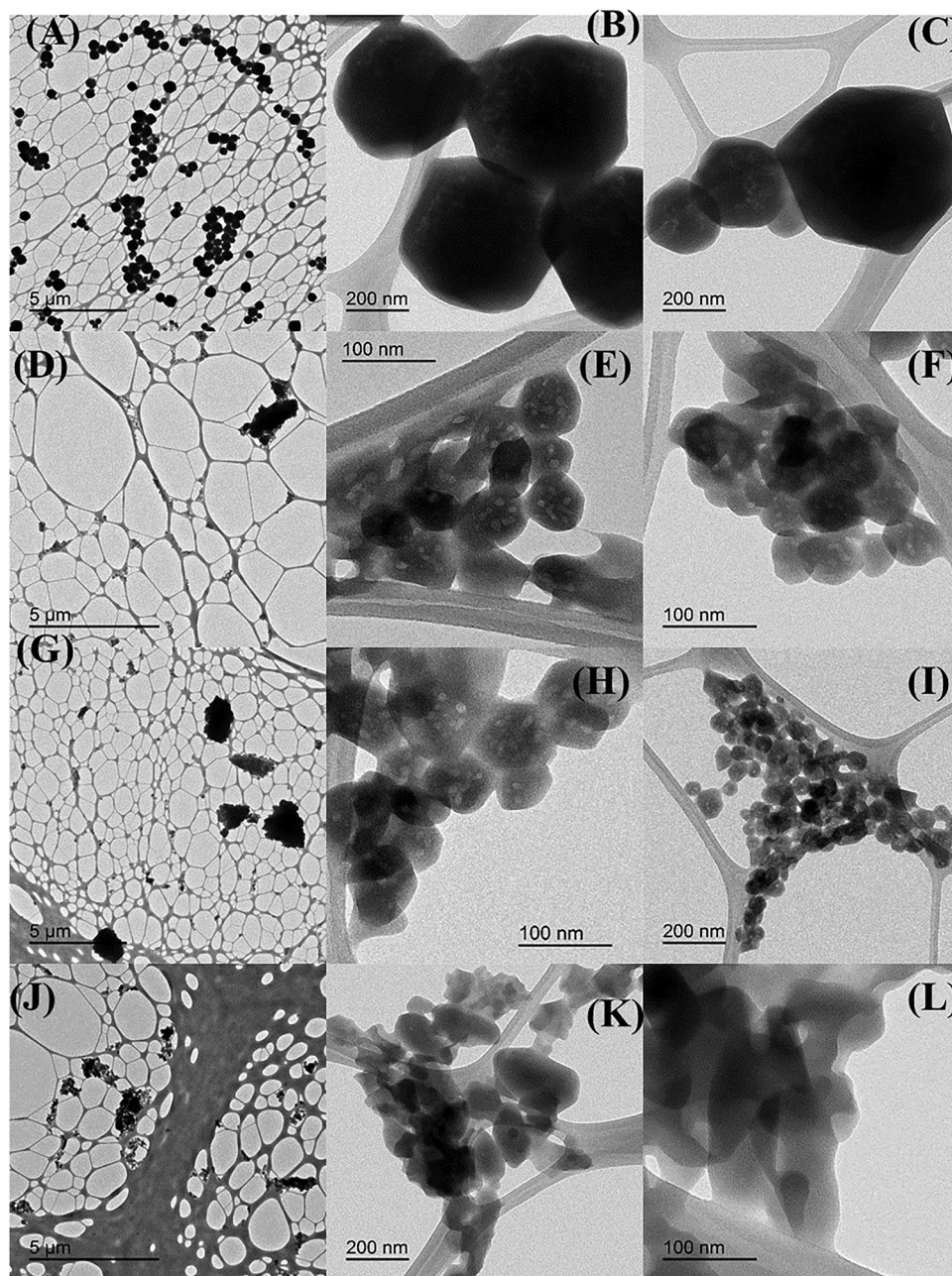
Fig. 16 Representative TEM images of MOFs after the complete drying of gel followed by activation in a vacuum oven. pZIF-8 (A)–(C), mZIF-8-R (D)–(F), mZIF-8-Δ (G)–(I) and mZIF-8-CS (J)–(L). Scale bars; 5 nm (A), (D), (G) and (J), 200 nm (B), (C), (I) and (K) and 100 nm (E), (F), (H) and (L).[44] Reproduced with permission from ref. 44 under the terms of the Creative Commons (CC BY) license.

The analysis of the resulting adsorption isotherm allows for the calculation of several key metrics: the Brunauer–Emmett–Teller (BET) surface area, which serves as the primary benchmark for comparing porosity; the pore volume, often delineated into micropore volume (pores <2 nm) and total pore volume; and the pore size distribution (PSD), determined using advanced models such as non-local density functional theory (NLDFT), which dictates a material's molecular sieving capabilities.[92]

However, a significant challenge arises when transitioning from laboratory powder to industrial application, which necessitates shaping the MOF into robust, handleable forms such as pellets or monoliths. Conventional techniques like pelletization under high mechanical pressure often incur a catastrophic loss of surface area and porosity. This makes the development of shaping methods that preserve porosity a key research focus.[93]

For instance, Pathak et al.[44] demonstrated that monolithic ZIF-8 (mZIF-8) possesses a hierarchical pore structure combining micro- and mesoporosity, which is a significant advancement over conventional powdered ZIF-8 (pZIF-8). While the powder form is exclusively microporous (Type-I isotherm, BET ~ 1450 m^2 g^{-1}), the monoliths exhibit a Type-IV isotherm with a distinct hysteresis loop, confirming the introduction of

mesopores with a mean size of 16 nm. Crucially, despite this architectural change, the optimal monolith (mZIF-8-Δ) retained a high BET surface area of 1421 $m^2 g^{-1}$. The key distinction lies in the density and volumetric performance; the monolith's much higher bulk density (0.76 g cm^{-3} vs. 0.35 g cm^{-3} for the powder) results in a far superior volumetric surface area (1080 $m^2 cm^{-3}$ vs. 508 $m^2 cm^{-3}$), making it far more practical for real-world applications where space is a constraint, without sacrificing its adsorptive capacity.

This principle of creating hierarchical structures within monoliths is further advanced in the work of Thakkar et al.,[47] who utilized 3D printing to structure MOF-74(Ni) and UTSA-16(Co). The results, summarized in Fig. 17, reveal significant structural insights: the pure MOF powders exhibited classic Type I isotherms, confirming their purely microporous nature with high BET surface areas (1180 $m^2 g^{-1}$ for MOF-74(Ni) and 727 $m^2 g^{-1}$ for UTSA-16(Co)). In contrast, the 3D-printed monoliths, particularly UTSA-16(Co), displayed a Type IV isotherm with a distinct hysteresis loop, confirming the successful introduction of mesoporosity during the printing process. While the incorporation of non-porous binders led to a reduction in gravimetric surface area and micropore volume, the highest-loaded monoliths retained substantial values (737 $m^2 g^{-1}$ and 0.32 $cm^3 g^{-1}$ for MOF-74(Ni); 568 $m^2 g^{-1}$ and 0.23 $cm^3 g^{-1}$ for UTSA-16(Co)). The UTSA-16(Co) monolith also exhibited an additional mesopore volume of 0.06 $cm^3 g^{-1}$ with a mean size of 25 nm.

The data showed that the structured monoliths retained 79–87% of the powder's CO_2 capacity. Furthermore, the intentionally introduced mesoporosity facilitated dramatically improved mass transfer kinetics as evidenced by a sharper breakthrough curve (10 minutes for the monolith vs. 15 minutes for the powder). This demonstrates that the 3D-printed form factor mitigates kinetic limitations without sacrificing core adsorption capacity, thereby validating this monolithic approach for practical CO_2 capture.

Mechanical strength

Powdered MOFs are characterised by poor mechanical strength compared to their monolithic counterparts.[94] The majority of research examining the mechanical properties of MOFs has primarily relied on nano indentation techniques. This technique involves pressing a hard indenter tip (often diamond) into a material's surface while precisely measuring the applied load and the resulting displacement, as illustrated in Fig. 18. In this representative molecular dynamics simulation model, a conical diamond indenter is pressed into a single-crystal specimen. The substrate is typically divided into layers: a fixed boundary layer to prevent slippage, a thermostatic layer to maintain the target temperature, and a Newtonian layer where the indentation occurs, and atomic motion is calculated. This approach which was established by Oliver and Pharr is mainly used to
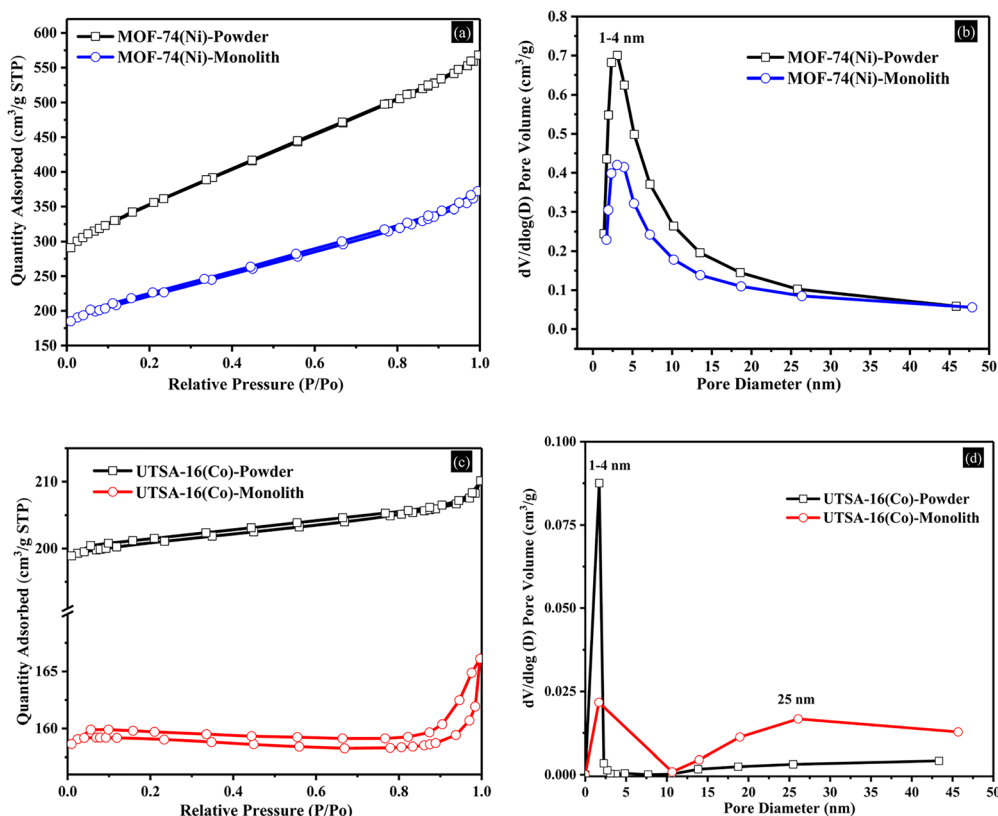
Fig. 17 Nitrogen physisorption isotherms and pore size distribution curves for 3D-printed MOF monoliths (a) an (b) MOF-74(Ni) and (c) an (d) UTSA-16(Co) and their corresponding powders.[47] Reproduced with permission from ref. 47, Copyright (2017) American Chemical Society.
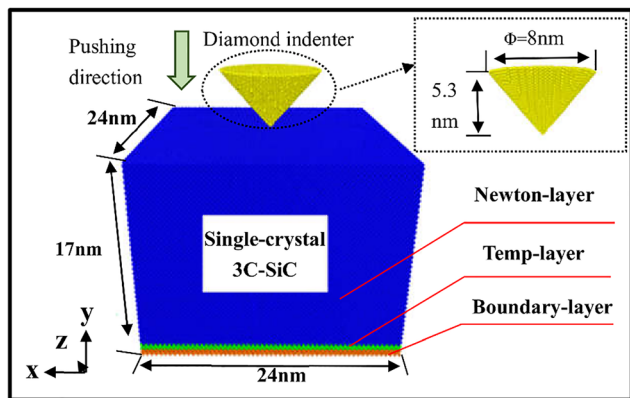
Fig. 18 Schematic of a molecular dynamics simulation model for nanoindentation on a single crystal, showing the indenter and the different atomic layers of substrate.[96] Reproduced from ref. 96, under the terms of the Creative Commons (CC BY) license.

determine two key properties: Young's modulus (E), which measures elasticity, and hardness (H).[95]

The monolithic samples are first made cylindrical by cold mounting, then they are polished to minimize roughness. A diamond indenter tip is then used to indent the smooth surface to a certain depth whilst the continuous stiffness measurement will be measuring the elastic modulus and hardness.[97,98] Young's modulus (E) represents the material's elastic stiffness, that is, its ability to resist elastic (reversible) deformation under applied stress. A high E value indicates that the material is rigid and can retain its shape under mechanical load, which is crucial for maintaining structural integrity in applications involving pressure, vibration, or mechanical agitation. This is particularly important for monolithic MOFs used in gas separation, flow reactors, or packed bed systems, where structural deformation could lead to channel blockage, pressure drops, or even framework collapse.

Hardness (H), on the other hand, measures a material's resistance to permanent (plastic) deformation, such as scratching or indentation. A high hardness value suggests that the material can withstand localized mechanical stress without sustaining damage.

In MOFs, higher hardness is advantageous for resisting wear and abrasion during processing, handling, or operation in dynamic environments, such as catalytic beds or adsorption columns. Monolithic MOFs preserve their structural integrity under conditions of cyclic loading, including repetitive compression and decompression as encountered in gas storage systems. Their stability without the inclusion of binders, coupled with a hierarchical porous structure, significantly enhances their mechanical properties and overall performance in practical applications. A notable example is that of ZIF-67 powder which was transformed into a monolith by the compression of the powder at 25 MPa for 5 min yielding a monolith after calcinating at 800 °C. The resulting monolith could withstand cyclic loadings of pressure up to 3 MPa.[99]

Tricarico et al.,[100] used nanoindentation method to evaluate the mechanical properties of four MOF monoliths: ZIF-8, HKUST-1, MIL-68, and MOF-808. Fig. 19 illustrates the load–depth curves from nanoindentation tests (Fig. 19A) and the relationship between elastic recovery and the H/E ratio (Fig. 19B), highlighting the distinct mechanical behaviour of each monolith. The results revealed a clear distinction in their mechanical responses, governed by their unique nanostructures. HKUST-1 exhibited the highest hardness (0.46 GPa) and an intermediate elastic recovery, contributing to its exceptional indentation fracture toughness ($K_c = 0.80 \pm 0.45$ MPa $\sqrt{m}$), the highest reported for any MOF material.

In contrast, ZIF-8 showed a high elastic recovery but intermediate hardness, making it more prone to radial cracking. Meanwhile, MIL-68 and MOF-808, characterized by smaller nanograins and a higher density of grain boundaries, displayed lower hardness and significantly reduced elastic recovery. This nanostructure promotes grain boundary sliding, which enhances ductility and energy dissipation, thereby providing remarkable resistance to crack propagation despite their lower inherent strength. These findings underscore how nanostructural features such as grain size, porosity, and framework topology directly influence both elastic and plastic deformation mechanisms. The superior hardness and fracture toughness of HKUST-1 make it highly suitable for industrial applications requiring durability under mechanical stress.
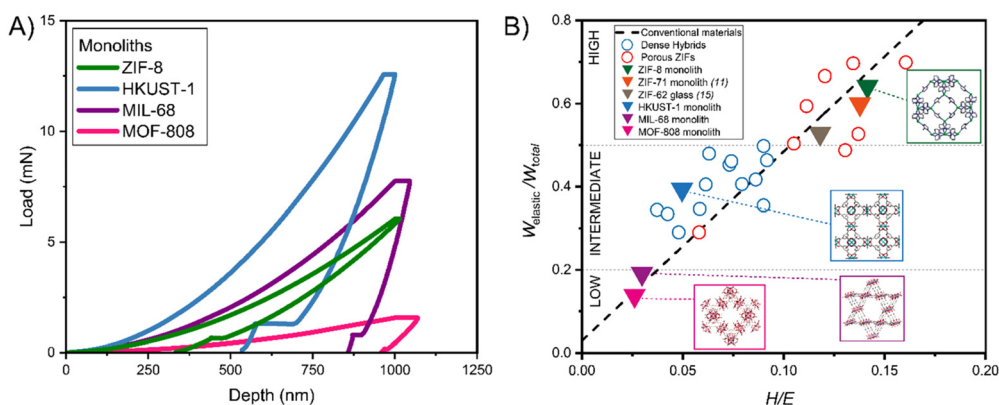

Fig. 19 Mechanical properties of monolithic MOFs, (A) nanoindentation load–depth curves and (B) elastic recovery versus hardness/modulus ratio.[100] Reproduced from ref. 100, under the terms of the Creative Commons (CC BY).

Recent upgrades to the nanoindentation technique have seen the emergence of two advanced mechanical testing methods: flat punch nanoindentation and micropillar compression.[94] Flat punch nanoindentation uses a cylindrical indenter with a flat end to compress a relatively large, flat area of a monolith. This technique is ideal for probing the bulk-like mechanical behaviour of porous monoliths since it minimizes localized densification that occurs with sharp tips usually used in conventional nanoindentation. As applied in the study of MOF monoliths, it enables the estimation of stress–strain relationships, providing insight into yielding and plastic flow under a constrained, triaxial stress state. It is commonly used to measure Young's modulus, yield strength, and to monitor fracture initiation under uniaxial loading. It helps in evaluating the structural stiffness and pore collapse behaviour in a more distributed stress field compared to standard indentation.

Fig. 20(a) and (b) shows the resulting load–depth (P–h) and stress–strain (σ–ε) curves from flat punch nanoindentation tests on ZIF-8 and MIL-68 monoliths, using a flat punch indenter with a diameter of 10.64 µm. The data, summarized in Table 3, reveal that both monoliths exhibit similar yield stresses (ZIF-8: 88.2 ± 16.4 MPa; MIL-68: 90.0 ± 10.5 MPa), but differ in their strain hardening behaviour, with ZIF-8 showing a higher strain hardening exponent ($n \approx 0.20$) compared to MIL-68 ($n \approx 0.11$). It was observed that MIL-68 exhibited an initial stiff response followed by softening for depths > 200 nm (as visible in the derivative dP/dh in Fig. 20(c)). This was contrary to the case of ZIF-8, which exhibited a softer response, without a drastic change in its slope. The authors attributed the initial stiff response of MIL-68 to its higher elastic modulus, prior to the onset of grain boundary sliding.

It was concluded that these MOF monoliths consists of stepwise microcracking, accommodating excessive build-up of stress, likely taking place at the grain boundaries between the nanocrystals. This mechanism is supported by the appearance of concentric ring-shaped cracks around the residual imprints (Fig. 20(d) and (e)), resembling shear faults, and the absence of pop-ins in the load–depth curves, indicating contained damage without catastrophic crack propagation.

Micropillar compression involves fabricating tiny cylindrical or square pillars (usually *via* focused ion beam milling) from a monolith and compressing them using a flat punch. This technique provides data on uniaxial compressive strength, yielding, and failure modes at the microscale. It is particularly useful for studying anisotropic mechanical responses, brittle-to-ductile transitions, or the effects of defects in monolithic frameworks. For MOFs and other fragile porous materials, it enables controlled study of plastic deformation or fracture mechanisms without bulk sample limitations. This technique has been used for studying the stress–strain relationships of ZIF-8 and MIL-68 monoliths, obtained by a sol–gel synthesis route.[94] The stress–strain curves obtained and the micropillar compression images are shown in Fig. 21 and they show distinctly different plastic behaviour of the two monoliths. From this study, it was concluded that ZIF-8 exhibited elastic crack propagation failure as shown in Fig. 21d, whereas MIL-68

had some plastic flow before failure (Fig. 21e).[94] The difference in failure modes is attributed to the distinct framework architectures and nanostructures: ZIF-8 fails by longitudinal splitting due to its brittle nature, while MIL-68 shows ductile flow and transverse cracking, enhanced by its finer nanoparticle size and stiffer framework.

Nanoindentation has been employed to evaluate the mechanical performance of a wide range of monolithic MOFs, as summarized in Table 4. These studies reveal that monolithic MOFs exhibit significantly enhanced mechanical durability compared to their powdered forms, making them suitable for high-pressure applications. Furthermore, their properties are not merely intrinsic but can be deliberately engineered. For instance, creating defects *via* thermolysis (*e.g.*, in monoUiO-66-NH-30%-A) results in a predictable decrease in hardness and elasticity.[71] Conversely, the encapsulation of guest molecules presents a exciting strategy for enhancing mechanical integrity. Recent work has shown that embedding rigid, planar dyes within monolithic UiO-66 frameworks increases both Young's modulus and hardness, suggesting a pore-filling stiffening effect.[98] This enhanced resistance to fracture and wear is critical for the sustained utilization of monolithic MOFs in demanding applications like catalysis and gas storage.

Emerging characterisation tools

While conventional techniques such as PXRD, gas sorption analysis, and electron microscopy provide essential information on the structure, porosity, and morphology of MOF monoliths, they often fall short of revealing the nanoscale features that dictate macroscopic mechanical and functional properties. The complex, often heterogeneous architecture of monoliths, comprising nanoparticles, grain boundaries, potential amorphous phases, and in composites, guest molecules demands characterisation tools with superior spatial resolution and multifunctional capabilities.[38] Recently, a suite of advanced nanocharacterisation techniques has been leveraged to provide these critical, mechanistic insights, moving beyond bulk averaging to probe local phenomena. Atomic force microscopy (AFM) has emerged as a pivotal technique for visualising the results of mechanical interaction at the nanoscale. Its primary advantage lies in its ability to generate high-resolution, three-dimensional topographical maps of a surface after testing, offering unambiguous evidence of deformation behaviour that complements quantitative data from nanoindentation.

This was demonstrated by Tian *et al.*[32] in their study of a sol–gel derived HKUST-1 monolith for methane storage. The mechanical robustness of the monoHKUST-1 monolith, a critical property for its application in high-pressure gas storage, was comprehensively characterized *via* nanoindentation and Atomic Force Microscopy (AFM), as summarized in Fig. 22. The nanoindentation results (Fig. 22a and b) quantified the bulk mechanical properties, showing that the monolith possessed a Young's modulus of 9.3 ± 0.3 GPa and, most notably, a hardness of 460 ± 30 MPa. This hardness value was more than double that of any conventional HKUST-1 material reported previously, a fact highlighted in the inset of Fig. 4b. An optical micrograph (Fig. 22c) of the sample
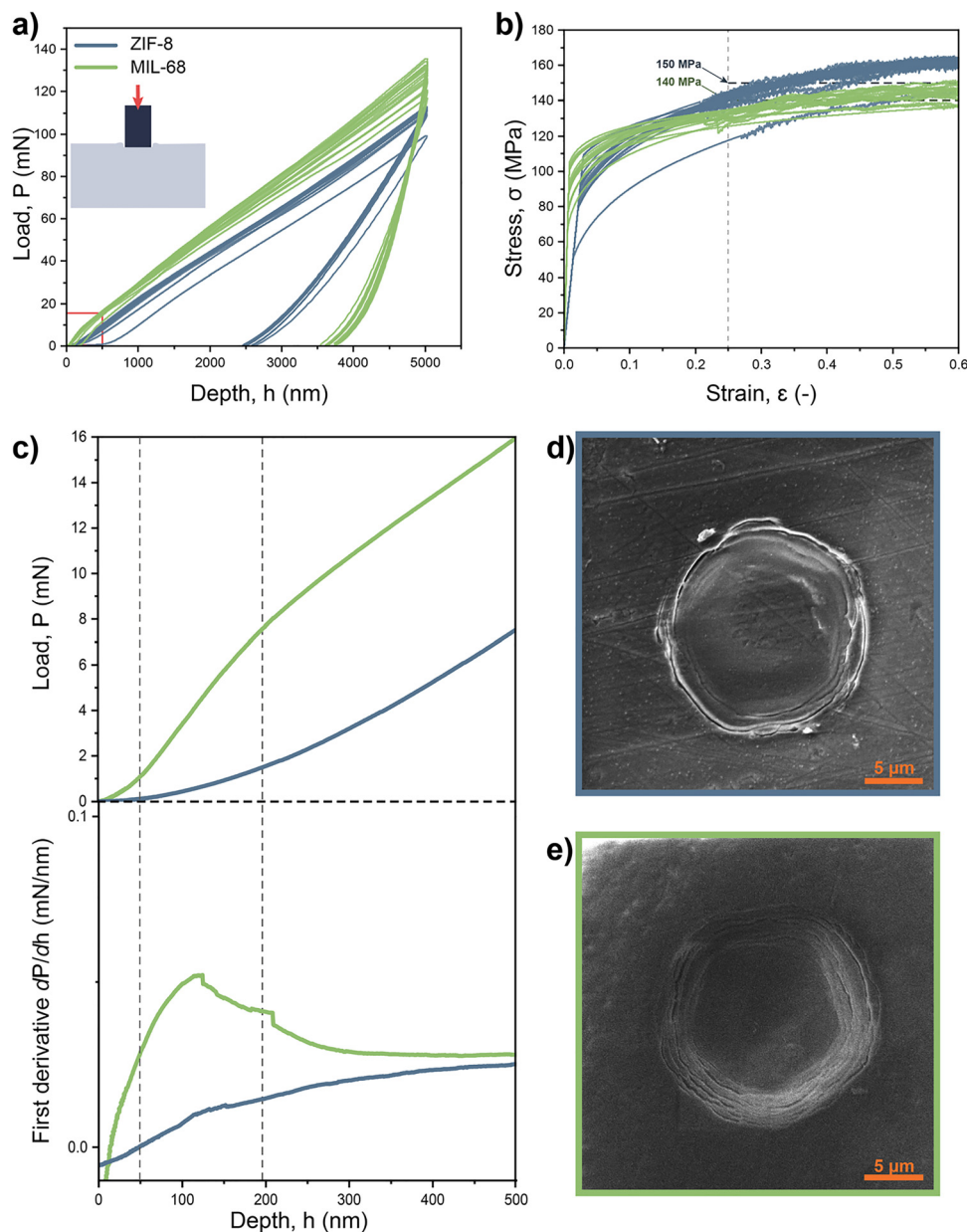
Fig. 20 Flat punch tests on ZIF-8 and MIL-68 monoliths (a) load-depth curves, (b) stress−strain curves, (c) load-depth curves in the 0−500 nm range, (d) SEM image for flat punched ZIF-8, and (e) SEM image for flat punched for MIL-68.[94] Reproduced with permission from ref. 94, under the terms of the Creative Commons Attribution License (CC BY).

surface showed an array of these indents, providing a macroscopic view that confirmed the tests were performed successfully and repeatedly across the material's surface.

Crucially, AFM imaging of the residual indents (Fig. 22d) was employed to move beyond numerical values and visualize the nanoscale quality of the deformation. The primary advantage

of AFM was its ability to provide a high-resolution, three-dimensional topographical map of the impression left by the indenter. The profile revealed a well-defined pit with smooth walls and, most importantly, a complete absence of surface cracking or radial fractures emanating from the edges. This evidence was the definitive visual proof of the monolith's

Table 3 Mechanical properties of ZIF-8 and MIL-68 monolith extrapolated from the stress−strain obtained by flat punch nanoindentation

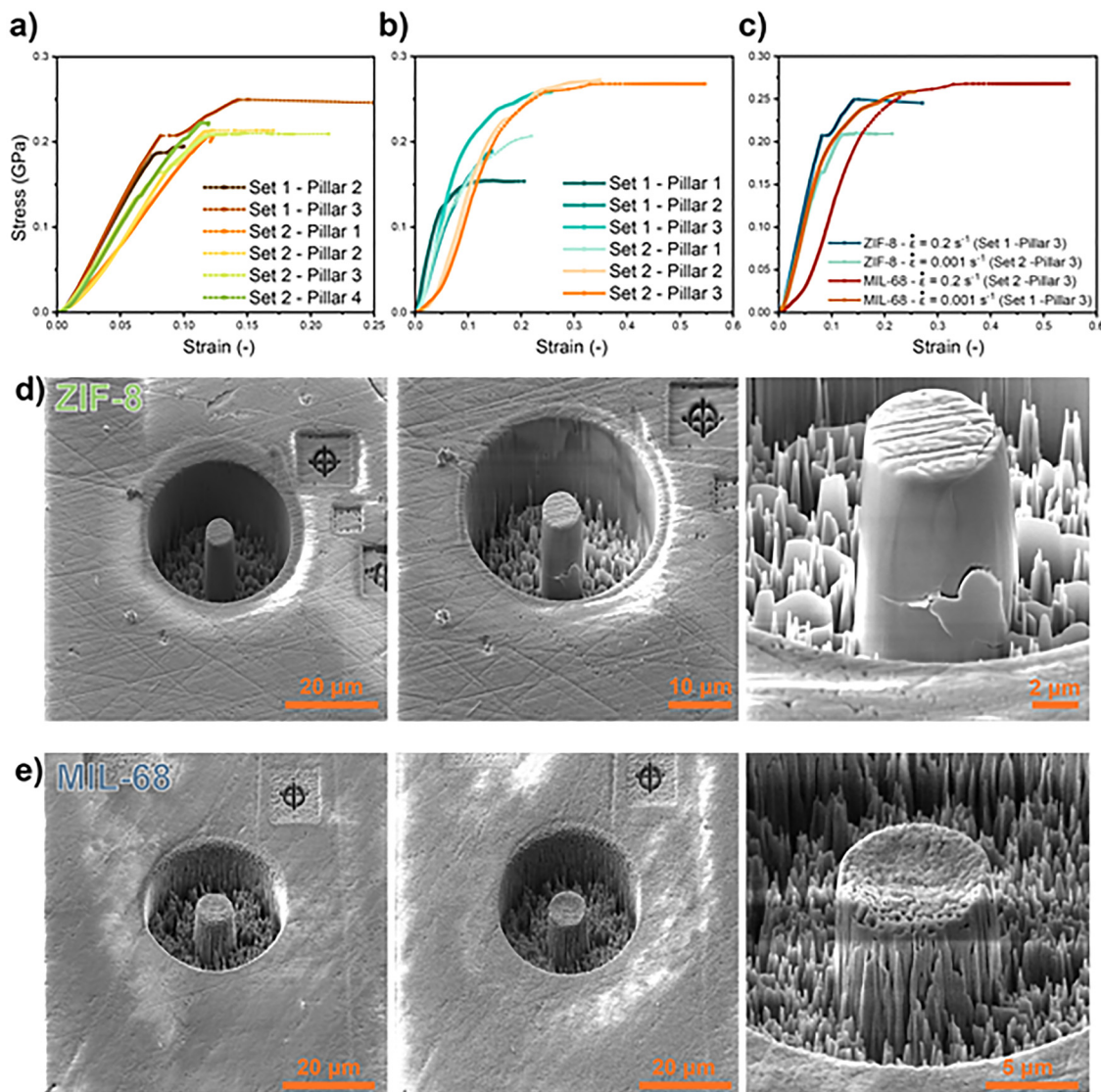| Material	Number of tests	Yield stress (MPa)	Yield strain (−)	K (MPa)	(n−)	Average flow stress (MPa)	Hardness (MPa)
ZIF-8	18	88.2 ± 16.4	0.00238 ± 0.0033	184.1 ± 9.5	0.1976 ± 0.0405	140 ± 10	452 ± 20
MIL-68	16	90.0 ± 10.5	0.0072 ± 0.0008	154.0 ± 6.6	0.1093 ± 0.029	150 ± 16	402 ± 13

Fig. 21   (a)–(c) Stress–strain curves of ZIF-8 and MIL-68 micropillars compression samples, (d) and (e) micropillars compression representative images.[94] Reproduced with permission from ref. 94 under the terms of the Creative Commons Attribution License (CC BY).

superior mechanical resilience. It demonstrated that under intense local stress, the material underwent plastic deformation rather than brittle fracture. This finding directly correlated with the high hardness values, confirming that the sol–gel process had successfully created a dense, monolithic structure capable of resisting permanent deformation and mechanical damage, a vital requirement for any material destined for practical, industrial use.

Tricarico *et al.*[35] combined nano-FTIR spectroscopy with AFM-based methods (tip force microscopy) to deconvolute the deformation mechanisms of ZIF-8 and ZIF-71 monoliths. The AFM topographical images and cross-sectional profiles, as illustrated in Fig. 23, showed that the residual indents from Berkovich, cube corner, and spherical tips exhibited quite an insignificant pile-up at their edges. This observation is a critical signature of a material that undergoes plastic deformation with negligible work hardening. Furthermore, the images confirmed

a complete absence of cracking around the indents, even those made with the sharp cube corner tip designed to initiate fractures. These AFM findings provided direct visual evidence that supported the authors' proposed deformation mechanism: grain boundary sliding (GBS). In the nanocrystalline structure of the monoliths, plastic flow is accommodated by nanograins sliding past one another, a process that does not lead to the dislocation accumulation that causes work hardening and pile-up. Thus, the AFM data served as the crucial visual proof linking the monoliths' unique sol–gel-derived nanostructure to their ductile, plastic mechanical behaviour under compressive load. The corresponding cross-sectional profiles show the depth of the indent and the minimal material pile-up at the edges, indicating ductile deformation with negligible work hardening.

Tricarico *et al.*[98] further advanced this approach by applying nano-FTIR to composite monoliths, using its nanochemical sensitivity to rule out framework alteration and prove that

Table 4 The nanoindentation data for selected monoliths

Monolith	Max depth (nm)	Indentation modulus (GPa)	Hardness (MPa)
ZIF-8[94]	2000	3.18 ± 0.04	452 ± 20
ZIF-71[35,94]	2000	1.67 ± 0.38	227 ± 47
MIL-68[94]	2000	13.24 ± 0.52	402 ± 13
UiO-66-30%-B[71]	1000	6.01 ± 0.2	185 ± 10
	2000	6.0 ± 0.2	180 ± 14
UiO-66-30%-A[71]	1000	4.8 ± 0.3	169 ± 16
	2000	4.6 ± 0.2	155 ± 13
HKUST-1[100]	1000	15.25 ± 0.61	761 ± 53
MOF-808[100]	1000	4.61 ± 0.32	122 ± 14
UiO-66-COOH[101]	3000	15.471 ± 0.25	589 ± 18
UiO-66-NH$_2$[101]	3000	11.959 ± 0.243	334 ± 9
UiO-66-(OH)$_2$[101]	3000	10.251 ± 0.142	331 ± 2
HKUST-1[32]	2000	9.3 ± 0.3	460 ± 30
UiO-66[98]	2000	2.06 ± 0.2	72 ± 12
RhB@UiO-66[98]	2000	3.02 ± 1.59	145 ± 101
FI@UiO-66[98]	2000	3.79 ± 0.42	151 ± 27
7MC@UiO-66[98]	2000	5.91 ± 1.38	263 ± 114

mechanical heterogeneity originated from physical guest distribution rather than chemical change. In their study, on luminescent monolithic MOFs, they employed an emerging nanoscale characterization tool known as near-field infrared nanospectroscopy (nano-FTIR) to unravel the complex structure–property relationships within their materials (Fig. 24). This advanced technique bypasses the diffraction limit of conventional infrared spectroscopy by utilizing a metallic atomic force microscope tip to act as an optical antenna, enabling the acquisition of local chemical fingerprints with a spatial resolution of approximately 20 nm.

The authors leveraged this powerful tool to investigate the origin of the significant scatter in mechanical properties observed across their monoliths. Analysis was performed on the two distinct morphological phases identified-"smooth" and "porous". The key finding was that the local IR spectra from both phases across all composites were virtually identical and matched the bulk spectrum of pristine UiO-66, as illustrated in Fig. 24d. This confirmed the preservation of the MOF's chemical framework integrity throughout the monolith despite the mechanical heterogeneity. However, the exquisite sensitivity of nano-FTIR did reveal a subtle yet crucial detail in the RhB@UiO-66 composite, the spectra from the mechanically softer "porous" phase showed a slight merging of the characteristic UiO-66 peak at ∼1390 cm^{-1} with peaks attributable to the rhodamine B dye. This indicated the presence of aggregated dye molecules residing in the intergranular macropores
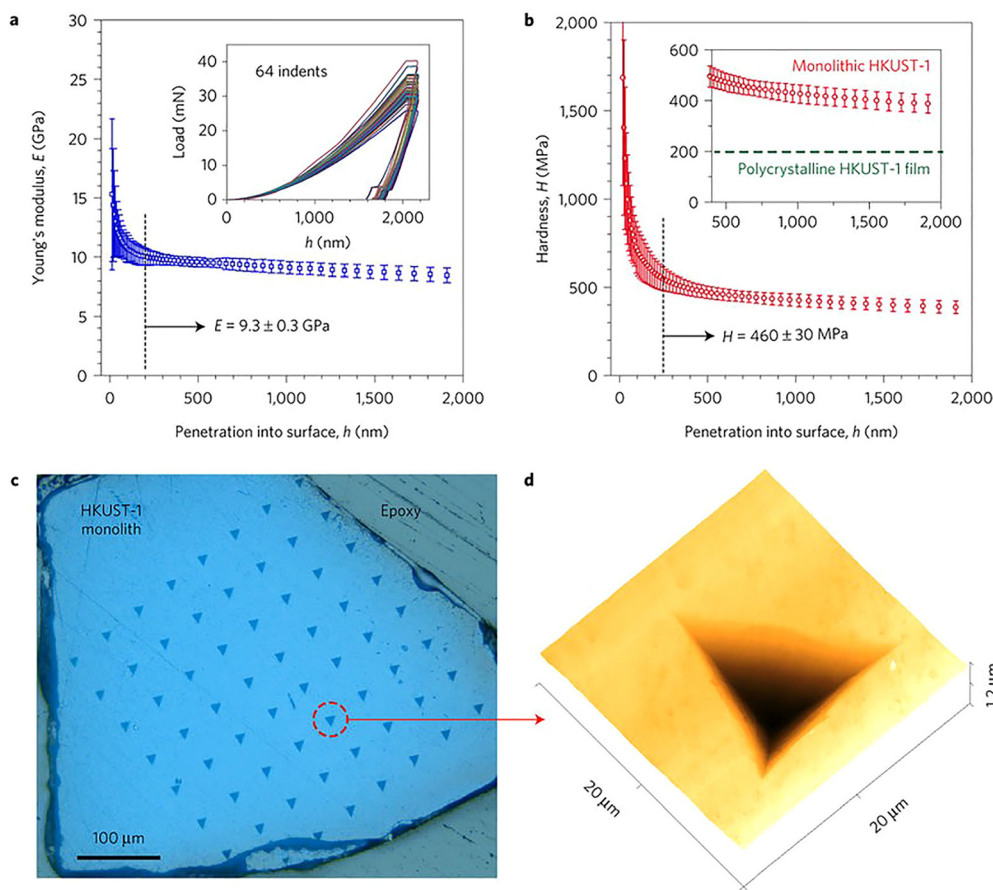
Fig. 22 Nanoindentation on $_{mono}$HKUST-1. (a) and (b) Young's modulus and hardness, respectively, as a function of indentation depth. (c) Optical micrograph showing the array of residual indents. (d) AFM profile depicting the 3D topography of a representative indent.[32] Reproduced with permission from ref. 32, under the terms of the Creative Commons Attribution License (CC BY).
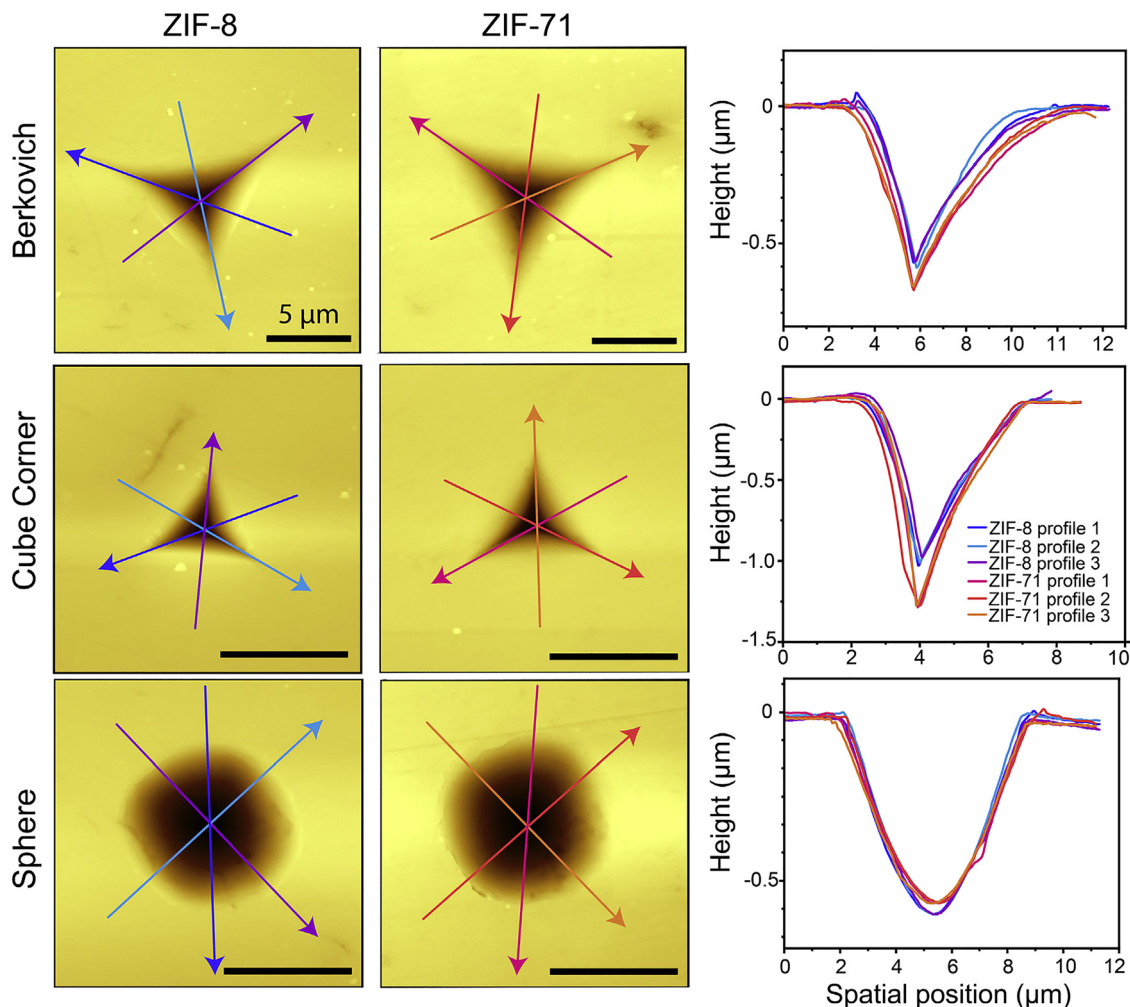
Fig. 23 AFM height topography of the residual indents of Berkovich, cube corner, and spherical indentations for ZIF-8 and ZIF-71 monoliths.[35] Reproduced with permission from ref. 35, Copyright (2022) Elsevier B.V.

between MOF nanoparticles, rather than being neatly confined within the framework's nanopores. This finding directly explained the reduced stiffness of the "porous" phase, as these aggregate-rich regions created mechanically weaker zones, while the "smooth" phase, with its well-confined guests, exhibited superior mechanical performance. Thus, by providing nanoscale chemical evidence, nano-FTIR was instrumental in correlating the physical location of the guest molecules with the macroscopic mechanical behaviour of the monolithic composites.

The adoption of these advanced techniques is transforming understanding of structure–property relationships in monolithic MOFs. Looking forward, the integration of techniques like nanoindentation mapping (*e.g.*, NanoBlitz 3D) to quantitatively spatialise mechanical properties, and *in situ* mechanical testing within electron microscopes to observe deformation in real-time, will provide the next level of insight. These emerging tools are not merely for characterisation; they are essential guides for the rational design of next-generation monoliths with bespoke mechanical and functional properties for targeted applications.

Application of monolithic MOFS

Catalysis

Monolithic MOFs offer significant advantages over their powdered counterparts in catalytic applications due to their structural integrity, enhanced mass transfer properties, and ease of handling.[25–27] Their high surface area provides a large number of active sites while also facilitating efficient substrate diffusion, which is crucial for improving catalytic performance. The interconnected hierarchical pore network typical of many monoliths combines microporosity, for size and shape selectivity, with meso- and macroporosity, which function as transport arteries to drastically reduce mass transfer limitations and prevent pore clogging. This enhanced mass transfer is less prone to clogging when applied in flow reactors, making them ideal for continuous processes. Additionally, their open porosity and interconnected networks enhance reactant accessibility to active sites, ensuring efficient conversion rates in both gas and liquid-phase reactions.[102]

The mechanical robustness of monolithic structures allows for easy integration into catalytic reactors, simplifying catalyst
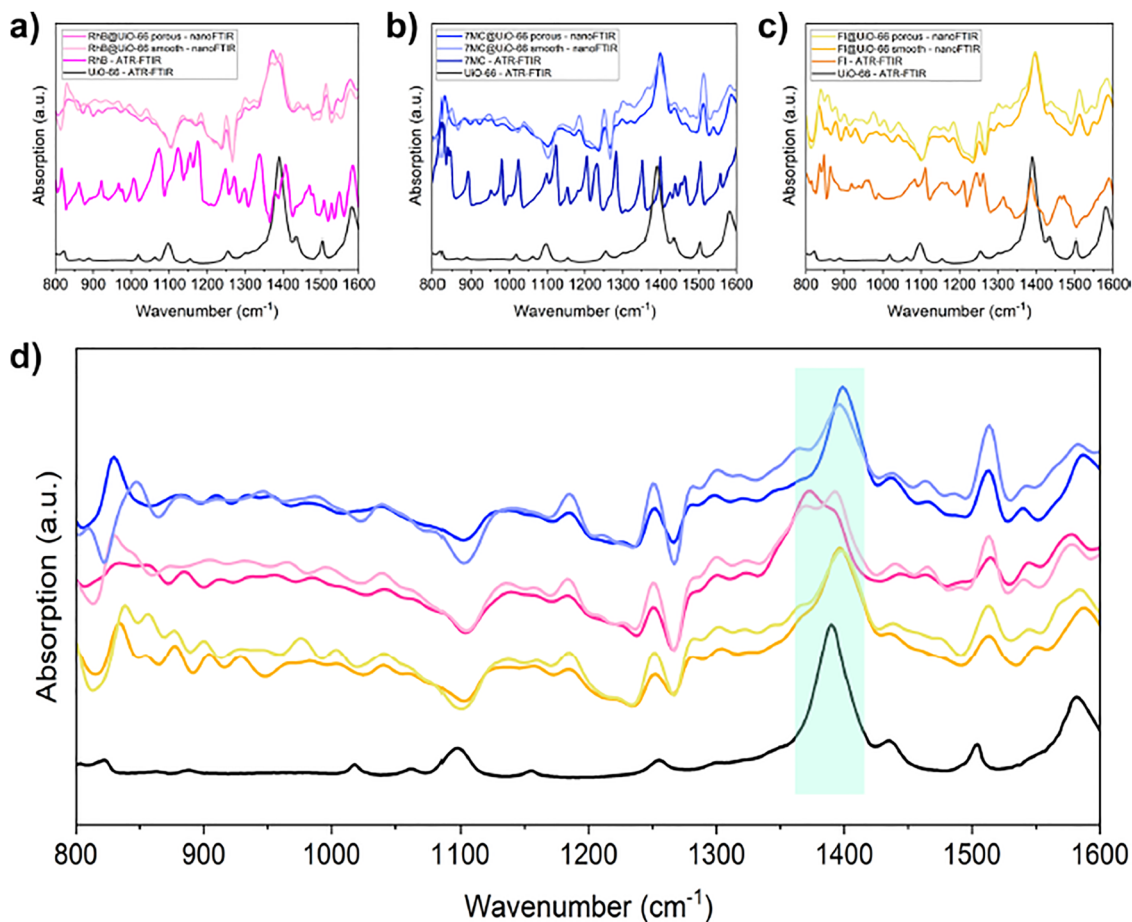
Fig. 24 Far-field ATR–FTIR and nearfield nano-FTIR spectra of (a) RhB@monoUiO-66, (b) 7MC@monoUiO-66, and (c) Fl@monoUiO-66. (d) Comparison of the nano-FTIR (local) spectra of the porous and smooth phase of the three composites and the ATR-FTIR (bulk) spectrum of the pristine UiO-66 monolith (black trace). Characteristic vibrational mode of UiO-66 at 1390 cm^{-1} is highlighted in green.[98] Reproduced with permission from ref. 98, Copyright (2024). America Chemical Society.

packing, recovery, and reuse, which is a critical advantage for industrial application.[103] Furthermore, the monolithic format provides a versatile platform for creating multi-functional systems, where the MOF itself can be the catalyst, or it can serve as a high-surface-area support for other catalytic species (*e.g.*, metal nanoparticles) distributed throughout the 3D framework.[103,104]

A study by Mehta *et al.*[103] demonstrated the advantage of monolithic MOFs in catalyst recovery and reuse. The authors developed a sol–gel method to synthesize a robust, monolithic ZIF-8 framework (monoZIF-8) and encapsulated SnO$_2$ nanoparticles (NPs) within it *in situ* to create a SnO$_2$@monoZIF-8 composite. This approach directly addressed the critical challenges of using powdered NP@MOF composites such as difficult handling, NP agglomeration, and catalyst loss. The monolithic MOF provided a rigid, high-density scaffold that prevented NP leaching and allowed for incredibly facile catalyst recovery after reaction cycles *via* simple gravity filtration (Fig. 25).

McIntyre *et al.*[102] investigated the use of monolithic MOFs, specifically MIL-88B, MIL-100, and ZIF-8@Pd(NO$_3$)$_2$, as catalysts for the transfer hydrogenation of levulinic acid (LA) to

γ-valerolactone (GVL), a valuable green solvent and fuel precursor. The study highlights the critical role of mass transport and diffusion limitations in determining catalytic selectivity and stability, particularly under basic aqueous conditions.

The monolithic forms of these MOFs were synthesized *via* modulated sol–gel methods, providing structural integrity, and facilitating handling compared to powdered analogues. As illustrated in Fig. 26, the reaction involves the conversion of LA over different monolithic MOF catalysts. The authors demonstrated that despite having lower noble metal content, the Fe-based MIL-88B and MIL-100 catalysts achieved comparable conversion rates to the Pd-doped ZIF-8 catalyst. However, the hydrophilic nature of the iron-based MOFs led to hydrolytic degradation over multiple cycles, reducing their long-term stability.

A key finding was the role of pore architecture in product selectivity. The smaller pore apertures of ZIF-8@Pd(NO$_3$)$_2$ (Fig. 27C) restricted side reactions, consistently yielding GVL selectivity above 80%, whereas the larger-pore MIL frameworks (Fig. 27A and B) showed decreased selectivity due to substrate accumulation and pore blockage.
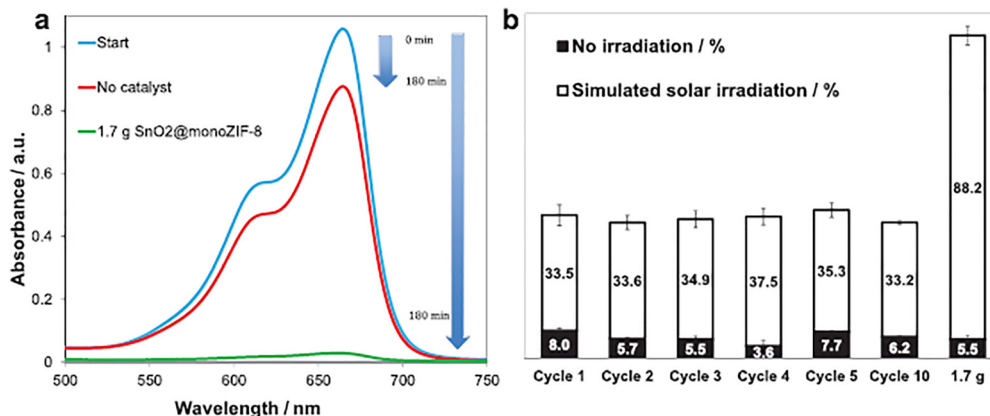
Fig. 25 (a) Photocatalytically induced spectral changes to aqueous MB dye (1.55×10^{-5} M) highlighting degradation of the absorption maximum at 664 nm in the absence of composite (red) and presence of 1.7 g $SnO_2@_{mono}ZIF$-8 (green) after 3 h of simulated solar irradiation. (b) Degradation of MB in the presence of 0.4 g (cycles 1–5 and 10) and 1.7 g of $SnO_2@_{mono}ZIF$-8.[103] Reproduced with permission from ref. 103, under Creative Attribution Licence (CC BY).
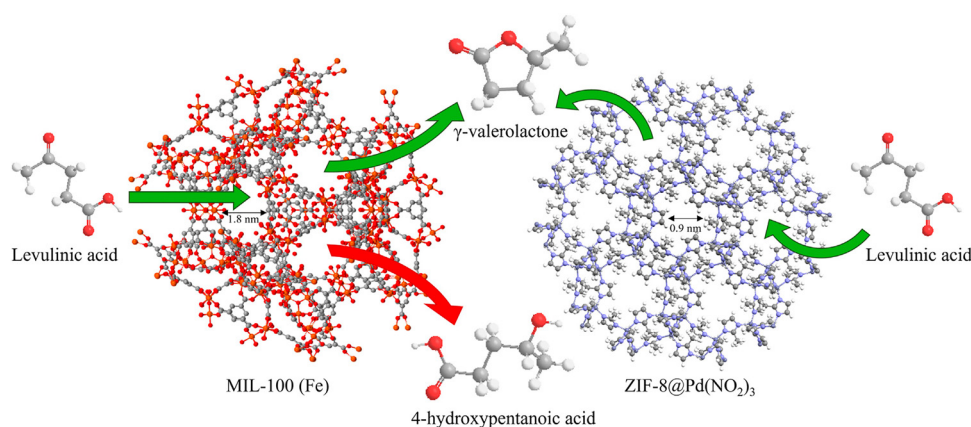

Fig. 26 Schematic representation of levulinic acid conversion over monolithic MOF catalysts.[102] Reproduced with permission from ref. 102, under Creative Attribution Licence (CC BY).

Using zero-length column (ZLC) methods, the authors quantified diffusion constants and mass transfer coefficients, revealing that ZIF-8 exhibited superior mass transfer properties due to its hydrophobic nature and hierarchical porosity. This enhanced transport contributed to higher selectivity and reduced fouling. In contrast, the hydrophilic MIL frameworks suffered from slower diffusion and eventual structural collapse under basic conditions. This study underscores the importance of
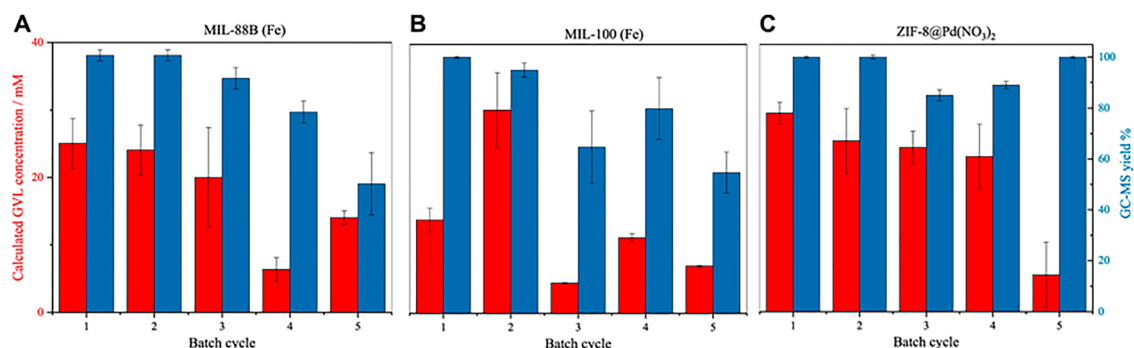

Fig. 27 Batch transfer hydrogenation of LA to GVL over (A) MIL-88B, (B) MIL-100, and (C) ZIF-8@Pd(NO$_3$)$_2$, showing conversion and selectivity over time.[102] Reproduced with permission from ref. 102, under Creative Attribution Licence (CC BY).

Table 5 A summary of selected monolith MOFs used in catalysis

$_{mono}$MOF	Catalytic activity	Comparison with powder counterpart
MIL-88B	Transfer hydrogenation of levulinic acid to γ-valerolactone[102]	Improved conversion ratio
MIL-100	Transfer hydrogenation of levulinic acid to γ-valerolactone[102]	Showed similar initial activity but had the poorest stability, with severe permanent deactivation after just 2 cycles caused by rapid framework collapse.
ZIF-8@Pd(NO$_3$)$_2$	Transfer hydrogenation of Levulinic acid to γ-valerolactone[102]	Displayed superior hydrolytic stability over 5 cycles due to its hydrophobic framework. Activity decline was attributed to pore blockage rather than structural degradation. Exhibited micropore diffusion limitations.
M-ZIF 8	Catalytic condensation of malononitrile and benzaldehyde into benzylidenemalononitrile	Presence of large mesopores in M-ZIF8 contributed to improved rate of catalytic activity compared to that of a general ZIF-8 MOF[105]
ZIF-8	Knoevenagel reaction between benzaldehyde and ref. 20	Enhanced reaction kinetics due to hierarchical macroporosity enabling efficient flow-through catalysis. The ZIF-8 monolith achieved 100% conversion in under 130 seconds, far surpassing the catalytic performance of ZIF-8 powder, which took ∼3 hours to complete the same reaction.
$_{mono}$UiO-66	Catalytic hydrolysis of methyl paraoxon to 4-nitrophenol	Turnover frequency for $_{mono}$UiO$_{66}$ was 0.48 s^{-1} while that of powder UiO$_{66}$ 0.94 s^{-1}. This suggests the monolith may have introduced diffusion limitations or reduce accessibility of active sites compared to the powdered form.[51]
SnO$_2$@$_{mono}$ZIF-8	Photocatalytic degradation of methylene blue	Improved photocatalytic activity and reusability, up to 10 times with no loss of activity.[103]
Cu-BTC silica monolith	Catalytic oxidation of alkylbenzene to ketones	Excellent yield with reduced reaction time.[104]

monolithic MOF design, combining micro- and mesoporosity-to optimize mass transfer and catalytic performance in liquid-phase biomass conversion reactions. It also highlights the trade-offs between activity, selectivity, and stability when selecting MOF platforms for sustainable catalytic processes.

Structuring MOFs into monolithic forms transcends mere shaping for practical handling; it is a critical strategy that fundamentally enhances their catalytic efficacy and viability. By integrating microporosity for molecular selectivity with meso- and macroporous networks that serve as transport arteries, monolithic MOFs drastically mitigate mass transfer limitations inherent to powdered counterparts, leading to improved reaction rates and selectivity. Furthermore, their macroscopic integrity facilitates seamless integration into continuous-flow reactors, eliminates issues of pressure drop and particle clogging, and enables effortless catalyst recovery and reuse, thereby addressing key barriers to the industrial adoption of MOF-based catalysts. This unique synergy of enhanced molecular-level performance and superior process-level operation solidifies monolithic MOFs as a transformative platform for advancing sustainable catalytic processes. Monolith MOFs that have been used for catalysis are presented in Table 5.

Gas storage and adsorption

The environmental benefits of cleaner gaseous fuels like natural gas and hydrogen are well-documented, yet their widespread adoption is hindered by limitations in current gas storage technologies.[106] Monolithic MOFs address these challenges by combining high surface areas, tunable pore sizes, and engineered geometries, making them ideal for gas storage applications. Their porous structure facilitates rapid gas diffusion, enabling faster adsorption/desorption cycles which are critical for practical storage systems. Unlike powdered MOFs, monoliths exhibit minimal pressure loss during adsorption, superior heat and mass transfer, and attrition resistance, owing to their uniform flow channels and dense, stable architectures.[49]

Madden et al.,[31] demonstrated that the exceptionally high-density structure of $_{mono}$HKUST-1 enables record-breaking hydrogen storage performance. The unique synthesis mechanism preserves porosity after shaping and yields benchmark volumetric BET areas, resulting in outstanding H$_2$ sorption characteristics. As illustrated in Fig. 28, $_{mono}$HKUST-1 displays a hydrogen adsorption capacity of 10.1 g L^{-1} at 25 °C and 100 bar, represents the highest measured H$_2$ capacity of a densified MOF using its true density under these conditions. At 100 bar, $_{mono}$HKUST-1 stores more hydrogen than compressed gas or powdered HKUST-1, owing to its compact morphology and minimized interparticle voids. Under cryogenic temperature-pressure swing conditions from 100 bar at 77 K to 5 bar at 160 K, it delivers a greater usable hydrogen amount, highlighting its excellent adsorption–desorption reversibility and structural integrity. At 77 K across varying pressures, $_{mono}$HKUST-1 consistently outperforms powdered MOF and even an empty tank in deliverable capacity. Notably, it achieves H$_2$ working capacity at 25 bars under cryogenic conditions, performance previously only possible by compressing hydrogen to 700 bars at ambient temperature. This reduction in operating pressure holds promise for lowering engineering demands and costs while enhancing the safety of onboard hydrogen storage systems for vehicular applications. Furthermore, the monolithic structure reduces material degradation typically seen in HKUST-1 powders, as an oxidized surface layer shields the internal particles from moisture, preserving high performance even after extended atmospheric exposure.

The same architectural advantages translate to methane storage, where $_{mono}$HKUST-1 approaches the US Department of Energy (DOE) target of 263 cm^3 (STP) cm^{-3}, a 30–50% improvement over pelletized/powdered forms.[32,106] The volumetric adsorption isotherms illustrated in Fig. 29 demonstrate $_{mono}$HKUST-1's superior capacity, approaching the target of 263 cm^3 (STP) cm^{-3} at high pressure, while pelletized forms show reduced uptake due to pore collapse from compression. Kinetic analysis reveals faster methane adsorption in the
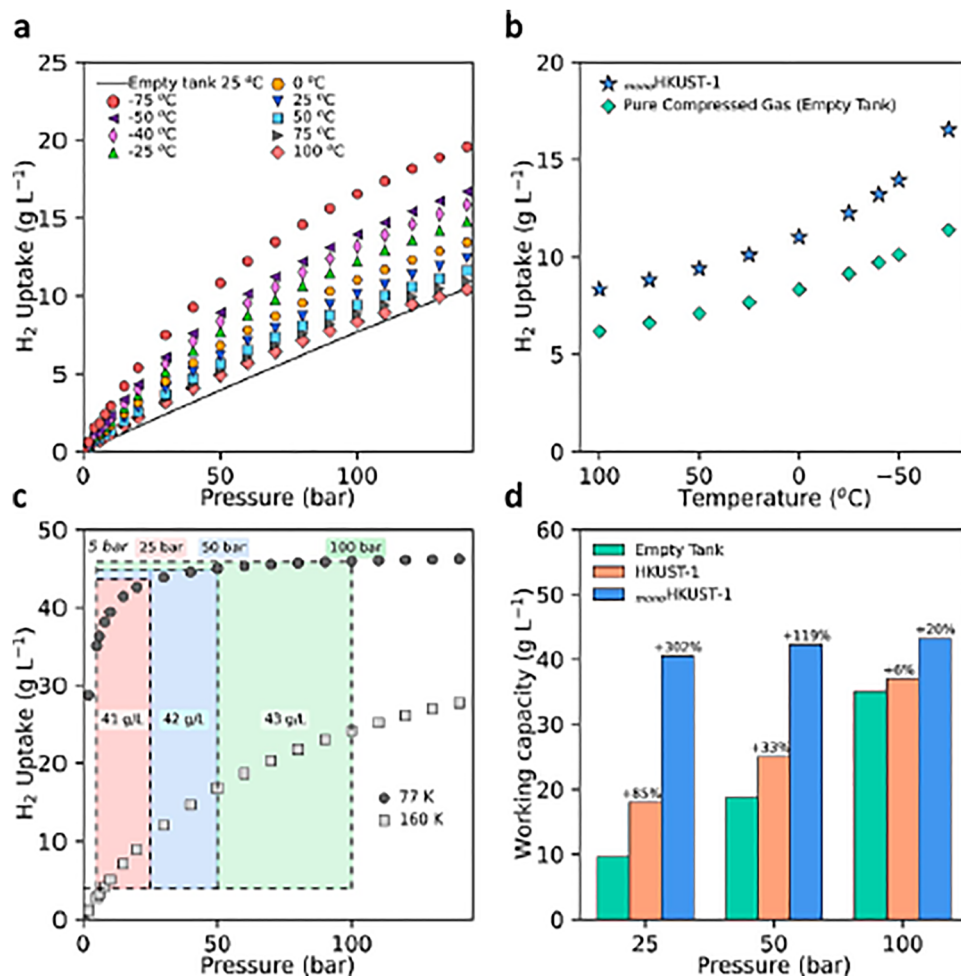
Fig. 28 (a) H_2 uptake of $_{mono}$HKUST-1 at different temperatures (b) volumetric storage of $_{mono}$HKUST-1 compared to compressed gas at 100 bars (c) H_2 delivery under cryogenic conditions and (d) deliverable H_2 capacity of $_{mono}$HKUST-1 compared to HKUST-1 powder and an empty tank at various adsorption pressures at 77 K.[31] Reproduced with permission from ref. 31. Copyright (2022) American Chemical Society.

monolith across all pressures, attributed to its hierarchical pore structure enhancing gas diffusion. Pressure decay measurements further confirm the monolith's stability, exhibiting slower pressure drop at 40 bar due to better heat dissipation and stronger gas–framework interactions. Together, these results establish monolithic HKUST-1 as technologically advantageous for methane storage, combining high capacity with rapid, stable adsorption–performance metrics that pelletized forms compromise for mechanical stability.

Lawson et al.[56] prepared polyethyleneimine (PEI) and tetra-ethylenepentamine (TEPA) impregnated MIL-101 monoliths MOFs using 3D printing technique, through pre- and post-functionalization approaches, and evaluated their CO_2 capture performances. The adsorption analysis results indicated that all impregnated monoliths showed improved CO_2 capacities from the pristine monolith at dilute concentrations, and pre-impregnation yielded higher CO_2 uptakes than post-impregnation. Specifically, the pre-impregnated TEPA and pre-impregnated PEI monoliths, with 3.5 and 5.5 mmol N g^{-1} amine content, respectively, displayed a capture capacity of 1.6 and 1.4 mmol g^{-1}, respectively, at 3000 ppm and 25 °C.

Fig. 30 compares the CO_2 adsorption performance of powdered and monolithic forms of HKUST-1, UiO-66, and UiO-66-NH_2 through gravimetric and volumetric isotherms at 298 K.[85] While powdered MOFs exhibit higher gravimetric uptake due to their greater surface area,[33] monolithic MOFs address a critical challenge in industrial deployment by combining high bulk density[32] with preserved sorption performance, enabling superior volumetric separation efficiency in applications like carbon capture and gas purification.[34]

Energy storage

MOFs have gained considerable attention for energy storage applications due to their tunable porosity, high surface areas, and chemical versatility. However, conventional MOF powders often suffer from poor electrical conductivity and mechanical instability, limiting their performance in devices such as super-conductors and batteries. The development of monolithic MOFs offers a promising route to overcome these challenges by creating robust, continuous structure with enhanced electrical properties.[34,57,107] The tunable architecture of monolithic MOFs provides high strength while maintaining lightweight,
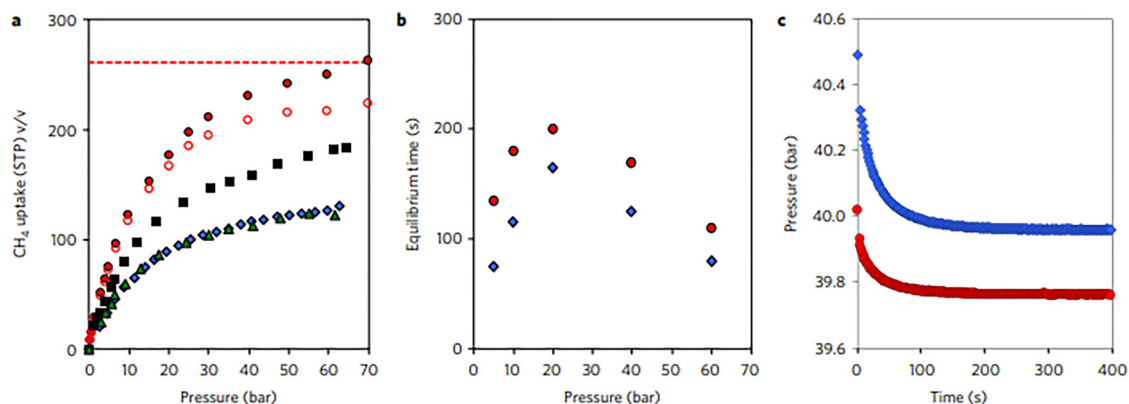
Fig. 29 Gas adsorption in HKUST-1. (a) Comparison of absolute volumetric methane adsorption isotherms at 298 K on $_{mono}$HKUST-1 (red filled circles), excess volumetric uptake on monoHKUST-1 (red open circles), HKUST-1 pellets under hand packing (blue diamonds), HKUST-1 pellets packed under 27.6 MPa (black squares), and HKUST-1 pellets under 68.9 MPa (green triangles). (b) Equilibrium time of methane adsorption at 298 K as a function of equilibrium pressure, and (c) decay of pressure with time at 40 bar for monoHKUST-1 (blue diamonds) and powdHKUST-1 (red circles).[32] Reproduced with permission from ref. 32. Copyright (2017) Springer Nature Limited.

making them portable energy storage systems.[108] Additionally, the use of MOF precursors allows the resulting derivatives to possess numerous active sites, thereby improving the utilisation of the intrinsic active sites. The structural advantage translates to impressive performances across a range of energy-related applications, including batteries, supercapacitors, and electrocatalysis.[109]

One innovative approach involves the fabrication of monolithic composites of MOFs and conductive additives like graphene. A particularly notable study[107] demonstrated the synthesis of a composite material based on HKUST-1 and commercial, non-modified graphene. In this method, a one-pot synthesis strategy was employed to produce a moldable composite without the need

for graphene oxidation or chemical functionalization, which can otherwise degrade the electrical properties of graphene. By carefully controlling the graphene loading during synthesis, researchers were able to tune the porosity and achieve high surface areas ranging between 1078 and 1156 m^2 g^{-1}. Furthermore, the electrical conductivity of the resulting monolithic coatings showed a significant dependence on graphene content, reaching values from 7.6×10^{-6} S m^{-1} up to 6.4×10^{-1} S m^{-1} (Fig. 31).

Moving forward, further research is needed to optimize the structural stability, conductivity, and scalability of monolithic MOFs for commercial energy storage applications. Strategies such as composite formation with conductive materials (e.g.,
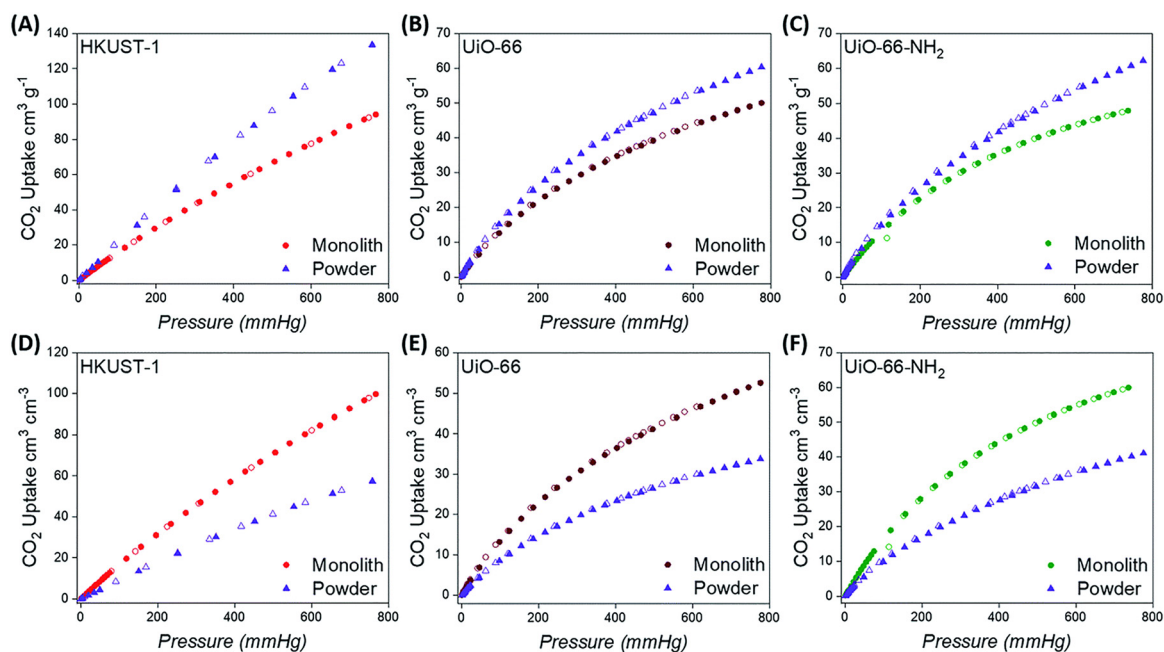

Fig. 30 Gravimetric (A)–(C) and volumetric (D)–(F) CO_2 adsorption isotherms at 298 K for monolithic and powdered HKUST-1, UiO-66 and UiO-66-NH_2 materials. Closed symbols represent adsorption while open symbols represent desorption.[85] Reproduced from ref. 85, with permission from the Royal Society of Chemistry.
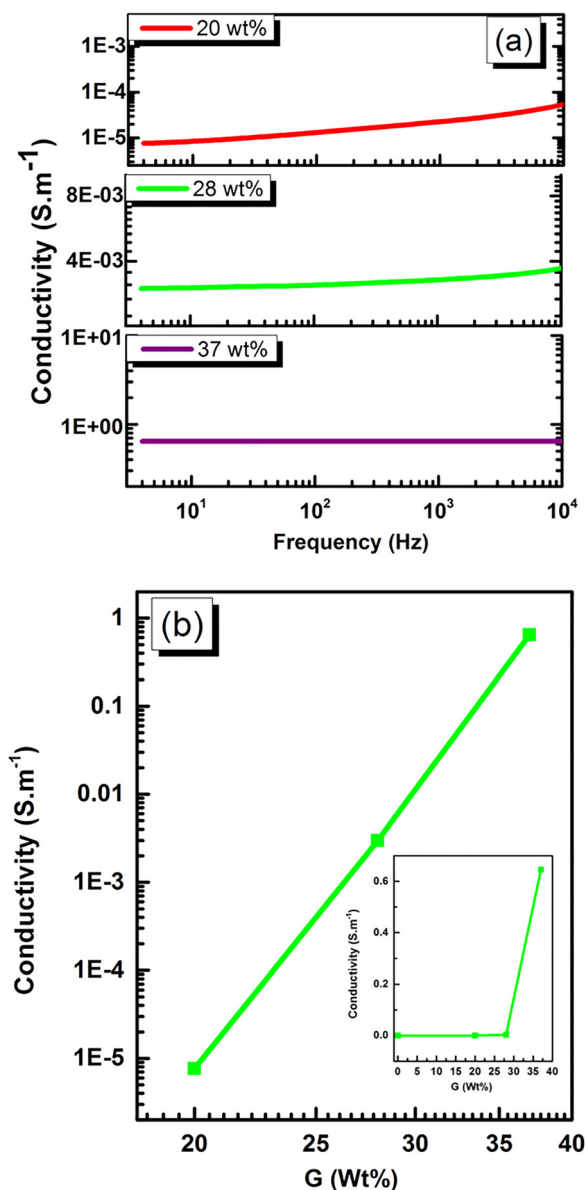
Fig. 31 (a) Conductivity measurements for several monoliths of HKUST-1 containing increasing loadings of G, and (b) electrical conductivity measured at 4 Hz for the three monolith composites.[107] Reproduced with permission from ref. 107. Copyright (2019) American Chemical Society.

graphene, carbon nanotubes),[110] doping with transition metals, and hybridizing with other porous materials could significantly enhance their electrochemical properties. With continued innovation, monolithic MOFs are poised to play a critical role in the development of next-generation energy storage systems.

Water purification

Monolithic MOFs excel in adsorption, catalytic degradation, and membrane-based separation of contaminants. Their interconnected porosity facilitates rapid diffusion of water pollutants such as heavy metals, organic dyes, pesticides and pharmaceuticals with uptake capacities rivalling powdered MOFs.[45,111,112] These contaminants are often challenging to

eliminate through conventional water treatment methods such as filtration, sedimentation, membrane bioreactors, and even advanced oxidation processes. To overcome these limitations, studies have demonstrated that monolith MOFs can be dispersed in wastewater to adsorb pollutants after which they can be recovered by filtration. Subsequently, the monolith MOFs can then be regenerated *via* solvent extraction, making them reusable and cost effective.[90]

For instance, Wang *et al.* developed a monolithic, hydrophobic ZIF-8 material (IPD-mesoMOF-12) by packing sufficiently small nanocrystals to create interparticle mesopores. The monolith exhibited a high BET surface area (1732 m^2 g^{-1}) and mesopore volume (up to 1.70 cm^3 g^{-1}). When tested for toluene removal from aqueous solution, it achieved a high Langmuir adsorption capacity of 242 mg g^{-1}, surpassing typical activated carbons, and reached equilibrium within 30 minutes. Critically, the monolith demonstrated excellent regenerability and the framework's structural integrity was maintained after recycling.[45]

Parsazadeh *et al.*[111] prepared HKUST-1 monolith MOF and used it as an adsorbent for the removal of eosin yellow and malachite green dyes. The study concluded that the HKUST-1 monolith MOF exhibited high efficiency for dye removal, highlighting its potential as an effective adsorbent material. Similarly, Yao *et al.*,[113] applied a freeze casting procedure in liquid nitrogen to prepare Ti-MOF monolith/polymer composites. Dye adsorption experiments were conducted on methylene blue, methyl orange and indigo carmine. It was observed that efficient adsorption occurred across pH range of 3–9. This work successfully demonstrated an alternative strategy for synthesising monolithic MOFs/polymer composites, offering a promising route for wastewater treatment application beyond the traditional use of powders. The results of the tests are shown in Fig. 32, where the monolithic composite displays superior activity in wastewater treatment coupled to easier separation from solution.

UiO-66-NH$_2$-CS aerogel monolith synthesised by Liu *et al.* through covalent cross linking was used to investigate the adsorption of Pb^{2+} from aqueous solutions. The success of this study shows that such synthesis methods may offer an effective route for transforming MOF powder particles into more flexible and mouldable forms, facilitating easier application in pollution treatment fields.[114] Similarly, Cu–BTC/NFC aerogel composites were synthesised using a direct mixing method, followed by gelation and freeze drying. Adsorption studies were carried out targeting the organic dye congo red and a heavy metal Mn^{7+}. The Cu-BTC/NFC monolith showed exceptional adsorption capacity for congo red and also acted as a reducing agent, removing permanganate ions by reducing them to manganese dioxide as illustrated in Fig. 33.[115]

Monolithic MOFs with large surface areas, tuneable wettabilities and good water resistance have been shown to play an important role in oil–water separations. In a recent study, a superhydrophobic (water contact angle of above 170°), water-stable MOF containing Cu^{2+} and hexafluorinated dicarboxylate linkers was prepared. After coating on a porous support, the

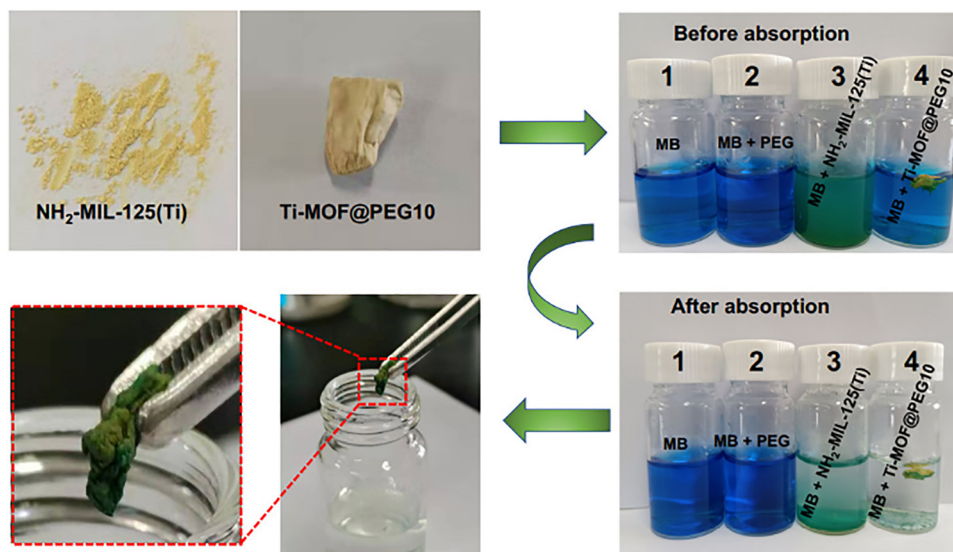**Fig. 32** Comparison of NH$_2$-MIL-125(Ti) powder and monolith Ti-MOF@PEG10 composite in dye absorption.[113] Reproduced with permission from ref. 113. Copyright (2025), Elsevier B.V.
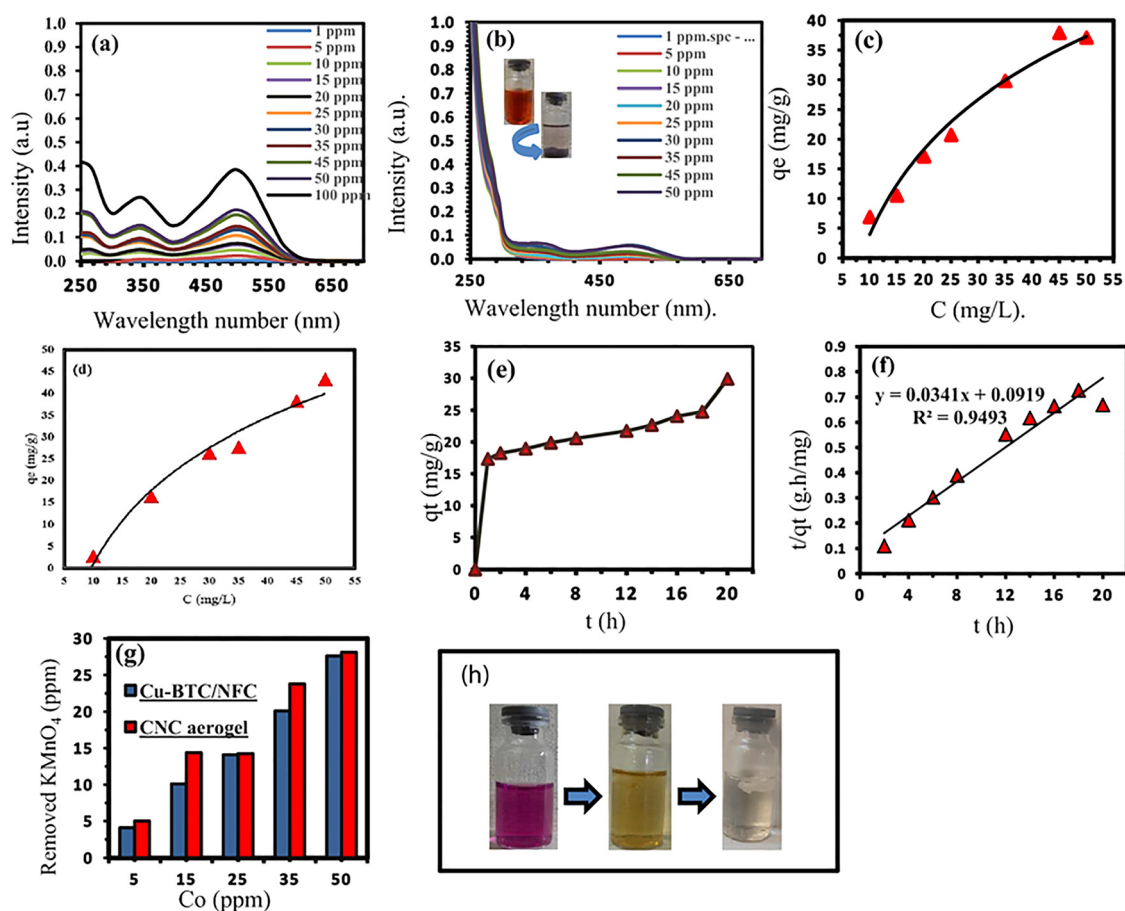

Fig. 33 (a) The UV-vis spectra of aqueous solutions of congo red before adsorption, (b) after exposing to Cu-BTC/NFC for 18 h, (c) adsorption isotherm of Cu-BTC/NFC aerogel composite for various concentrations of Congo Red, (d) adsorption isotherm for different concentrations of Congo Red in Cu-BTC/CNC aerogel composite, (e) the time dependency of the adsorption, (f) the pseudo-second-order model for the kinetics of the reaction, (g) the CNC aerogel and Cu-BTC/NFC aerogel composite adsorption isotherm for various concentrations of KMnO$_4$. (h) The colour change process during the reduction of KMnO$_4$.[115] Reproduced with permission from ref. 115. Copyright (2025) Springer Nature Limited.
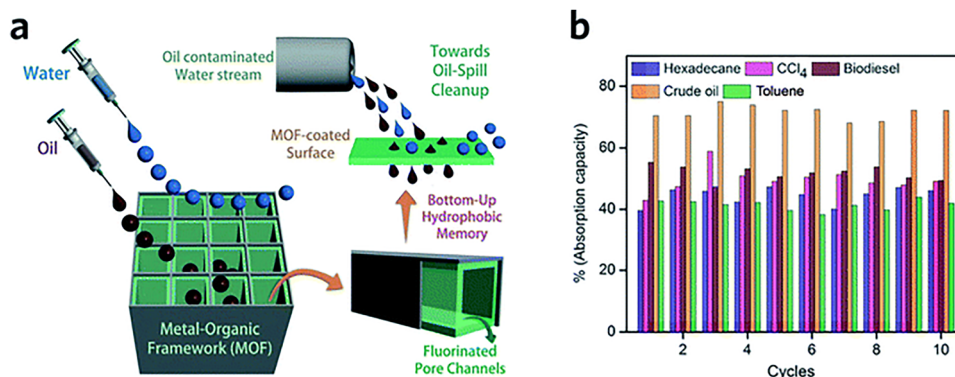
Fig. 34 Oil–water separation using monolithic MOF materials. (a) Schematic diagram of oil–water separation with the monolith MOF containing fluorinated linkers. (b) Oil absorption capacities of the monolithic MOF containing fluorinated linkers.[90] Reproduced with permission from ref. 90. Copyright (2020) Royal Society of Chemistry.

monolithic MOF film exhibits excellent oil absorption capacities and reusability, during the separation of hexadecane, biodiesel, toluene and crude oil from water[90] (Fig. 34).

Sensing

Detection is a critical process across many sectors of the chemical industry, driving essential operations such as pollution monitoring, industrial safety and medical diagnostics. In this context, monolithic materials have gained significant attention, offering unique advantages over traditional sensing materials.[32] A variety of sensing techniques have been developed utilising monoliths, particularly the electrical/chemi-resistive method.[116,117]

A unique monolithic chemiresistor sensor was utilised for detection of formaldehyde, a probable carcinogen (Fig. 35).
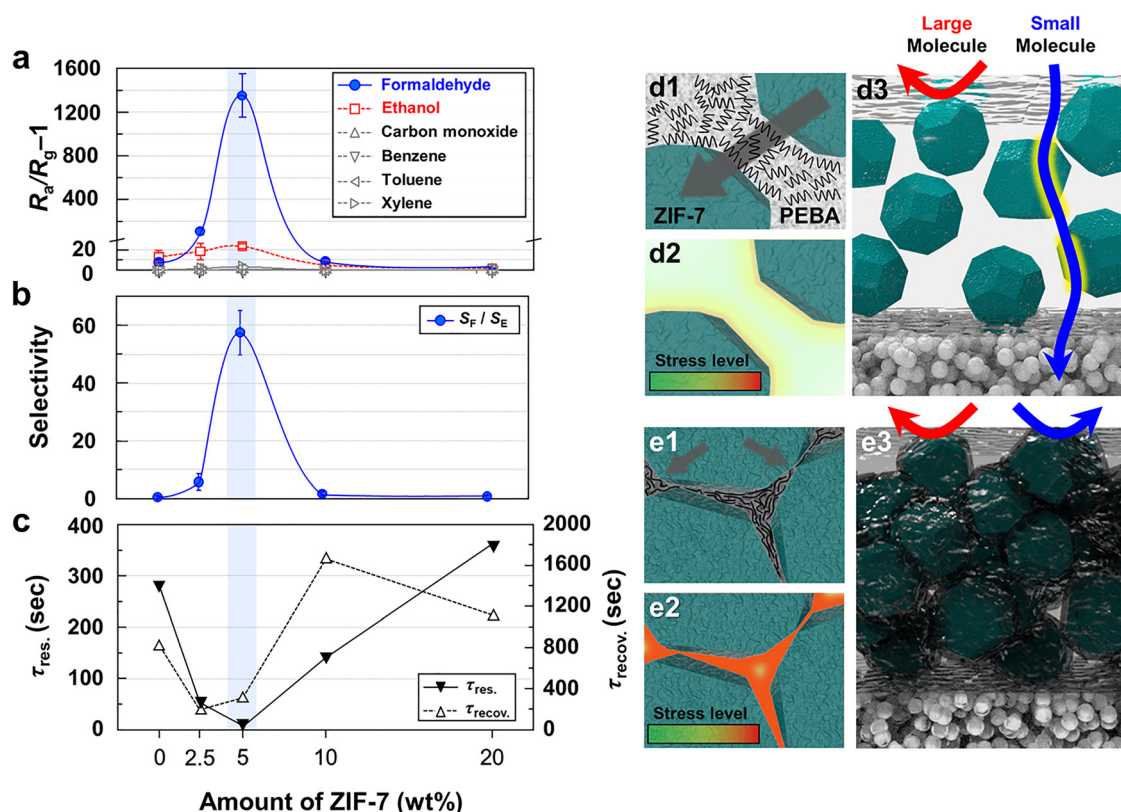

Fig. 35 Gas response, formaldehyde selectivity, response/recovery times, and gas-sensing mechanism. (a) Gas response of pure PEBA/TiO$_2$, 2.5MMM/TiO$_2$, 5MMM/TiO$_2$, 10MMM/TiO$_2$, 20MMM/TiO$_2$ sensors (temperature: 23 °C). (b) Formaldehyde selectivity to ethanol of pure PEBA/TiO$_2$, 2.5MMM/TiO$_2$, 5MMM/TiO$_2$, 10MMM/TiO$_2$, 20MMM/TiO$_2$ sensors. (c) 90% response time ($\tau_{res.}$, left) and 90% recovery times ($\tau_{recov.}$, right) of pure PEBA/TiO$_2$, 2.5MMM/TiO$_2$, 5MMM/TiO$_2$, 10MMM/TiO$_2$, and 20MMM/TiO$_2$ sensors. (d) and (e) Schematic illustration of gas penetration model, stress level, and polymer configuration when mild amount of ZIF-7 loading in PEBA (d) and excessively high amount of ZIF-7 loading in PEBA (e).[116] Reproduced with permission from ref. 116, Copyright (2024) American Chemical Society.

TiO_2 was coated with $_{mono}$ZIF-7 providing a distinctive and selective pathway for formaldehyde detection.[116] The key innovation lies in the synergistic combination of two mechanisms: UV light activation of the TiO_2 layer at room temperature, which selectively enhances sensitivity to highly reactive gases like formaldehyde and ethanol while ignoring other interferents, and the molecular sieving effect of the ZIF-7/PEBA MMM overlayer. The precisely tuned pore aperture of ZIF-7 ($\sim$0.3 nm) allows the smaller formaldehyde molecules (0.373 nm) to diffuse through to the sensor surface while effectively blocking larger interfering gases such as ethanol (0.45 nm), benzene, and toluene (0.585 nm). This strategy resulted in exclusive, ultrasensitive detection of formaldehyde down to 25 ppb with an ultrahigh selectivity ratio ($>$50) over ethanol at room temperature. This monolithic design led to improved sensitivity and stability compared to conventional sensor coatings.

In a related study, MOF(Tb) xerogel presented its application as chemosensor for the selective detection of nitroaromatics such as 2,4-dinitrophenol (2,4-DNT) and 2,6-dinitrophenol (2,6-DNT). Further experiments demonstrated excellent selectivity and recyclability, maintaining its performance across multiple sensing cycles.[118] ZIF-8 monolithic membranes have been applied in humidity sensing, taking advantage of their hydrophobic/hydrophilic balance, although improvements are needed to address water stability challenges.[119] Humidity sensing is another area where monoliths have shown potential. However, challenges remain, particularly regarding the fragility of many materials under aqueous conditions, which necessitates further research and development to improve their stability and durability.[120,121]

In a recent study by Li et al.,[117] a monolithic MOF-based metal–insulator–metal (MIM) resonator was developed for high-performance optical chemical sensing. The device was constructed by sandwiching a monolithic HKUST-1 surface-mounted metal–organic framework (SURMOF) film between two gold layers, fabricated via a layer-by-layer deposition method. The structure exhibited high reflectivity ($>$95%) and tunable coloration across the visible spectrum by varying the MOF thickness. To overcome the diffusion limitation imposed by the top metal layer, femtosecond laser-processing was used to create microwell arrays on the surface, which significantly enhanced the adsorption and diffusion of analyte molecules into the porous MOF layer without compromising optical performance.

The optimized device with a microwell period of 40 μm and height of 220 nm demonstrated rapid response (5.2 s) and high sensitivity to xylene vapours, with a detection limit of 17.39 ppm, as shown in Fig. 36(a)–(c). The real-time reflectance response, detailed in Fig. 36(d)–(f), further confirmed the fast kinetics and high dynamic range of the sensor. The integration of monolithic MOFs into MIM resonators represents a significant advancement in optical sensing platforms, combining high structural integrity with enhanced analyte accessibility and real-time monitoring capability.

Multifunctional composites and emerging applications

The integration of monolithic MOFs with other functional materials represents a frontier in designing advanced composites that leverage synergetic effects. By moving beyond pure MOF monoliths, these composites address limitations such as poor electrical conductivity, limited stability, or lack of specific functionality, opening doors to emerging applications.

A significant direction involves the combination of MOFs with ionic liquids (ILs). ILs, known for their high ionic conductivity, thermal stability, and tunable chemistry, can be encapsulated within MOF pores or used to form composite monoliths. For example, as highlighted in recent reviews, IL/MOF composites are being explored as advanced solid electrolytes in energy storage devices, highly selective membranes for gas separation, supported catalysts for CO_2 conversion,[122] and as specialized stationary phases for chromatographic separations.[123] The monolithic form of such composites ensures ease of handling and integration into devices while the IL enhances host–guest interactions and ionic transport.

Similarly, the incorporation of two-dimensional materials like MXenes or molybdenum disulfide (MoS_2) with MOFs into monolithic structures has garnered significant interest. MXenes offer high electrical conductivity and rich surface chemistry, while MoS_2 is a renowned semiconductor catalyst.[124,125] A monolithic MOF–MXene composite could synergize the high surface area and selectivity of the MOF with the excellent electrical conductivity of MXenes, creating ideal electrodes for supercapacitors or electrocatalysis. Likewise, combining photoactive MoS_2 with MOFs in a monolithic scaffold can facilitate efficient charge separation and mass transport, significantly enhancing photocatalytic performance for reactions like water splitting or pollutant degradation.[126,127]

Beyond integrating other materials into MOF monoliths, a powerful strategy is the functionalization of the MOF's external surface to impart new properties to the entire monolithic structure. A recent pioneering study by Bogdanova et al.[128] demonstrates this by grafting long-chain hydrocarbons (C18) onto the surface of highly oriented UiO-66-NH$_2$ MOF thin films. The key innovation lies in the well-defined, large spacing ($\sim$0.8 nm) between grafting sites on the monolith MOF lattice. These spacing forces the hydrocarbon chains to adopt a coiled, brush-like conformation with high conformational entropy. When a water droplet contacts this surface, the chains must stretch to accommodate it, incurring a large entropic penalty that effectively pushes the water away, resulting in a superhydrophobic surface with water contact angles exceeding 160°, as illustrated in Fig. 37. Counterintuitively, this entropy-driven mechanism outperforms traditional chemical strategies, as using less flexible fluorinated chains yielded lower hydrophobicity. This approach creates a novel type of functional composite where the MOF monolith is not just a porous scaffold but an engineered platform for controlling macroscopic interfacial properties like wettability and adhesion through nanoscale architectural design.

A highly impactful emerging application for these advanced materials is in atmospheric water harvesting (AWH), where the inherent powdery nature and poor mechanical stability of pure MOFs are major obstacles to practical implementation. Research is advancing on two key fronts: the creation of pure
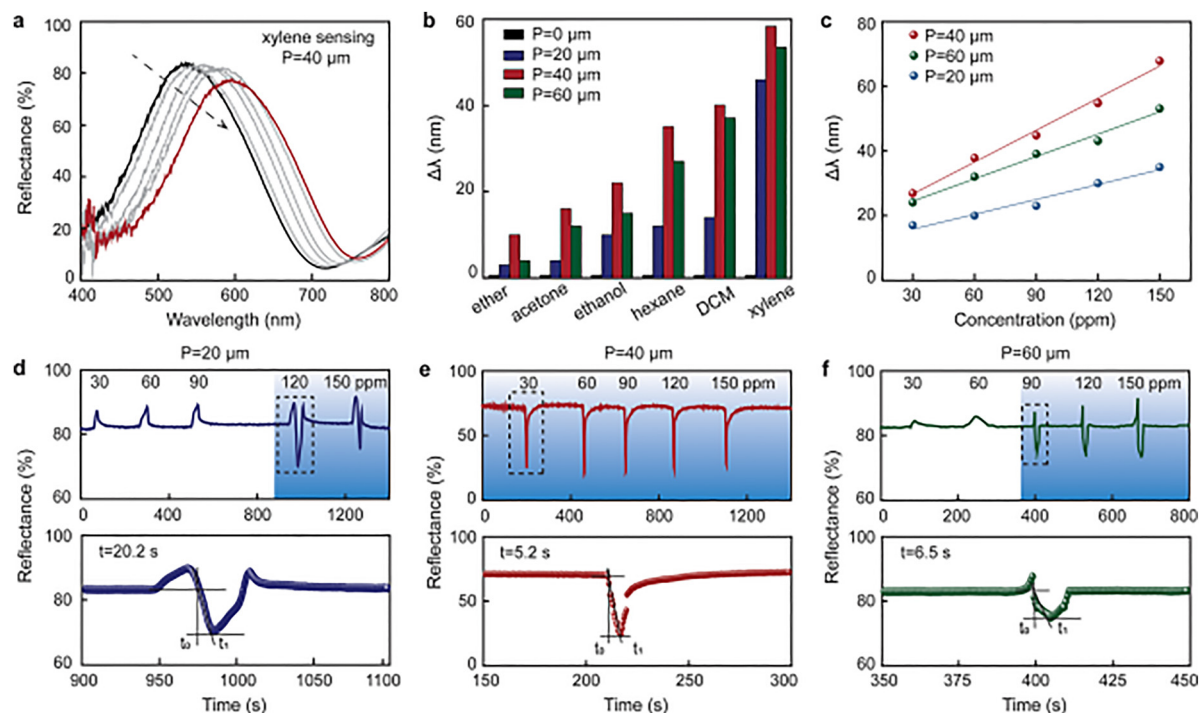
Fig. 36 Chemical sensing on the monolithic MOF-based MIM resonator with different periods of the microwell arrays. (a) Reflection spectral shifts of the MOF-based MIM resonator with microwell arrays during xylene sensing. (b) Reflection band shifts upon exposure to various saturated chemical vapours. (c) Concentration-dependent sensing performance and (d)–(f) time-dependent reflectance changes for different microwell periods.[117] Adapted with permission from ref. 117. Copyright (2023) American Chemical Society.

MOF monoliths and the integration of MOFs into composite matrices. The review by Panahi-Sarmad *et al.*[23] details how integrating MOFs into macroporous monoliths like aerogels, cryogels, or foams creates a hierarchical structure that combines the nanoscale adsorption properties of MOFs with the mechanical integrity and rapid mass transport of the monolith scaffold. The paper highlights a composite where MOF-801 particles are integrated into a cross-linked calcium alginate (CA) matrix with polypyrrole (PPy) to form a porous monolith (denoted as PMC). This composite leverages the MOF's high-water affinity at low humidity, the alginate's structural support and hydrophilicity, and the polypyrrole's photothermal properties for efficient solar-driven desorption. The results showed a water uptake capacity of 1.106 g g^{-1} at 60% RH (relative humidity) and a remarkable daily water harvesting rate of 1.081 kg of water per kg of sorbent in field tests, demonstrating the practical viability of such composites for arid regions. The synthesis, structure, and performance of this specific composite are illustrated in Fig. 38.

Furthermore, the authors discussed advanced fabrication techniques like 3D printing to create monolithic structures with optimized millimetre-scale grids for enhanced air circulation and water vapor interaction. This approach, combined with the encapsulation of hygroscopic salts like LiCl within the MOF-monolith matrix, preventing leakage and agglomeration issues associated with pure salts while significantly boosting water uptake capacity under low-humidity conditions.

In a parallel, the synthesis of pure robust monolithic MOFs, such as the hierarchically porous MOF-801 monolith prepared

via sol–gel phase separation (as previously discussed and shown in Fig. 3),[39] directly addresses the critical barriers of poor mass transfer and high pressure drop inherent in packed powder beds. The performance of this binder free monolith is compelling: it achieves excellent water uptake at 30% RH even at a 4 g scale, providing a viable pathway for industrial-scale water harvesting devices by avoiding the pore blockage and reduced capacity typical of composite sorbents. Quantitatively, the material demonstrated a superior water vapor sorption capacity, exceeding that of conventional MOF-801 powder by 1.2 times in small batches and outperforming compressed tablets by 1.4 times in large-scale tests at 30% RH. Furthermore, the structure showed excellent cyclic stability. Crucially, for scale-up, the monolith possessed remarkable mechanical robustness, with a compressive Young's modulus of up to 61.3 MPa, enabling it to withstand practical handling, as comprehensively illustrated in Fig. 39.

Together, these studies underscore a major trend in the field: the move beyond powder synthesis towards engineering monolithic structures, whether pure or composite, with tailored hierarchies that are essential for real-world applications requiring efficient fluid transport, rapid sorption kinetics, and mechanical durability.

Beyond compositing, monolithic MOFs represent a promising class of precursors for the synthesis of shaped, derived functional materials. The thermal decomposition of MOFs under controlled atmospheres (a process known as calcination) is a well-established route to transform powdered MOFs into
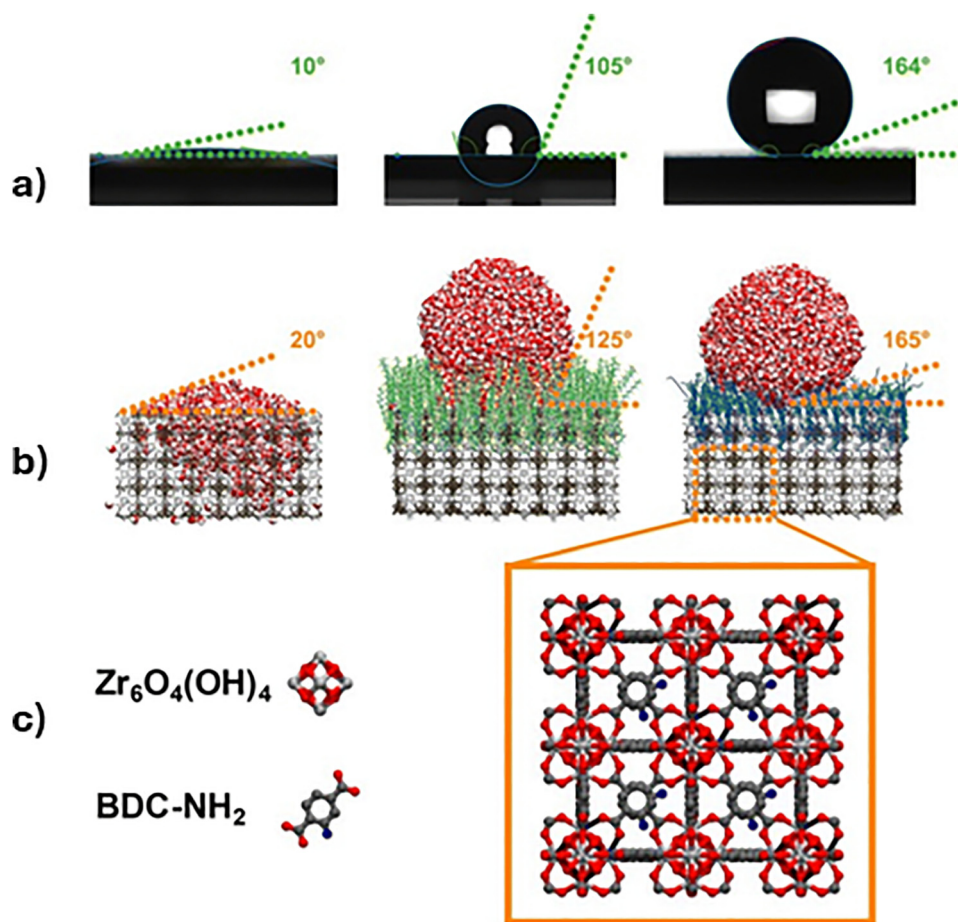
Fig. 37 Engineered super hydrophobicity showing the transition from a hydrophilic pristine monolith MOF surface to a super hydrophobic surface after entropy-driven functionalization with C18 hydrocarbon chains. (a) Experimental (b) Simulated and (c) monolith MOF structure.[128] Reproduced from ref. 128 Copyright (2025) Royal Society of Chemistry.
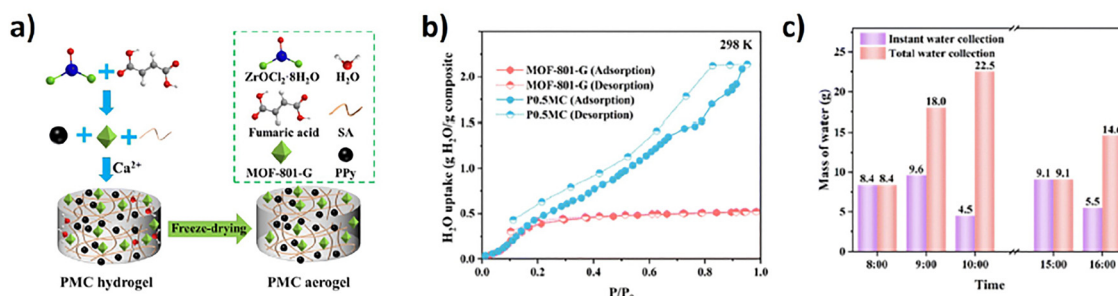

Fig. 38 (a) Schematic of the PMC monolith synthesis *via* freeze-drying. (b) Water adsorption isotherm of the P0.5MC composite showing high capacity. (c) Real-world AWH performance data demonstrating high daily water yield.[23] Reproduced with permission from ref. 23, under Creative Commons Attribution Licence (CC BY).

functional derivatives like metal oxides, carbon-based composites, or single-atom catalysts. This concept of using MOFs as sacrificial templates is extensively demonstrated in the literature for powdered systems, yielding a wide range of materials for applications in catalysis and sensing. For instance, a zeolitic imidazolate framework (ZIF) can be converted into nitrogen-doped porous carbon with high electrical conductivity for electrocatalysis,[129] and sophisticated materials like CuO/Cu$_2$O can be derived from HKUST-1,[130] exhibiting excellent performance in applications such as pollutant degradation.

In a related study, cobalt-based zeolitic imidazolate frameworks (ZIF-67) was converted into hollow cobalt sulphide (Co$_3$S$_4$) nanopolyhedrons through a solvothermal sulphidation process.[131] The resulting material inherits the high surface area
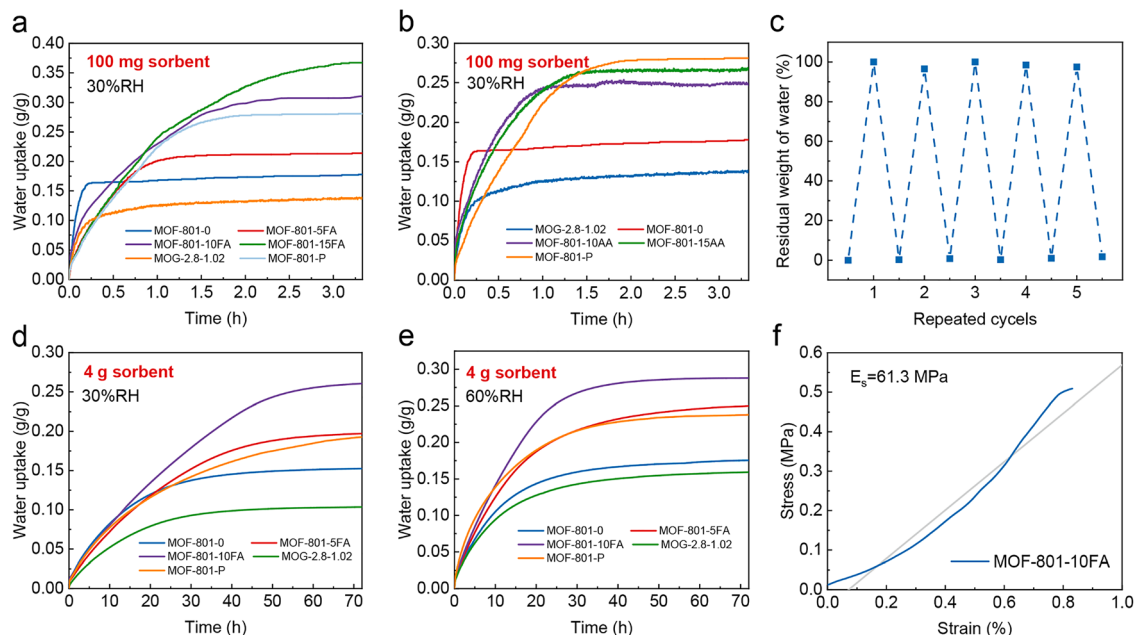
Fig. 39 Water vapor sorption kinetics at 30% RH and 25 °C of the sorbents (all in powder form) treated by formic acid (FA) (a) and acetic acid (AA) (b) with a mass of 100 mg. The repeated sorption and desorption performance of MOF-801-10FA (c). Water vapor sorption kinetics at 30% RH (d) and 60% RH (e) and at 25 °C of the sorbents (all in monolithic form) with a mass of 4 g. The stress–strain curve of MOF-801-10FA with a slope equal to compressive Young's modulus (f).[39] Reproduced with permission from ref. 39. Copyright (2023) Elsevier B.V.
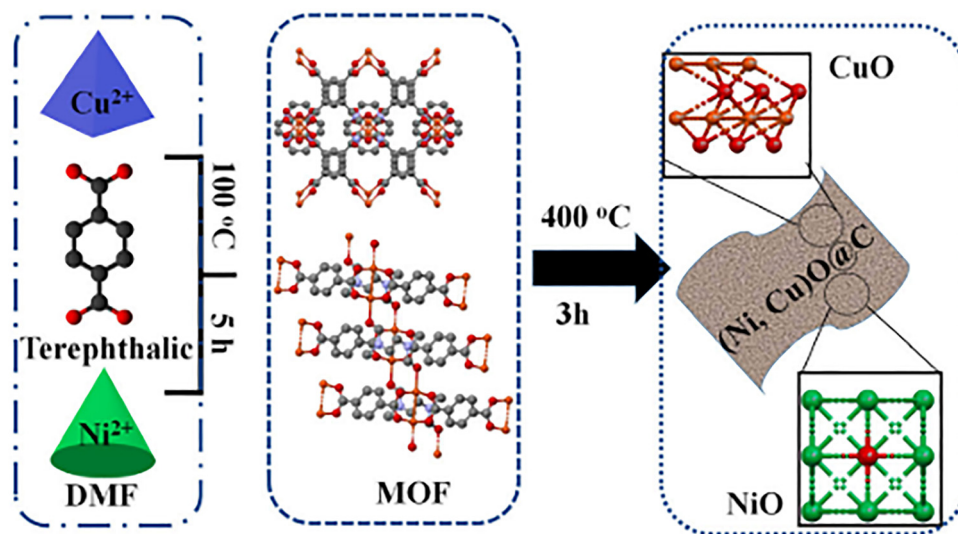

Fig. 40 Schematic illustration of the synthesis of hierarchical (Ni,Cu)O@C derivatives *via* calcination of a terephthalate-based MOF precursor.[132] Reproduce with permission ref. 132, under the terms of Creative Commons Attribution Licence (CC BC).

and porous morphology of the ZIF-67 precursor but gains significantly enhanced electrochemical activity due to the formation of a metal sulphide. When applied as an electrode material, these hollow Co_3S_4 structures demonstrate excellent supercapacitive performance, highlighting the potential of this top-down synthesis route for creating advanced energy storage materials.

The exciting potential for monolithic MOFs lies in applying this same principle to a pre-formed macroscopic structure.

While the current literature on the direct calcination of pre-formed, macroscopic MOF monoliths into shaped derivatives is more limited, the work on powders provides a strong foundational proof-of-concept. It indicates that the calcination pathway could be effectively transferred to monolithic MOFs to create robust, structured functional materials with retained macroscopic integrity. This potential is underscored by research that utilizes structured MOF precursors. A compelling example is the work by Zhang *et al.*,[132] who used a solvothermal

method to synthesize a terephthalate-based MOF precursor, which was then calcined in air at 400 °C for 3 h to yield (Ni, Cu)O@C derivatives with a hierarchical porous composite structure containing macropores (Fig. 40). This pathway from a structured MOF to a structured derivative effectively demonstrates how the advantages of a monolithic form can be transferred to a new class of materials with distinct properties, highlighting the viability of this approach for future monolithic systems.

Challenges and future perspectives

Monolithic MOFs represent a significant advancement in porous materials engineering, offering a unique combination of hierarchical porosity, mechanical stability, and enhanced processability into integrated structures. Although these attributes position them as strong candidates for advanced applications, the technology is still in its early stages. Several critical challenges must be addressed to fully unlock the potential of monolithic MOFs.

According to Lorignon et al.,[57] during 3D printing of monolith MOFs there is a possible loss of key properties, particularly porosity and crystallinity. Such loses can restrict the final shape and architecture of the monolith, ultimately limiting its applicability in practical systems. Another significant challenge relates to the workability of monolithic MOFs, largely due to their limited stability in water, as noted by Duan et al.[34] In their study they further highlighted that the synthesis mechanisms of monolith MOFs are still unclear. Additionally, for monolithic MOFs to be viable across a wide range of applications, large-scale production is essential; however, current synthetic strategies often require long reaction times.[34] For example, as highlighted in the synthesis sections, certain sol–gel processes require extended aging times of up to 120 hours,[71] and DIW ink preparation can be a multi-step process taking 1–2 days,[51,52] directly impacting production throughput.

While monolithic MOFs hold great potential for diverse applications, several environmental concerns must also be addressed. In particular, there is need to explore fabrication methods that enable the mass production of complex monolithic structures, preferably through solvent-free techniques or employing environmentally benign solvents in the synthesis process.[90]

Combining MOFs with other materials, such as polymers and nanoparticles, presents and effective strategy for creating multifunctional composites that leverage the strengths of each component, resulting in materials well-suited for a variety of applications. Although this concept remains under active investigation, several researchers have already explored its potential.[23,128] For instance, Tian et al.[133] encapsulated polyvinylpyrrolidone (PVP)-stabilized gold nanoparticles (Au NPs) within ZIF-67 particles to form monolithic Au@ZIF-67 composites. The composites combine the benefits of both constituents, retaining the characteristic porosity and high bulk density from $_{mono}$ZIF-67 along with the localized surface plasmonic resonance (LSPR) properties from Au NPs. This results in an enhanced CO_2 photoreduction rate as compared to pristine

ZIF-67. Under visible irradiation, the optimal monolithic Au@ZIF-67, $_{8mL}$Au@ZIF-67, achieved a volumetric CO production rate 1.5 and 3 times higher than $_{mono}$ZIF-67 and $_{pow}$ZIF-67, respectively. Additionally, the monolithic composite exhibits excellent mechanical stability, as indicated by their high elastic modulus and hardness.

In another notable study, Avila et al.[134] synthesised a perovskite@ MOF monolith composite, which demonstrated exceptional stability against humidity, temperature variations, and exposure to different solvents (Fig. 41). Overall, the integration of nanoparticles with monolithic MOFs offers exciting opportunities for enhancing functionality and broadening the range of potential applications.

Sustainability and environmental impact

When assessing sustainability and environmental footprint of MOFs, several factors come into play. Typically, the materials are composed of metal ions and organic linkers. Metals like iron, zinc, and copper are relatively benign, whereas rare, energy-intensive to extract, or toxic metals like cadmium carry a higher environmental cost. Similarly, the choice of organic linkers and their synthetic origin (petrochemical, bio-based, etc.) also matters.[135]

A major determinant of impact is the synthesis route, including solvents, energy inputs, and purification. Traditional synthesis often relies on toxic solvents like dimethylformamide (DMF),[136] raising concerns about waste and safety, alongside energy-intensive processes. Recent life cycle assessment (LCA) studies (Ntouros et al., 2021)[135] highlight that solvent use (e.g., DMF and methanol) can constitute over 80% of the total environmental burden, with post-synthetic washing sometimes costing more than the MOF formation itself. This context has driven interest in solvent-free approaches for synthesizing monolithic MOFs.

Several alternative strategies have been explored to minimize solvent usage and reduce environmental impact. Mechanochemical synthesis and freeze casting are among the most promising solvent-free or low-solvent methods. For instance, a reusable NH_2-MIL-125(Ti)@polymer monolith fabricated via freeze casting exhibited an impressive adsorption capacity of 747.4 mg g^{-1} for wastewater dyes, outperforming pure MOF powders and demonstrating mechanical integrity for multiple reuses.[113] Mechanochemical synthesis, in particular, offers high space-time yields with lower energy and solvent consumption.[137] Reactive extrusion, another emerging approach, allows for continuous processing and significantly lowers the environmental impact compared to conventional solvothermal synthesis.[138]

Although some MOF synthesis processes still demand considerable energy, contributing to their overall environmental footprint, the production of monolithic MOFs represents a more sustainable alternative. Their enhanced mechanical strength not only facilitates easier handling and recycling but also helps reduce material waste, further aligning with the principles of green chemistry. It is important to emphasize, however, that shaping methods such as freeze casting or extrusion only contribute to sustainability when the MOF
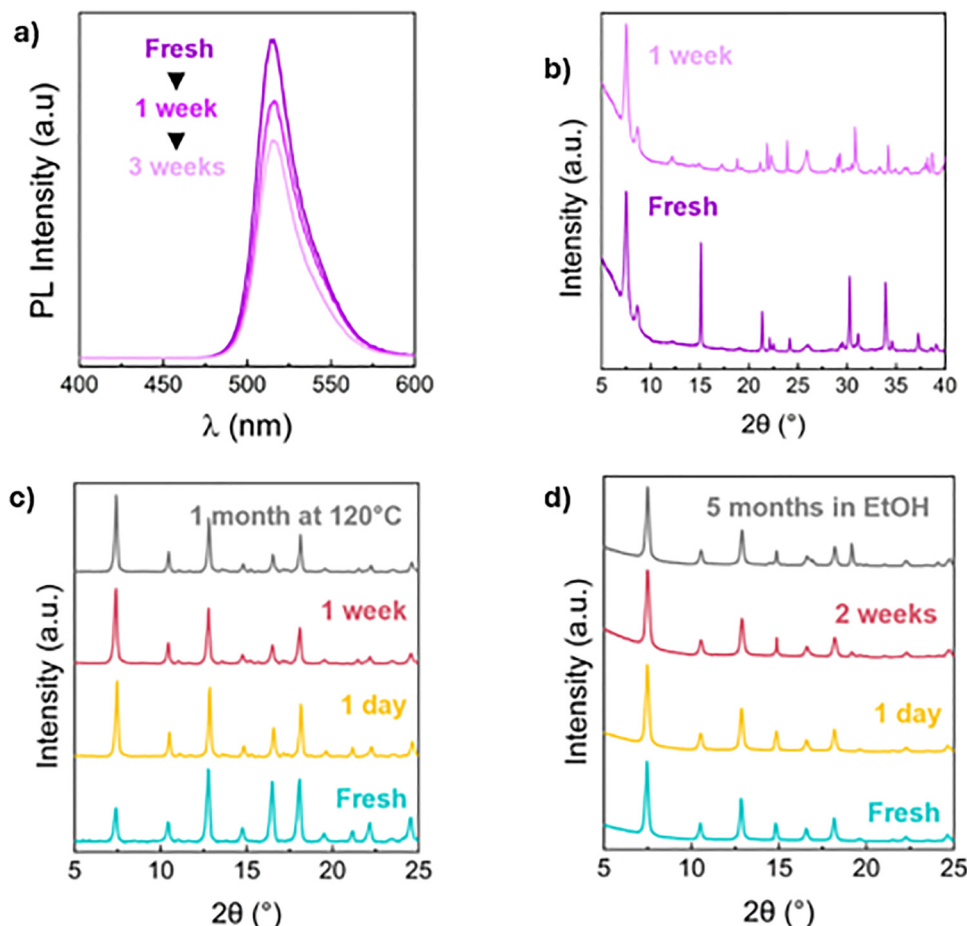
Fig. 41 (a) Temporal evolution of the photoluminescence spectrum of a MAPbBr$_3$@UiO-66 monolith over 3 weeks at 75% relative humidity, (b) PXRD patterns of the MAPbBr$_3$@UiO-66 monolith before (dark purple) and after (light purple) immersion in water for 1 week, (c) Evolution of PXRD patterns of the MAPbBr$_3$@ZIF-8 monolith when thermally stressed at 120 °C for 1 month, and (d) when immersed in EtOH for 5 months.[134] Reproduced with permission from ref. 134, under the terms of the Creative Commons CC-BY.

synthesis itself is green. Simply structuring a monolith using a sustainable technique does not offset the environmental burden of an upstream solvent-intensive MOF synthesis. Full sustainability must be evaluated across the entire lifecycle, from raw material sourcing, synthesis, purification, shaping, to end-of-life disposal or reuse.

Emerging trends and future directions

As the applications of monolithic MOFs continue to grow, there is increasing emphasis on enhancing functionality, scalability and sustainability.[22] This shift is evident in recent innovations in synthesis methods, which increasingly adopt green approaches such as solvent-free or aqueous-phase techniques, to minimize environmental impact.[139] Techniques like sol–gel and hydrothermal synthesis have been refined to support these goals, offering more environmentally friendly pathways while preserving material quality.[90,140] These methods also help reduce pollutant generation and often incorporate bio-based precursors.

In parallel, additive manufacturing techniques, particularly 3D printing, have emerged as powerful tools for engineering the hierarchical structure of monoliths. These approaches

enable the creation of complex architectures with improved functionality.[141] Looking forward, strategies such as roll-to-roll production and biomimetic design are gaining traction.[140] These aim is to bridge the gap between laboratory-scale research and industrial-scale production by enhancing cost-effectiveness and mechanical robustness under harsh operating conditions.

Another key development is the creation of hybrid composites through the incorporation of nanoparticles, polymers, ionic liquids or MXenes into monolithic MOFs.[126,127,133,134] These composites enhance multifunctionality, making them highly suitable for catalysis, sensing, and environmental remediation. For instance, hierarchical porous monoliths are increasingly used in water treatment and catalysis due to their superior mass transfer, catalytic activity, and separation efficiency, which are benefits arising from their integrated macro-, meso-, and microporous structures.

Recent advances in nanocharacterization techniques have been essential in supporting these developments. While scanning electron microscopy (SEM) and transmission electron microscopy (TEM)[142] provide detailed analyses of pore architectures and

phase distributions, and nanoparticle arrangements, a suite of newer tools is providing critical, mechanistic insights. Atomic force microscopy (AFM) is now pivotal for visualizing nanoscale deformation and damage resilience after mechanical testing, providing unambiguous evidence to complement quantitative data.[30] Furthermore, techniques like nano-FTIR spectroscopy offer nanochemical mapping with $\sim$20 nm resolution, enabling the correlation of local chemical environments (e.g., guest molecule distribution) with macroscopic mechanical and functional properties.[98] The integration of these methods with established techniques like nanoindentation is transforming the understanding of structure–property relationships in monolithic MOFs, guiding the rational design of next-generation materials with tailored properties. Mechanical and thermal testing further ensure that monolithic materials can withstand elevated pressures and temperatures.

Conclusion

The synthesis methods for monolithic MOFs are moving towards more green and efficient pathways, while their applications are also evolving into a wide range of fields including biomedical, energy and environmental sectors. Continued research in synthesis and application is expected to generate novel multifunctional composites, further broadening the practical use of these materials. Inherent challenges traditionally associated with conventional MOFs, such as poor mechanical stability, difficult handling and processing, have been significantly mitigated through the development of monolithic MOFs. Their enhanced structural integrity, ease of handling, and tunable properties position them as strong candidates for industrial applications including gas storage, catalysis, separation and drug delivery. Key methods for synthesis of monolith MOFs particularly sol–gel techniques and 3D printing, have shown significant potential in producing monolithic MOFs with tailored architectures and functionalities while offering routes to greener synthesis methods. As research progresses, overcoming issues related to scalability, reproducibility, mass transport limitations, and optimization of both physical and chemical properties will be crucial. Prospective work should focus on refining synthesis approaches, developing advanced nanocharacterisation tools, exploring innovative fabrication methods, and expanding the scope of applications into areas like atmospheric water harvesting and advanced sensing. With the rapid pace of advancements in this field, monolithic MOFs are on the verge of playing a pivotal role in addressing complex scientific and industrial challenges, ultimately contributing to the development of more efficient, sustainable technologies.

Author contributions

Donald Muringaniza – investigation, writing, original draft preparation; Laurencia Zulu – investigation, writing, original draft preparation; Linia Gedi Marazani – reviewing and editing; Piwai Tshuma –supervision, reviewing and editing; Gift Mehlana – conceptualization, supervision, resources, reviewing and editing.

Conflicts of interest

The authors declare no conflict of interest.

Data availability

No primary research results, software or code have been included and no new data were generated or analysed as part of this review.

Acknowledgements

References

1 S. Kaushal, G. Kaur, J. Kaur and P. P. Singh, First Transition Series Metal–Organic Frameworks: Synthesis, Properties and Applications, *Mater. Adv.*, 2021, **2**(22), 7308–7335, DOI: **10.1039/d1ma00719j**.

2 W. Xiang, Y. Zhang, Y. Chen, C. J. Liu and X. Tu, Synthesis, Characterization and Application of Defective Metal–Organic Frameworks: Current Status and Perspectives, *J. Mater. Chem. A*, 2020, **8**(41), 21526–21546, DOI: **10.1039/d0ta08009h**.

3 H. Furukawa, N. Ko, Y. B. Go, N. Aratani, S. B. Choi, E. Choi, A. Ö. Yazaydin, R. Q. Snurr, M. O'Keeffe, J. Kim and O. M. Yaghi, Ultrahigh Porosity in Metal–Organic Frameworks, *Science*, 2010, **329**(5990), 424–428, DOI: **10.1126/science.1192160**.

4 M. S. Alhumaimess, Metal–Organic Frameworks and Their Catalytic Applications, *J. Saudi Chem. Soc.*, 2020, **24**(6), 461–473, DOI: **10.1016/j.jscs.2020.04.002**.

5 C. Xu, R. Fang, R. Luque, L. Chen and Y. Li, Functional Metal–Organic Frameworks for Catalytic Applications, *Coord. Chem. Rev.*, 2019, **388**, 268–292, DOI: **10.1016/j.ccr.2019.03.005**.

6 S. Singh, N. Sivaram, B. Nath, N. A. Khan, J. Singh and P. C. Ramamurthy, Metal Organic Frameworks for Wastewater Treatment, Renewable Energy and Circular Economy Contributions, *npj Clean Water*, 2024, **7**(1), 124, DOI: **10.1038/s41545-024-00408-4**.

7 F. Gao, R. Yan, Y. Shu, Q. Cao and L. Zhang, Strategies for the Application of Metal–Organic Frameworks in Catalytic Reactions, *RSC Adv.*, 2022, **12**(16), 10114–10125, DOI: **10.1039/d2ra01175a**.

8 E. Linnane, S. Haddad, F. Melle, Z. Mei and D. Fairen-Jimenez, The Uptake of Metal–Organic Frameworks: A Journey into the Cell, *Chem. Soc. Rev.*, 2022, **51**(14), 6065–6086, DOI: **10.1039/d0cs01414a**.

9 F. Zhan, H. Wang, Q. He, W. Xu, J. Chen, X. Ren, H. Wang, S. Liu, M. Han, Y. Yamauchi and L. Chen, Metal–Organic Frameworks and Their Derivatives for Metal-Ion (Li, Na, K and Zn) Hybrid Capacitors, *Chem. Sci.*, 2022, **13**(41), 11981–12015, DOI: **10.1039/d2sc04012c**.

10 K. Sonowal and L. Saikia, Metal–Organic Frameworks and Their Composites for Fuel and Chemical Production via CO_2 Conversion and Water Splitting, *RSC Adv.*, 2022, **12**(19), 11686–11707, DOI: **10.1039/d1ra09063a**.

11 H. I. Adil, M. R. Thalji, S. A. Yasin, I. A. Saeed, M. A. Assiri, K. F. Chong and G. A. M. Ali, Metal–Organic Frameworks (MOFs) Based Nanofiber Architectures for the Removal of Heavy Metal Ions, *RSC Adv.*, 2022, **12**(3), 1433–1450, DOI: **10.1039/d1ra07034g**.

12 A. Schneemann, R. Dong, F. Schwotzer, H. Zhong, I. Senkovska, X. Feng and S. Kaskel, 2D Framework Materials for Energy Applications, *Chem. Sci.*, 2021, **12**(5), 1600–1619, DOI: **10.1039/d0sc05889k**.

13 M. Sai Bhargava Reddy, D. Ponnamma, K. K. Sadasivuni, B. Kumar and A. M. Abdullah, Carbon Dioxide Adsorption Based on Porous Materials, *RSC Adv.*, 2021, **11**(21), 12658–12681, DOI: **10.1039/d0ra10902a**.

14 D. Li, A. Yadav, H. Zhou, K. Roy, P. Thanasekaran and C. Lee, Advances and Applications of Metal–Organic Frameworks (MOFs) in Emerging Technologies: A Comprehensive Review, *Glob. Challenges*, 2024, **8**(2), 2300244, DOI: **10.1002/gch2.202300244**.

15 H. Ghasempour, K. Wang, J. A. Powell, F. Zarekarizi, X. Lv and A. Morsa, Metal – Organic Frameworks Based on Multicarboxylate Linkers, *Coord. Chem. Rev.*, 2021, **426**, 213524, DOI: **10.1016/j.ccr.2020.213542**.

16 B. Yeskendir, J. P. Dacquin, Y. Lorgouilloux, C. Courtois, S. Royer and J. Dhainaut, From Metal–Organic Framework Powders to Shaped Solids: Recent Developments and Challenges, *Mater. Adv.*, 2021, **2**(22), 7139–7186, DOI: **10.1039/d1ma00630d**.

17 J. Fonseca and T. Gong, Fabrication of Metal–Organic Framework Architectures with Macroscopic Size: A Review, *Coord. Chem. Rev.*, 2022, **462**, 214520, DOI: **10.1016/j.ccr.2022.214520**.

18 D. Bazer-Bachi, L. Assié, V. Lecocq, B. Harbuzaru and V. Falk, Towards Industrial Use of Metal–Organic Framework: Impact of Shaping on the MOF Properties, *Powder Technol.*, 2013, **255**(2014), 52–59, DOI: **10.1016/j.powtec.2013.09.013**.

19 R. E. Morris and L. Brammer, Coordination Change, Lability and Hemilability in Metal–Organic Frameworks, *Chem. Soc. Rev.*, 2017, **46**(17), 5444–5462, DOI: **10.1039/c7cs00187h**.

20 Y. Sun, Y. Zhu, S. Zhang and B. P. Binks, Fabrication of Hierarchical Macroporous ZIF-8 Monoliths Using High Internal Phase Pickering Emulsion Templates, *Langmuir*, 2021, **37**(28), 8435–8444, DOI: **10.1021/acs.langmuir.1c00757**.

21 Y. R. Lee, M. S. Jang, H. Y. Cho, H. J. Kwon, S. Kim and W. S. Ahn, ZIF-8: A Comparison of Synthesis Methods, *Chem. Eng. J.*, 2015, **271**, 276–280, DOI: **10.1016/j.cej.2015.02.094**.

22 X. Yu, B. Li, L. Wu, D. Shi and S. Han, Review and Perspectives of Monolithic Metal–Organic Frameworks: Toward Industrial Applications, *Energy Fuels*, 2023, **37**, 9938–9955, DOI: **10.1021/acs.energyfuels.3c00858**.

23 M. Panahi-Sarmad, T. Guo, S. A. Hashemi, A. Ghaffarkhah, S. Wuttke, O. Rojas and F. Jiang, Hierarchically MOF-Based Porous Monolith Composites for Atmospheric Water Harvesting, *Adv. Mater.*, 2025, e2413353, DOI: **10.1002/adma.202413353**.

24 S. Vilela, P. Salcedo-Abraira, L. Micheron, E. Solla, P. Yot and P. Horcajada, A Robust Monolithic Metal–Organic Framework with Hierarchical Porosity, *Chem. Commun.*, 2018, **54**, 13088–13091, DOI: **10.1039/C8CC07252C**.

25 C. Y. Chaparro-Garnica, E. Bailón-García, D. Lozano-Castelló and A. Bueno-López, Design and Fabrication of Integral Carbon Monoliths Combining 3D Printing and Sol–Gel Polymerization: Effects of the Channel Morphology on the CO-PROX Reaction, *Catal. Sci. Technol.*, 2021, **11**(19), 6490–6497, DOI: **10.1039/d1cy01104a**.

26 Y. Cao, W. Han, Z. Pu, X. Wang, B. Wang, C. Liu, H. Uyama and C. Shen, Fabrication of Hierarchically Porous Super-hydrophilic Polycaprolactone Monolith Based on Nonsolvent-Thermally Induced Phase Separation, *RSC Adv.*, 2020, **10**(44), 26319–26325, DOI: **10.1039/d0ra04687f**.

27 K. B. Spilstead, S. J. Haswell, N. W. Barnett, X. A. Conlan, P. G. Stevenson and P. S. Francis, Development of a Resin Based Silica Monolithic Column Encapsulation, *Anal. Methods*, 2015, **7**(12), 4908–4911, DOI: **10.1039/c5ay00722d**.

28 Y. Hinamoto, A. Sugawara, T.-A. Asoh, M. Nandi and H. Uyama, Functionalized Cellulose Monolith Based Affinity Chromatography Columns for Efficient Separation of Protein Molecules, *RSC Appl. Polym.*, 2023, **1**(1), 82–96, DOI: **10.1039/d3lp00041a**.

29 A. Lambarska, K. Szymańska and U. Hanefeld, Monoliths Enabling Biocatalysis in Flow Chemistry, *Green Chem.*, 2024, 10718–10738, DOI: **10.1039/d4gc03535f**.

30 T. Tian, Z. Zeng, D. Vulpe, M. E. Casco, G. Divitini, P. A. Midgley, J. Silvestre-Albero, J. C. Tan, P. Z. Moghadam and D. Fairen-Jimenez, A Sol–Gel Monolithic Metal–Organic Framework with Enhanced Methane Uptake, *Nat. Mater.*, 2018, **17**(2), 174–179, DOI: **10.1038/NMAT5050**.

31 D. G. Madden, D. O'Nolan, N. Rampal, R. Babu, C. Çamur, A. N. Al Shakhs, S. Y. Zhang, G. A. Rance, J. Perez, M. Casati, N. Pietro, C. Cuadrado-Collados, D. O'Sullivan, N. P. Rice, T. Gennett, P. Parilla, S. Shulda, K. E. Hurst, V. Stavila, M. D. Allendorf, J. Silvestre-Albero, A. C. Forse, N. R. Champness, K. W. Chapman and D. Fairen-Jimenez, Densified HKUST-1 Monoliths as a Route to High Volumetric and Gravimetric Hydrogen Storage Capacity, *J. Am. Chem. Soc.*, 2022, **144**(30), 13729–13739, DOI: **10.1021/jacs.2c04608**.

32 T. Tian, Z. Zeng, D. Vulpe, M. E. Casco, G. Divitini, P. A. Midgley, J. Silvestre-Albero, J. C. Tan, P. Z. Moghadam and D. Fairen-Jimenez, A Sol–Gel Monolithic Metal–Organic Framework with Enhanced Methane Uptake, *Nat. Mater.*, 2018, **17**(2), 174–179, DOI: **10.1038/NMAT5050**.

33 B. M. Connolly, M. Aragones-Anglada, J. Gandara-Loe, N. A. Danaf, D. C. Lamb, J. P. Mehta, D. Vulpe, S. Wuttke, J. Silvestre-Albero, P. Z. Moghadam, A. E. H. Wheatley and D. Fairen-Jimenez, Tuning Porosity in Macroscopic Monolithic Metal–Organic Frameworks for Exceptional Natural Gas Storage, *Nat. Commun.*, 2019, **10**(1), 1–11, DOI: **10.1038/s41467-019-10185-1**.

34 C. Duan, Y. Yu, J. Li, L. Li, B. Huang, D. Chen and H. Xi, Recent Advances in the Synthesis of Monolithic Metal–Organic Frameworks, *Sci. China Mater.*, 2021, **64**(6), 1305–1319, DOI: **10.1007/s40843-020-1585-1**.

35 M. Tricarico and J. C. Tan, Mechanical Properties and Nanostructure of Monolithic Zeolitic Imidazolate Frameworks: A Nanoindentation, Nanospectroscopy, and Finite Element Study, *Mater. Today Nano*, 2022, **17**, 100166, DOI: **10.1016/j.mtnano.2021.100166**.

36 K. Ploner, P. Delir Kheyrollahi Nezhad, A. Gili, F. Kamutzki, A. Gurlo, A. Doran, P. Cao, M. Heggen, N. Köwitsch, M. Armbrüster, M. Watschinger, B. Klötzer and S. Penner, The Sol–Gel Autocombustion as a Route towards Highly CO$_2$-Selective, Active and Long-Term Stable Cu/ZrO$_2$ methanol Steam Reforming Catalysts, *Mater. Chem. Front.*, 2021, **5**(13), 5093–5105, DOI: **10.1039/d1qm00641j**.

37 D. K. Pattadar and F. P. Zamborini, Effect of Size, Coverage, and Dispersity on the Potential-Controlled Ostwald Ripening of Metal Nanoparticles, *Langmuir*, 2019, **35**(50), 16416–16426, DOI: **10.1021/acs.langmuir.9b02421**.

38 M. Tricarico, C. Besnard, G. Cinque, A. M. Korsunsky and J. C. Tan, Stress–Strain Relationships and Yielding of Metal–Organic Framework Monoliths, *Commun. Mater.*, 2023, **4**(1), 1–9, DOI: **10.1038/s43246-023-00412-0**.

39 Y. He, T. Fu, L. Wang, J. Liu, G. Liu and H. Zhao, Self-Assembly of MOF-801 into Robust Hierarchically Porous Monoliths for Scale-up Atmospheric Water Harvesting, *Chem. Eng. J.*, 2023, **472**, 144786, DOI: **10.1016/j.cej.2023.144786**.

40 S. A. Holey and R. R. Nayak, Harnessing Glycolipids for Supramolecular Gelation: A Contemporary Review, *ACS Omega*, 2024, **9**(24), 25513–25538, DOI: **10.1021/acsomega.4c00958**.

41 E. Hunter-Sellars, P. A. Saenz-Cavazos, A. R. Houghton, S. R. McIntyre, I. P. Parkin and D. R. Williams, Sol–Gel Synthesis of High-Density Zeolitic Imidazolate Framework Monoliths via Ligand Assisted Methods: Exceptional Porosity, Hydrophobicity, and Applications in Vapor Adsorption, *Adv. Funct. Mater.*, 2021, **31**(5), 2008357, DOI: **10.1002/adfm.202008357**.

42 M. Borlaf and R. Moreno, Colloidal Sol–Gel: A Powerful Low-Temperature Aqueous Synthesis Route of Nanosized Powders and Suspensions, *Open Ceram.*, 2021, **8**, 100200, DOI: **10.1016/j.oceram.2021.100200**.

43 E. Hunter-Sellars, P. A. Saenz-Cavazos, A. R. Houghton, S. R. McIntyre, I. P. Parkin and D. R. Williams, Sol–Gel Synthesis of High-Density Zeolitic Imidazolate Framework Monoliths via Ligand Assisted Methods: Exceptional Porosity, Hydrophobicity, and Applications in Vapor Adsorption (Advanced Functional Materials, (2021), 31, 5, (2008357), 10.1002/Adfm.20200), *Adv. Funct. Mater.*, 2021, 12–14, DOI: **10.1002/adfm.202102716**.

44 A. Pathak, L. A. Alghamdi, J. Fernández-Catalá, M. Tricarico, D. Cazorla-Amorós, J. C. Tan, Á. Berenguer-Murcia, G. Mehlana and A. E. H. Wheatley, Understanding Metal–Organic Framework Densification: Solvent Effects and the Growth of Colloidal Primary Nanoparticles in Monolithic ZIF-8, *Small*, 2025, **21**(21), 1–27, DOI: **10.1002/smll.202500510**.

45 A. Wang, M. Jin, N. Li, Y. Ma, L. Chen, D. Ma, B. X. Chen, F. Gao, Y. Q. Tian and Y. K. Shi, Zeolitic Imidazolate Framework Monoliths with High Mesoporosity and Effective Adsorption of Toluene from Aqueous Solution, *New J. Chem.*, 2017, **41**(16), 8031–8035, DOI: **10.1039/c7nj02024d**.

46 W. Y. Hong, S. P. Perera and A. D. Burrows, Manufacturing of Metal–Organic Framework Monoliths and Their Application in CO$_2$ Adsorption, *Microporous Mesoporous Mater.*, 2015, **214**, 149–155, DOI: **10.1016/j.micromeso.2015.05.014**.

47 H. Thakkar, S. Eastman, Q. Al-Naddaf and F. Rezaei, 3D-Printed Metal–Organic Framework Monoliths for Gas Adsorption Processes, *ACS Appl. Mater. Interfaces*, 2017, **9**(41), 35908–35916, DOI: **10.1021/acsami.7b11626**.

48 G. J. H. Lim, Y. Wu, B. B. Shah, J. J. Koh, C. K. Liu, D. Zhao, A. K. Cheetham, J. Wang and J. Ding, 3D-Printing of Pure Metal–Organic Framework Monoliths, *ACS Mater. Lett.*, 2019, **1**(1), 147–153, DOI: **10.1021/acsmaterialslett.9b00069**.

49 H. Molavi, K. Mirzaei, M. Barjasteh, S. Y. Rahnamaee, S. Saeedi, A. Hassanpouryouzband and M. Rezakazemi, *3D-Printed MOF Monoliths: Fabrication Strategies and Environmental Applications*, Springer Nature Singapore, 2024, vol. 16, DOI: **10.1007/s40820-024-01487-1**.

50 R. L. Truby and J. A. Lewis, Printing Soft Matter in Three Dimensions, *Nature*, 2016, **540**(7633), 371–378, DOI: **10.1038/nature21003**.

51 A. J. Young, R. Guillet-Nicolas, E. S. Marshall, F. Kleitz, A. J. Goodhand, L. B. L. Glanville, M. R. Reithofer and J. M. Chin, Direct Ink Writing of Catalytically Active UiO-66 Polymer Composites, *Chem. Commun.*, 2019, **55**(15), 2190–2193, DOI: **10.1039/c8cc10018g**.

52 R. Pei, L. Fan, F. Zhao, J. Xiao, Y. Yang, A. Lai, S. F. Zhou and G. Zhan, 3D-Printed Metal–Organic Frameworks within Biocompatible Polymers as Excellent Adsorbents for Organic Dyes Removal, *J. Hazard. Mater.*, 2020, **384**, 121418, DOI: **10.1016/j.jhazmat.2019.121418**.

53 B. Verougstraete, D. Schuddinck, J. Lefevere, G. V. Baron and J. F. M. Denayer, A 3D-Printed Zeolitic Imidazolate Framework-8 Monolith For Flue- and Biogas Separations by Adsorption: Influence of Flow Distribution and Process Parameters, *Front. Chem. Eng*, 2020, **2**, 1–8, DOI: **10.3389/fceng.2020.589686**.

54 B. Claessens, N. Dubois, J. Lefevere, S. Mullens, J. Cousin-Saint-Remi and J. F. M. Denayer, 3D-Printed ZIF-8 Monoliths for Biobutanol Recovery, *Ind. Eng. Chem. Res.*, 2020, **59**(18), 8813–8824, DOI: **10.1021/acs.iecr.0c00453**.

55 C. A. Grande, R. Blom, V. Middelkoop, D. Matras, A. Vamvakeros, S. D. M. Jacques, A. M. Beale, M. Di Michiel, K. Anne Andreassen and A. M. Bouzga, Multiscale Investigation of Adsorption Properties of Novel 3D Printed UTSA-16 Structures, *Chem. Eng. J.*, 2020, **402**, 126166, DOI: **10.1016/j.cej.2020.126166**.

56 S. Lawson, C. Griffin, K. Rapp, A. A. Rownaghi and F. Rezaei, Amine-Functionalized MIL-101 Monoliths for CO_2 Removal from Enclosed Environments, *Energy Fuels*, 2019, **33**(3), 2399–2407, DOI: **10.1021/acs.energyfuels.8b04508**.

57 F. Lorignon, A. Gossard and M. Carboni, Hierarchically Porous Monolithic MOFs: An Ongoing Challenge for Industrial-Scale Effluent Treatment, *Chem. Eng. J.*, 2020, **393**, 124765, DOI: **10.1016/j.cej.2020.124765**.

58 X. Liu, D. Zhao and J. Wang, Challenges and Opportunities in Preserving Key Structural Features of 3D-Printed Metal/Covalent Organic Framework, *Nano-Micro Lett.*, 2024, **16**(1), 1–20, DOI: **10.1007/s40820-024-01373-w**.

59 X. D. Do, V. T. Hoang and S. Kaliaguine, MIL-53(Al) Mesostructured Metal–Organic Frameworks, *Microporous Mesoporous Mater.*, 2011, **141**(1–3), 135–139, DOI: **10.1016/j.micromeso.2010.07.024**.

60 S. Lawson, M. Snarzyk, D. Hanify, A. A. Rownaghi and F. Rezaei, Development of 3D-Printed Polymer-MOF Monoliths for CO2 Adsorption, *Ind. Eng. Chem. Res.*, 2020, **59**(15), 7151–7160, DOI: **10.1021/acs.iecr.9b05445**.

61 M. C. Kreider, M. Sefa, J. A. Fedchak, J. Scherschligt, M. Bible, B. Natarajan, N. N. Klimov, A. E. Miller, Z. Ahmed and M. R. Hartings, Toward 3D Printed Hydrogen Storage Materials Made with ABS-MOF Composites, *Polym. Adv. Technol.*, 2018, **29**(2), 867–873, DOI: **10.1002/pat.4197**.

62 R. Li, S. Yuan, W. Zhang, H. Zheng, W. Zhu, B. Li, M. Zhou, A. Wing-Keung Law and K. Zhou, 3D Printing of Mixed Matrix Films Based on Metal–Organic Frameworks and Thermoplastic Polyamide 12 by Selective Laser Sintering for Water Applications, *ACS Appl. Mater. Interfaces*, 2019, **11**(43), 40564–40574, DOI: **10.1021/acsami.9b11840**.

63 A. Pustovarenko, B. Seoane, E. Abou-Hamad, H. E. King, B. M. Weckhuysen, F. Kapteijn and J. Gascon, Rapid Fabrication of MOF-Based Mixed Matrix Membranes through Digital Light Processing, *Mater. Adv.*, 2021, **2**(8), 2739–2749, DOI: **10.1039/d1ma00023c**.

64 O. Halevi, J. M. R. Tan, P. S. Lee and S. Magdassi, Hydrolytically Stable MOF in 3D-Printed Structures, *Adv. Sustainable Syst.*, 2018, **2**(2), 1–5, DOI: **10.1002/adsu.201700150**.

65 S. Lawson and F. Rezaei, Effects of Process Parameters on CO_2/H_2 Separation Performance of 3D-Printed MOF-74 Monoliths, *ACS Sustainable Chem. Eng.*, 2021, **9**(32), 10902–10912, DOI: **10.1021/acssuschemeng.1c03443**.

66 B. Verougstraete, D. Schuddinck, J. Lefevere, G. V. Baron and J. F. M. Denayer, A 3D-Printed Zeolitic Imidazolate Framework-8 Monolith For Flue- and Biogas Separations by Adsorption: Influence of Flow Distribution and Process Parameters, *Front. Chem. Eng*, 2020, **2**, 1–8, DOI: **10.3389/fceng.2020.589686**.

67 L. Figueroa–Quintero, E. V. Ramos–Fernández and J. Narciso, 3D-Printed Brass Monoliths for ZIF-8 Synthesis and CO_2 Conversion: A Novel Approach Using Selective Laser Melting, *J. Environ. Chem. Eng.*, 2025, **13**(2), 1–10, DOI: **10.1016/j.jece.2025.115453**.

68 Q. Fu, L. Wen, L. Zhang, X. Chen, D. Pun, A. Ahmed, Y. Yang and H. Zhang, Preparation of Ice-Templated MOF-Polymer Composite Monoliths and Their Application for Wastewater Treatment with High Capacity and Easy Recycling, *ACS Appl. Mater. Interfaces*, 2017, **9**(39), 33979–33988, DOI: **10.1021/acsami.7b10872**.

69 M. Herrmann, P. B. Kempa, H. Fietzek, T. Altenburg, A. Polyzoidis, C. G. Piscopo and S. Löbbecke, Characterization of Metal–Organic Frameworks Using X-Ray Diffraction, *Chem. Ing. Tech.*, 2016, **88**(7), 967–970, DOI: **10.1002/cite.201500123**.

70 C. Alberoni, I. Barroso-Martin, A. Infantes-Molina, E. Rodriguez-Castellon, A. Talon, H. Zhao, S. You, A. Vomiero and E. Moretti, Ceria Doping Boosts Methylene Blue Photodegradation in Titania Nanostructures, *Mater. Chem. Front.*, 2021, **5**(11), 4138–4152, DOI: **10.1039/d1qm00068c**.

71 L. G. Marazani, V. Gascon-Perez, A. Pathak, M. Tricarico, J. C. Tan, M. J. Zaworotko, A. E. H. Wheatley, B. C. E. Makhubela and G. Mehlana, Water Sorption Studies with Mesoporous Multivariate Monoliths Based on UiO-66, *Mater. Adv.*, 2024, **5**(19), 7679–7689, DOI: **10.1039/d4ma00522h**.

72 M. Rivera-Torrente, L. D. B. Mandemaker, M. Filez, G. Delen, B. Seoane, F. Meirer and B. M. Weckhuysen, Spectroscopy, Microscopy, Diffraction and Scattering of Archetypal MOFs: Formation, Metal Sites in Catalysis and Thin Films, *Chem. Soc. Rev.*, 2020, **49**(18), 6694–6732, DOI: **10.1039/d0cs00635a**.

73 J. Zhu, P. M. Usov, W. Xu, P. J. Celis-Salazar, S. Lin, M. C. Kessinger, C. Landaverde-Alvarado, M. Cai, A. M. May, C. Slebodnick, D. Zhu, S. D. Senanayake and A. J. Morris, A New Class of Metal-Cyclam-Based Zirconium Metal–Organic Frameworks for CO_2 Adsorption and Chemical Fixation, *J. Am. Chem. Soc.*, 2018, **140**(3), 993–1003, DOI: **10.1021/jacs.7b10643**.

74 Y. Zheng, H. Kasai, S. Kobayashi, S. Kawaguchi and E. Nishibori, In Situ Observation of a Mechanically Induced Self-Sustaining Reaction for Synthesis of Silver, *Mater. Adv.*, 2022, **4**(4), 1005–1010, DOI: **10.1039/d2ma00903j**.

75 H. L. Nguyen, Reticular Design and Crystal Structure Determination of Covalent Organic Frameworks, *Chem. Sci.*, 2021, **12**(25), 8632–8647, DOI: **10.1039/d1sc00738f**.

76 L. Bourda, C. Krishnaraj, P. Van Der Voort and K. Van Hecke, Conquering the Crystallinity Conundrum: Efforts to Increase Quality of Covalent Organic Frameworks, *Mater. Adv.*, 2021, **2**(9), 2811–2845, DOI: **10.1039/d1ma00008j**.

77 G. Odling, H. Logan, A. Chan, A. J. Bissel, C. R. Pulham and D. E. Oliver, Large Scale Recyclable Monolithic Methyltrimethoxysilane Aerogels Formed by Self-Reinforcement, *Mater. Adv.*, 2023, **4**(17), 3724–3732, DOI: **10.1039/d3ma00085k**.

78 M. Khan, F. Ali, S. Ramzan and Z. A. AlOthman, N-Phenyl Acrylamide-Incorporated Porous Silica-Bound Graphene Oxide Sheets with Excellent Removal Capacity for Cr(III) and Cr(VI) from Wastewater, *RSC Adv.*, 2023, **13**(24), 16047–16066, DOI: **10.1039/d3ra02568c**.

79 Y. Wang, L. Zhang, T. A. Asoh and H. Uyama, Hydrophobic and Hydrophilic Modification of Hierarchically Porous Monolithic Polyimide Derivatives as Functional Liquid Absorbers, *Mater. Adv.*, 2021, **2**(11), 3560–3568, DOI: **10.1039/d1ma00185j**.

80 S. Shekhar and C. Chowdhury, Topological Data Analysis Enhanced Prediction of Hydrogen Storage in Metal–Organic Frameworks (MOFs), *Mater. Adv.*, 2023, **5**(2), 820–830, DOI: **10.1039/d3ma00591g**.

81 C. Altintas and S. Keskin, Role of Partial Charge Assignment Methods in High-Throughput Screening of MOF Adsorbents and Membranes for CO_2/CH_4 Separation, *Mol. Syst. Des. Eng.*, 2020, **5**(2), 532–543, DOI: **10.1039/c9me00163h**.

82 G. M. Neville, R. Jagpal, J. Paul-Taylor, M. Tian, A. D. Burrows, C. R. Bowen and T. J. Mays, Freeze Casting of Porous Monolithic Composites for Hydrogen Storage, *Mater. Adv.*, 2022, **3**(6861), 8934–8946, DOI: **10.1039/d2ma00710j**.

83 T. Toyao, K. Liang, K. Okada, R. Ricco, M. J. Styles, Y. Tokudome, Y. Horiuchi, A. J. Hill, M. Takahashi, M. Matsuoka and P. Falcaro, Positioning of the HKUST-1 Metal–Organic Framework ($Cu_3(BTC)_2$) through Conversion from Insoluble Cu-Based Precursors, *Inorg. Chem. Front.*, 2015, **2**(5), 434–441, DOI: **10.1039/c4qi00215f**.

84 Y. Si, X. Li, G. Yang, X. Mie and L. Ge, Fabrication of a Novel Core–Shell CQDs@ZIF-8 Composite with Enhanced Photocatalytic Activity, *J. Mater. Sci.*, 2020, **55**(27), 13049–13061, DOI: **10.1007/s10853-020-04909-8**.

85 D. G. Madden, R. Babu, C. Çamur, N. Rampal, J. Silvestre-Albero, T. Curtin and D. Fairen-Jimenez, Monolithic Metal–Organic Frameworks for Carbon Dioxide Separation, *Faraday Discuss.*, 2021, **231**, 51–65, DOI: **10.1039/d1fd00017a**.

86 J. I. Lovitt, T. Gorai, E. Cappello, J. M. Delente, S. T. Barwich, M. E. Möbius, T. Gunnlaugsson and C. S. Hawes, Supramolecular Aggregation Properties of 4-(1-Morpholino)-1,8-Naphthalimide Based Fluorescent Materials, *Mater. Chem. Front.*, 2021, **5**(8), 3458–3469, DOI: **10.1039/d1qm00091h**.

87 S. Weber, S. Schäfer, M. Saccoccio, K. Seidel, H. Kohlmann, R. Gläser and S. A. Schunk, Mayenite-Based Electride C12A7e⁻: An Innovative Synthetic Methodviaplasma Arc Melting, *Mater. Chem. Front.*, 2021, **5**(3), 1301–1314, DOI: **10.1039/d0qm00688b**.

88 S. Noh, H. Oh, J. Kim, S. Jung and J. H. Shim, Cobalt-Copper-Embedded Nitrogen-Doped Carbon Nanostructures Derived from Zeolite Imidazolate Frameworks as Electrocatalysts for the Oxygen Reduction Reaction, *ACS Omega*, 2024, **9**(27), 29431–29441, DOI: **10.1021/acsomega.4c01667**.

89 L. León-Alcaide, J. López-Cabrelles, M. Esteve-Rochina, E. Ortí, J. Calbo, B. A. H. Huisman, M. Sessolo, J. C. Waerenborgh, B. J. C. Vieira and G. Mínguez Espallargas, Implementing Mesoporosity in Zeolitic Imidazolate Frameworks through Clip-Off Chemistry in Heterometallic Iron-Zinc ZIF-8, *J. Am. Chem. Soc.*, 2023, **145**(42), 23249–23256, DOI: **10.1021/jacs.3c08017**.

90 J. Hou, A. F. Sapnik and T. D. Bennett, Metal–Organic Framework Gels and Monoliths, *Chemical Science*, Royal Society of Chemistry, 2020, pp. 310–323, DOI: **10.1039/c9sc04961d**.

91 H. Furukawa, K. E. Cordova, M. O'Keeffe and O. M. Yaghi, The Chemistry and Applications of Metal–Organic Frameworks, *Science*, 2013, **341**(6149), 1230444, DOI: **10.1126/science.1230444**.

92 M. Thommes, K. Kaneko, A. V. Neimark, J. P. Olivier, F. Rodriguez-Reinoso, J. Rouquerol and K. S. W. Sing, Physisorption of Gases, with Special Reference to the Evaluation of Surface Area and Pore Size Distribution (IUPAC Technical Report), *Pure Appl. Chem.*, 2015, **87**(9–10), 1051–1069, DOI: **10.1515/pac-2014-1117**.

93 Z. Wang, L. Liu, Z. Li, N. Goyal, T. Du, J. He and G. K. Li, Shaping of Metal–Organic Frameworks: A Review, *Energy Fuels*, 2022, **36**(6), 2927–2944, DOI: **10.1021/acs.energyfuels.1c03426**.

94 M. Tricarico, C. Besnard, G. Cinque, A. M. Korsunsky and J. C. Tan, Stress–Strain Relationships and Yielding of Metal–Organic Framework Monoliths, *Commun. Mater.*, 2023, **4**(1), 1–35, DOI: **10.1038/s43246-023-00412-0**.

95 D. F. Bahr, J. A. Reid, W. M. Mook, C. A. Bauer, R. Stumpf, A. J. Skulan, N. R. Moody, B. A. Simmons, M. M. Shindel and M. D. Allendorf, Mechanical Properties of Cubic Zinc Carboxylate IRMOF-1 Metal–Organic Framework Crystals, *Phys. Rev. B: Condens. Matter Mater. Phys.*, 2007, **76**(18), 1–7, DOI: **10.1103/PhysRevB.76.184106**.

96 X. Ning, N. Wu, M. Zhong, Y. Wen, B. Li and Y. Jiang, Molecular Dynamics Simulation Analysis of Damage and Expansion Process of Nanoindentation Single-Crystal 3C-SiC Carbide Specimens at Different Temperature, *Nanomaterials*, 2023, **13**(2), 235, DOI: **10.3390/nano13020235**.

97 T. Tian, J. Velazquez-Garcia, T. D. Bennett and D. Fairen-Jimenez, Mechanically and Chemically Robust ZIF-8 Monoliths with High Volumetric Adsorption Capacity, *J. Mater. Chem. A*, 2015, **3**(6), 2999–3005, DOI: **10.1039/c4ta05116e**.

98 M. Tricarico, S. Mollick, V. Kachwal, D. A. Sherman and J. C. Tan, Exploring the Photophysical and Mechanical Behavior of Fluorescent Metal–Organic Framework Monoliths, *Chem. Mater.*, 2024, **36**(17), 8247–8254, DOI: **10.1021/acs.chemmater.4c00963**.

99 Z. Le, W. Zhang, W. Li, J. Tan, R. Li, X. Wang, Y. V. Kaneti, X. Jiang, J. Chu, Y. Yamauchi and M. Hu, Metal–Organic Powder Thermochemical Solid–Vapor Architectonics toward Gradient Hybrid Monolith with Combined

Structure-Function Features, *Matter*, 2020, **3**(3), 879–891, DOI: **10.1016/j.matt.2020.07.002**.

100 M. Tricarico and J.-C. Tan, Nanostructure-Dependent Indentation Fracture Toughness of Metal–Organic Framework Monoliths, *Next Mater.*, 2023, **1**(1), 100009, DOI: **10.1016/j.nxmate.2023.100009**.

101 X. Duan, L. Feng, D. Wu, Z. Kong, D. Shi, L. Zhang and J. He, Tuning the Mechanical Properties of Sol–Gel Monolithic Metal–Organic Frameworks by Ligand Engineering, *J. Colloid Interface Sci.*, 2024, **654**, 1312–1319, DOI: **10.1016/j.jcis.2023.10.150**.

102 S. R. McIntyre, P. A. Saenz-Cavazos, E. Hunter-Sellars and D. R. Williams, Product Selectivity and Mass Transport in Levulinic Acid Transfer Hydrogenation by Monolithic MIL-100, MIL-88B and ZIF-8@Pd MOFs, *Front. Chem.*, 2023, **10**, 1–12, DOI: **10.3389/fchem.2022.1087939**.

103 J. P. Mehta, T. Tian, Z. Zeng, G. Divitini, B. M. Connolly, P. A. Midgley, J. C. Tan, D. Fairen-Jimenez and A. E. H. Wheatley, Sol–Gel Synthesis of Robust Metal–Organic Frameworks for Nanoparticle Encapsulation, *Adv. Funct. Mater.*, 2018, **28**(8), 1–7, DOI: **10.1002/adfm.201705588**.

104 G. Q. Song, Y. X. Lu, Q. Zhang, F. Wang, X. K. Ma, X. F. Huang and Z. H. Zhang, Porous Cu-BTC Silica Monoliths as Efficient Heterogeneous Catalysts for the Selective Oxidation of Alkylbenzenes, *RSC Adv.*, 2014, **4**(57), 30221–30224, DOI: **10.1039/c4ra04076g**.

105 A. Ganesan, J. Leisen, R. Thyagarajan, D. S. Sholl and S. Nair, Product Selectivity and Mass Transport in Levulinic Acid Transfer Hydrogenation by Monolithic MIL-100, MIL-88B and ZIF-8@Pd MOFs, *ACS Appl. Mater. Interfaces*, 2023, **15**(34), 40623–40632, DOI: **10.1021/acsami.3c08344**.

106 B. M. Connolly, D. G. Madden, A. E. H. Wheatley and D. Fairen-Jimenez, Shaping the Future of Fuel: Monolithic Metal–Organic Frameworks for High-Density Gas Storage, *J. Am. Chem. Soc.*, 2020, **142**(19), 8541–8549, DOI: **10.1021/jacs.0c00270**.

107 M. H. Hassan, R. R. Haikal, T. Hashem, J. Rinck, F. Koeniger, P. Thissen, S. Stefan Heißler, C. Wöll and M. H. Alkordi, Electrically Conductive, Monolithic Metal–Organic Framework-Graphene (MOF@G) Composite Coatings, *ACS Appl. Mater. Interfaces*, 2019, **11**(6), 6442–6447, DOI: **10.1021/acsami.8b20951**.

108 F. Heidarizadeh, X. Jin and Y. Xu, Significance of Copper Benzene 1,3,5-Tricarboxylate Metal Organic Framework: Environmental and Biomedical Applications, *Mater. Chem. Horiz.*, 2023, **2**(2), 155–170.

109 A. J. A. Abubakar, R. L. S. Canevesi, D. A. L. Sanchez and C. A. Grande, Monoliths for Gas Storage Manufactured with Precision Pore Engineering Using 3D-Printed Templates, *Chem. Eng. J.*, 2024, **489**, 151450, DOI: **10.1016/j.cej.2024.151450**.

110 D. M. Teffu, K. Makgopa, T. R. Somo, M. S. Ratsoma, S. Honey, E. Makhado and K. D. Modibane, Metal and Covalent Organic Frameworks (MOFs and COFs): A Comprehensive Overview of Their Synthesis, Characterization and Enhanced Supercapacitor Performance, *Coord. Chem. Rev.*, 2025, **540**, 216798, DOI: **10.1016/j.ccr.2025.216798**.

111 N. Parsazadeh, F. Yousefi, M. Ghaedi, K. Dashtian and F. Borousan, Preparation and Characterization of Monoliths HKUST-1 MOF: Via Straightforward Conversion of Cu(OH)$_2$-Based Monoliths and Its Application for Wastewater Treatment: Artificial Neural Network and Central Composite Design Modeling, *New J. Chem.*, 2018, **42**(12), 10327–10336, DOI: **10.1039/c8nj01067f**.

112 P. Yao, Y. Liu, X. Tang, S. Lu, Z. Li and Y. Yao, Green Chemical Engineering Synthesis of Reusable NH$_2$-MIL-125(Ti)@Polymer Monolith as Ef Fi Cient Adsorbents for Dyes Wastewater Remediation Polyvinyl, *Alcohol.*, 2023, **4**, 439–447.

113 P. Yao, Y. Liu, X. Tang, S. Lu, Z. Li and Y. Yao, Synthesis of Reusable NH$_2$-MIL-125(Ti)@polymer Monolith as Efficient Adsorbents for Dyes Wastewater Remediation, *Green Chem. Eng.*, 2023, **4**(4), 439–447, DOI: **10.1016/j.gce.2022.06.004**.

114 Q. Liu, S. Li, H. Yu, F. Zeng, X. Li and Z. Su, Covalently Crosslinked Zirconium-Based Metal–Organic Framework Aerogel Monolith with Ultralow-Density and Highly Efficient Pb(II) Removal, *J. Colloid Interface Sci.*, 2020, **561**(Ii), 211–219, DOI: **10.1016/j.jcis.2019.11.074**.

115 N. Shaheed, S. Javanshir, M. Esmkhani, M. G. Dekamin and M. R. Naimi-Jamal, Synthesis of Nanocellulose Aerogels and Cu-BTC/Nanocellulose Aerogel Composites for Adsorption of Organic Dyes and Heavy Metal Ions, *Sci. Rep.*, 2021, **11**(1), 1–11, DOI: **10.1038/s41598-021-97861-9**.

116 Y. K. Jo, S. Y. Jeong, Y. K. Moon, Y. M. Jo, J. W. Yoon and J. H. Lee, Exclusive and Ultrasensitive Detection of Formaldehyde at Room Temperature Using a Flexible and Monolithic Chemiresistive Sensor, *Nat. Commun.*, 2021, **12**(1), 1–9, DOI: **10.1038/s41467-021-25290-3**.

117 Z. Li, J. Liu, L. Feng, Y. Pan, J. Tang, H. Li, G. Cheng, Z. Li, J. Shi, Y. Xu and W. Liu, Monolithic MOF-Based Metal-Insulator-Metal Resonator for Filtering and Sensing, *Nano Lett.*, 2023, **23**(2), 637–644, DOI: **10.1021/acs.nanolett.2c04428**.

118 Z. S. Qin, W. W. Dong, J. Zhao, Y. P. Wu, Q. Zhang and D. S. Li, A Water-Stable Tb(III)-Based Metal–Organic Gel (MOG) for Detection of Antibiotics and Explosives, *Inorg. Chem. Front.*, 2018, **5**(1), 120–126, DOI: **10.1039/c7qi00495h**.

119 D. Zhao, Y. Wang, J. Shao, P. Zhang, Y. Chen, Z. Fu, S. Wang, W. Zhao, Z. Zhou, Y. Yuan, D. Fu and Y. Zhu, Temperature and Humidity Sensor Based on MEMS Technology, *AIP Adv.*, 2021, **11**, 085126, DOI: **10.1063/5.0053342**.

120 M. González-Gómez, E. Martínez Medina, J. Kovač, O. Casals, M. Martínez López, E. Xuriguera-Martín and C. Fàbrega, A Low-Cost Colorimetric HKUST-1 Sensor for Ppm-Level Humidity Detection, *Sens. Actuators, B*, 2025, **25**, 18724–18730, DOI: **10.1016/j.snb.2025.137973**.

121 K. Wu, T. Fei and T. Zhang, Humidity Sensors Based on Metal – Organic Frameworks, *Nanomaterials*, 2022, **12**, 4208, DOI: **10.3390/nano12234208**.

122 I. Pandya, O. A. El Seoud, M. A. Assiri, S. Kumar Kailasa and N. I. Malek, Ionic Liquid/Metal Organic Framework Composites as a New Class of Materials for CO$_2$ Capture: Present Scenario and Future Perspective, *J. Mol. Liq.*, 2024, **395**, 123907, DOI: **10.1016/j.molliq.2023.123907**.

123 Y. Han, S. Wang, Y. Liu, L. Bai, H. Yan and H. Liu, Preparation of Poly(Ionic Liquid@MOF) Composite Monolithic Column and Its Application in the Online Enrichment and Purification of Tectochrysin in Medicinal Plants, *Anal. Methods*, 2022, **14**(4), 401–409, DOI: **10.1039/D1AY01954F**.

124 N. Khosroshahi, M. Bakhtian, A. Asadi and V. Safarifard, Revolutionizing Energy Storage: The Emergence of MOF/MXene Composites as Promising Supercapacitors, *Nano Express*, 2023, **4**, 042002, DOI: **10.1088/2632-959X/ad0446**.

125 F. Mu, J. Zhao, Q. Rong, C. Gu and Q. Zhao, Co/Ni-MOF@MXene Electrode Material for High-Performance Supercapacitor, *Membr. Technol.*, 2025, 117–124.

126 C. He, W. Yin, X. Li, J. Zheng, B. Tang and Y. Rui, Molybdenum Disulfide Synthesized by Molybdenum-Based Metal Organic Framework with High Activity for Sodium Ion Battery, *Electrochim. Acta*, 2021, **365**, 137353, DOI: **10.1016/j.electacta.2020.137353**.

127 Z. Dourandish, I. Sheikhshoaie and S. Maghsoudi, Molybdenum Disulfide/Nickel-Metal Organic Framework Hybrid Nanosheets Based Disposable Electrochemical Sensor for Determination of 4-Aminophenol in Presence of Acetaminophen, *Biosensors*, 2023, **13**(5), 524, DOI: **10.3390/bios13050524**.

128 E. Bogdanova, M. Liu, P. Hodapp, A. Borbora, W. Wenzel, S. Bräse, A. Jung, Z. Dong, P. A. Levkin, U. Manna, T. Hashem and C. Wöll, Functionalization of Monolithic MOF Thin Films with Hydrocarbon Chains to Achieve Superhydrophobic Surfaces with Tunable Water Adhesion Strength, *Mater. Horiz.*, 2024, **12**(4), 1274–1281, DOI: **10.1039/d4mh00899e**.

129 J. Xu, Z. Sun, F. Li, Q. An, Y. Bao, D. Han and L. Niu, Nitrogen-Doped Porous Carbon Derived from Zeolitic Imidazolate Framework-67 Strung into Necklace with Carbon Nanotubes for the Detection of Calcium at Ultralow Level, *J. Electrochem. Soc.*, 2020, **167**, 1–7, DOI: **10.1149/1945-7111/ab91cb**.

130 B. Peng, C. Feng, S. Liu and R. Zhang, Synthesis of CuO Catalyst Derived from HKUST-1 Temple for the Low-Temperature NH_3-SCR Process, *Catal. Today*, 2018, **314**, 122–128, DOI: **10.1016/j.cattod.2017.10.044**.

131 M. Zhu, Y. Yang, X. Zhang, Y. Liang and J. Tang, Cobalt-Based Zeolitic Imidazole Framework Derived Hollow Co_3S_4 Nanopolyhedrons for Supercapacitors, *Appl. Organomet. Chem.*, 2024, **38**(8), 1–11, DOI: **10.1002/aoc.7533**.

132 Y. Zhang and R. Wang, Metal–Organic Framework (MOF)-Derived Metal Oxides for Selective Catalytic Reduction (SCR) of NOx, *Molecules*, 2025, **30**(13), 2836, DOI: **10.3390/molecules30132836**.

133 T. Tian, J. Xu, A. Abdolazizi, C. Ji, J. Hou, D. J. Riley, C. Yan, M. P. Ryan, F. Xie and C. Petit, A Monolithic Gold Nanoparticle@Metal–Organic Framework Composite as CO_2 Photoreduction Catalyst, *Mater. Today Nano*, 2023, **21**, 1–10, DOI: **10.1016/j.mtnano.2022.100293**.

134 E. Avila, H. Salway, E. Ruggeri, C. Çamur, N. Rampal, T. A. S. Doherty, O. D. I. Moseley, S. D. Stranks, D. Fairen-Jimenez and M. Anaya, Better Together: Monolithic Halide Perovskite@Metal–Organic Framework Composites, *Matter*, 2024, 4319–4331, DOI: **10.1016/j.matt.2024.08.022**.

135 V. Ntouros, I. Kousis, D. Papadaki, A. L. Pisello and M. N. Assimakopoulos, Life Cycle Assessment on Different Synthetic Routes of Zif-8 Nanomaterials, *Energies*, 2021, **14**(16), 1–22, DOI: **10.3390/en14164998**.

136 H. U. Escobar-Hernandez, R. Shen, M. I. Papadaki, J. A. Powell, H.-C. Zhou and Q. Wang, Hazard Evaluation of Metal–Organic Framework Synthesis and Scale-up: A Laboratory Safety Perspective, *ACS Chem. Health Saf.*, 2021, **28**(5), 358–368, DOI: **10.1021/acs.chas.1c00044**.

137 J. M. Marrett, F. Effaty, X. Ottenwaelder and T. Friščić, Mechanochemistry for Metal–Organic Frameworks and Covalent–Organic Frameworks (MOFs, COFs): Methods, Materials, and Mechanisms, *Adv. Mater.*, 2025, 2418707, DOI: **10.1002/adma.202418707**.

138 F. Al-Ghazzawi, L. Conte, M. W. Potts, C. Richardson and P. Wagner, Reactive Extrusion Printing of Zeolitic Imidazolate Framework Films, *ACS Appl. Mater. Interfaces*, 2024, **16**(33), 44270–44277, DOI: **10.1021/acsami.4c08609**.

139 M. Sakai, H. Hori, T. Matsumoto and M. Matsukata, One-Pot Synthesis Method of MIL-96 Monolith and Its CO_2 Adsorption Performance, *ACS Appl. Mater. Interfaces*, 2023, **15**(18), 22395–22402, DOI: **10.1021/acsami.2c22955**.

140 Y. Chen, S. Zhang, S. Cao, S. Li, F. Chen, S. Yuan, C. Xu, J. Zhou, X. Feng, X. Ma and B. Wang, Roll-to-Roll Production of Metal–Organic Framework Coatings for Particulate Matter Removal, *Adv. Mater.*, 2017, **29**(15), 4–9, DOI: **10.1002/adma.201606221**.

141 Y. Li, S. Chen, X. Cai, J. Hong, X. Wu, Y. Xu, J. Zou and B. H. Chen, Rational Design and Preparation of Hierarchical Monoliths through 3D Printing for Syngas Methanation, *J. Mater. Chem. A*, 2018, **6**(14), 5695–5702, DOI: **10.1039/c8ta01597j**.

142 E. Hunter-Sellars, P. A. Saenz-Cavazos, A. R. Houghton, S. R. McIntyre, I. P. Parkin and D. R. Williams, Sol–Gel Synthesis of High-Density Zeolitic Imidazolate Framework Monoliths via Ligand Assisted Methods: Exceptional Porosity, Hydrophobicity, and Applications in Vapor Adsorption, *Adv. Funct. Mater.*, 2021, **31**(5), 1–10, DOI: **10.1002/adfm.202008357**.